Functional Characterization of the RNA Helicase MOV10

Inaugural-Dissertation

to obtain the academic degree

Doctor rerum naturalium (Dr. rer. nat.)

submitted to

the Department of Biology, Chemistry and Pharmacy of Freie Universität Berlin

by

Lea Haarup Gregersen

Submitted 26.9.2013

1st Reviewer: **Dr. Markus Landthaler**
Berlin Institute for Medical Systems Biology (BIMSB)
Max-Delbrück-Center for Molecular Medicine (MDC)
Robert-Rössle-Str. 10
13125 Berlin
Tel.: +49 30 9406 3026
Email: markus.landthaler@mdc-berlin.de

2nd Reviewer: **Prof. Dr. Markus Wahl**
Institut für Chemie und Biochemie
Freie Universität Berlin
Takustr. 6
14195 Berlin
Tel.: +49 30 838 53456
Email: mwahl@chemie.fu-berlin.de

Date of 14.1.2014 defense:

ACKNOWLEDGMENTS

Firstly I would like to thank my supervisor Markus Landthaler for the opportunity to work in his lab and his guidance throughout my PhD. I have learned numerous valuable lessons from my time in his lab not only scientifically but also personally which I will benefit from in my future scientific whereabouts.

I owe a huge thanks to Markus Schüler who took it upon himself to make sense of the vast amount of high-throughput sequencing data generated in this project. Without his enthusiasm and skilled analysis this project wouldn't be anywhere near to where it is now. I would also like to thank all other Landthaler lab members for valuable input, especially Mathias Munschauer, who got involved in the later stages of this project. Emanuel Wyler, Christin Zasada and Miha Milek for comments on this thesis.

I would like to thank Ouidad Benlasfer for her assistance in growing and crosslinking hundreds of cell culture plates consumed in this project. I would also like to acknowledge Nikolaus Rajewsky (BIMSB, MDC) and members of his lab for sharing the PAR-CLIP computational analysis pipeline for this study as well as. Jonas Maaskola for an initial secondary structure analysis around MOV10 PAR-CLIP sites. Katrin Bagola from the lab of Thomas Sommer (MDC) for help and advice with yeast culturing.

Last, but definitely not least, I would like to thank Richard, Nina, Maya, and my parents for their never ending support, encouragement and patience with me throughout this PhD. Ruth, Nuria, Pinar, Lena, Christin, Jordi, Matt and Matze for many hours of great company over a countless number of coffees and beers. You guys all made my PhD time an unforgettable and joyful experience.

STATEMENT OF CONTRIBUTIONS

This project was a collaboration between Markus Schüler from the lab of Christoph Dietherich (BIMSB, MDC, currently Max Planck Institute for Biology of Ageing) and myself. Markus Schüler carried out all of the bioinformatic analysis of our PAR-CLIP data as well as RNA-Seq data. Guido Mastrobuoni from the lab of Stefan Kempa (BIMSB, MDC) carried out mass spectrometry runs and ran MaxQuant. Mirjam Feldkamp and Claudia Langnick from the laboratory of Wei Chen (BIMSB, MDC) carried out sequencing runs. Wei Chen calculated mRNA half-lives from RNA-Seq data. Mathias Munschauer from the lab of Markus Landthaler carried out UPF1 PAR-CLIP and MOV10 PAR-CLIP of puromycin treated cells. This data will not be presented here, but only briefly mentioned in the context of understanding the functional role of MOV10.

TABLE OF CONTENT

SUMMARY

RNA helicases are important regulators of gene expression, which act by remodeling local RNA secondary structures as well as RNA-protein interactions to allow dynamic association of RNA-binding proteins to their targets. Here, I demonstrate that the helicase MOV10 has an ATP-dependent 5’ to 3’ *in vitro* RNA unwinding activity and comprehensively determine the RNA-binding sites of wild-type MOV10 and helicase mutants in human cells using photoactivatable-ribonucleoside-enhanced crosslinking and immunoprecipitation (PAR-CLIP). I find that MOV10 predominantly binds to 3’ untranslated regions (UTRs) immediately upstream of regions predicted to form local secondary structures and provide evidence that MOV10 helicase mutants are impaired in their ability to translocate 5’ to 3’ on their mRNA targets. MOV10 interacts with UPF1, the key component of the nonsense-mediated decay (NMD) pathway and co-occupies the same RNA sites. Knockdown of MOV10 results in increased mRNA half-lives of MOV10-targeted mRNAs as well as an NMD reporter transcript, suggesting that MOV10 functions in mRNA degradation as an mRNP clearance factor that resolves local secondary structures and displaces proteins from 3’UTRs.

ZUSAMMENFASSUNG

RNA-Helikasen können lokale RNA-Sekundärstrukturen sowie Protein-RNA-Interaktionen verändern. Dadurch ermöglichen sie flexible Änderungen der an RNA gebundene Proteine und sind somit wichtige Regulatoren der Genexpression. In dieser Dissertation zeige ich, dass die Helikase MOV10 ATP-abhängig doppelsträngige RNA in 5’ zu 3’-Richtung entwindet. Zudem bestimme ich transkriptomweit die RNA-Bindungsstellen von Wildtyp-MOV10 und Helikase-defizienten Mutanten vermittels Immunopräzipitation von UV-vernetzten Protein-RNA-Komplexen (PAR-CLIP). So kann ich darlegen, dass MOV10 vor allem in den nicht-translatierten Regionen am 3'-Ende der Boten-RNA (3’-UTRs) bindet, gleich vor Stellen für die RNA-Sekundärstrukturen berechnet werden. Für die MOV10-Mutanten zeige ich, dass sie sich im Gegensatz zum Wildtyp-Enzym vermutlich nicht auf der RNA fortbewegen können. MOV10 bindet an UPF1, eine Schlüsselkomponente im Abbau von Nonsense-Boten-RNA (NMD) und besetzt die selben RNA-Bindungsstellen wie dieses Protein. Depletion von MOV10 führt zu Stabilisierung von MOV10-gebundenen Boten-RNAs sowie eines NMD-Reporter-transkripts. Dies ist ein Hinweis darauf, dass MOV10 den Abbau von Boten-RNA begünstigt, indem es RNA-Sekundärstrukturen in 3'-UTRs entwindet sowie daran gebundene Proteine entfernt.

ABBREVIATIONS

4SU	4-thiouridine
4TU	4-thiouracil
6SG	6-thioguanosine
AREs	AU-rich elements
ATP	Adenosine triphosphate
CH domain	Cysteine-histidine rich domain
CLIP	UV-crosslinking and immunoprecipitation
DEAD	Aspartic acid- glutamic acid - alanine - aspartic acid
DEAH	Aspartic acid - glutamic acid - alanine - histidine
DExH	Aspartic acid - glutamic acid -x- histidine
dsRNA	Double stranded RNA
EJC	Exon junction complex
FPKM	Fragments per kilobase of exon per million fragments mapped
HITS-CLIP	High-throughput sequencing CLIP
HIV-1	Human immunodeficiency virus type 1
hrs	Hours
IAP	Intracisternal A particles
iCLIP	Individual-nucleotide-resolution CLIP
IP	Immunoprecipitation
KH	hnRNP K homology
LINE-1	Long interspersed element 1
miRISC	miRNA-induced silencing complex
miRNA	microRNA
NMD	Nonsense-mediated decay
NTP	Nucleoside triphosphate
PAR-CLIP	Photoactivatable-ribonucleoside-enhanced CLIP
P-bodies	Processing bodies
piRNA	PIWI-interacting RNAs
poly(A)	Polyadenylated
PRC	Polycomb repressive complex
PTC	Premature termination codon
qRT-PCR	Quantitative real-time PCR
RIP	RNA immunoprecipitation
RNP	Ribonucleoprotein complex
RRM	RNA recognition motif
SILAC	Stable isotope labeling by amino acid in cell culture

siRNA	Small interference RNA
SQ domain	Serine-glutamine rich domain
ssDNA	Single stranded DNA
ssRNA	Single stranded RNA
SURF complex	SMG-1-UPF1-eRF1-eRF3 complex
UTR	Untranslated region
UV	Ultraviolet

INTRODUCTION

The Life Cycle of an mRNA is Dependent on Continuous mRNP Remodeling

From transcription to degradation, RNA molecules are covered with RNA-binding proteins forming ribonucleoprotein complexes (RNPs) (Lee and Lykke-Andersen, 2013; Muller-McNicoll and Neugebauer, 2013; Wahl et al., 2009). During transcription, RNA-binding proteins are recruited to nascent transcripts to dictate co-transcriptional processes including 5-capping, splicing and RNA editing (Neugebauer, 2002). Many proteins involved in co-transcriptional mRNA processing interact with the C-terminal domain of RNA polymerase II that serves as a recruitment platform for proteins involved in co-transcriptional processes, and numerous RNA-binding proteins, such as U1 snRNP splicing factors and SR splicing regulators, co-purifies with the RNA polymerase II subunit (Bentley, 2005; Das et al., 2007; Meinhart and Cramer, 2004). In addition, mRNA-binding proteins are involved in ensuring correct formation of nascent transcripts and to prevent erroneous mRNP formation in a co-transcriptional manner (Jensen et al., 2003). Nascent mRNPs that do not pass the quality control are retained within the nucleus and targeted for degradation (Jensen et al., 2003). If the RNA polymerase II pauses during transcription, the RNA-DNA helicase Senataxin (SETX) is recruited to these sites to resolve structures formed between the single stranded DNA (ssDNA) and nascent transcripts to promote XRN2-mediated 5’ to 3’ degradation (Mischo et al., 2011; Skourti-Stathaki et al., 2011). As a final step in co-transcriptional processing, the nascent pre-mRNA is cleaved downstream of the polyadenylation (poly(A)) site by a multisubunit cleavage/polyadenylation complex and polyadenylated by the poly(A) polymerase (Bentley, 2005).

During the following steps of an mRNA’s life cycle, involving export of the mRNA from the nucleus into the cytoplasm and translation, the mRNA transcripts are continuously associated with a different repertoire of mRNA-binding proteins, forming distinct mRNP structures dictating the fate of the mRNA. Most mRNPs exported from the nucleus will initially form an ‘actively translating mRNP’ by assembly of the translation initiation complex in the 5’ untranslated region (UTR), followed by joining of the 60S ribosomal subunit and assembly of the 80S initiation complex (Aitken and Lorsch, 2012). Assembly of the translation machinery promotes the formation of a closed-loop structure of the mRNP, by bringing the 5’ and 3’ ends of the mRNA into proximity allowing efficient recycling of translating ribosomes (Aitken and

Lorsch, 2012; Schoenberg and Maquat, 2012). mRNA molecules are protected from degradation by their 5' cap and 3' poly(A)-tail. During translation, the poly(A)-tail is continuously shortened which eventually makes the mRNA susceptible to 3' to 5' exosome-mediated exonucleolytic decay (Garneau et al., 2007; Schoenberg and Maquat, 2012). Alternatively, mRNA transcripts can be made susceptible to decay by decapping or endonucleolytic cleavage (Garneau et al., 2007; Schoenberg and Maquat, 2012).

Some actively translating mRNPs are removed from the translating pool of mRNAs either on the basis of recognition of specific gene regulatory elements within the mRNA transcript, mRNA surveillance mechanisms or as a response to changes in cellular conditions. These translationally repressed mRNPs are typically sequestered into either processing bodies (P-bodies) or stress-granules (Eulalio et al., 2007; Garneau et al., 2007). Both are highly dynamic foci consisting of numerous mRNA-binding proteins, including proteins involved in translational repression and mRNA degradation (Eulalio et al., 2007; Parker and Sheth, 2007). mRNAs containing premature termination codons (PTCs), introduced either during erroneous splicing or due to frameshift mutations, are targeted for rapid degradation in P-bodies by the nonsense-mediated decay (NMD) pathway (Franks et al., 2010; Lykke-Andersen et al., 2000). This prevents the synthesis of truncated proteins with potential harmful effects to the cell. In addition, several proteins involved in regulation of a subset of mRNA targets such as Argonaute proteins involved in microRNA (miRNA)-mediated regulation are also located in P-bodies (Eulalio et al., 2007).

mRNPs Consist of a Diverse Repertoire of mRNA-binding Proteins

Correct gene expression and post-transcriptional regulation rely on a tight interplay between mRNA-binding proteins that bind to a subset of mRNAs and housekeeping mRNA-binding proteins, which are bound to most mRNAs. Two recent studies employing ultraviolet (UV) light based crosslinking approaches to capture proteins bound to poly(A) mRNAs in human cells, identified 797 and 860 mRNA-bound proteins, respectively (Baltz et al., 2012; Castello et al., 2012). These proteins represent a catalog of mRNA-binding proteins that at any given state can be bound to poly(A) mRNAs. Many of the identified proteins are involved in regulation of RNA stability, RNA splicing, translation, RNA modification or RNA localization and most, but not all, contain canonical RNA recognition domains (Baltz et al., 2012; Castello et al., 2012). Overrepresented domains among the captured mRNA-bound proteins included classical RNA-binding domains such as the RNA recognition motif (RRM), hnRNP K homology (KH), and DEAD (aspartic acid-glutamic acid-alanine-aspartic acid) box helicase domains (Baltz et al.,

2012; Castello et al., 2012). Both KH domains and RRM domains interact with single-stranded RNA (ssRNA) in a sequence-specific manner, whereas the DEAD box helicase domain interacts with RNA in a sequence independent manner (Auweter et al., 2006). The different RNA interacting domains provide different modes of RNA recognition, which can be based on a more or less well defined sequence motif, local RNA structural elements or RNA modifications, all of which can be further complemented and/or regulated by accessory domains involved in protein-protein interactions.

RNA Helicases Represent an Important Class of mRNP Remodeling Enzymes

Since mRNAs are continuously associated with a changing repertoire of mRNA-binding proteins, the proteins need to constantly cycle between binding to their targets and removal from their targets. Even though much is known about the different individual mRNA-binding proteins and their functional role in mRNA processing, surprisingly little is known about how mRNP transitions are facilitated and which mRNA-binding proteins are involved in these processes. One class of mRNA-binding proteins that plays a key role in mRNP transitions are RNA helicases. RNA helicases are nucleotide triphosphate (NTP)-dependent enzymes that work to remodel both RNA-RNA structures (RNA unwinding activity), and RNA-protein complexes (RNPase activity) (Fairman et al., 2004; Jankowsky et al., 2001; Pyle, 2008). This implies a key role of RNA helicases in regulating mRNP transitions. In line with this, RNA helicases have been implicated in every step of RNA metabolism, from transcription, ribosomal biogenesis, splicing, RNA localization, translation, to RNA surveillance and turnover (Bleichert and Baserga, 2007; Fairman-Williams et al., 2010; Jankowsky and Fairman, 2007; Rocak and Linder, 2004; Wahl et al., 2009). In human cells 47 and 46 out of the poly(A) mRNA-interacting proteins contained a helicase domain (Baltz et al., 2012; Castello et al., 2012). Based on homolog searches it is estimated that 95 helicases are encoded within the human genome, whit 64 of these representing RNA helicases and the remaining 31 representing DNA helicases (Umate et al., 2011).

RNA helicases are found in all three kingdoms of life, but the number of RNA helicases among eukaryotes is significantly higher than in bacteria (Anantharaman et al., 2002). Strikingly, RNA helicases are the most abundant group of enzymes involved in RNA metabolism in eukaryotes (Anantharaman et al., 2002). RNA helicases are often found in multisubunit complexes such as the RNA helicase Brr2 which is stably associated with the catalytic core of the spliceosome, eIF4A3 (also known as DDX48) in the exon junction complex (EJC), and UPF1 in the

surveillance complex or eIF4A in the cap-binding complex (Ballut et al., 2005; Bessonov et al., 2008; Kashima et al., 2006; Linder and Jankowsky, 2011). Common for these RNA helicases is that they are responsible for induction of NTP-dependent conformational changes of their associated protein complexes and/or RNA bound by these complexes.

RNA Helicases and Their Mechanism of Action

DNA and RNA helicases are classified into six super families termed SF1 to SF6 (Fairman-Williams et al., 2010). All currently known RNA helicases, with the exception of some viral RNA helicases, belong to SF1 or SF2 and share similar dual RecA-like domains, 1A and 2A, which make up the helicase core (Jankowsky and Fairman, 2007) (Figure 1A). The SF1 and SF2 helicase core domains contain 13 signature helicase motifs (Q, I, Ia, Ib, Ic, II, III, IV, V, Va, Vb and VI) (Fairman-Williams et al., 2010). The conserved motifs directly participate in NTP-binding and hydrolysis (Q, I, II and VI), RNA recognition (Ia, Ib, Ic, IV, V and Vb) and connection between the two sites (III and Va). The two most conserved motifs, motif I and II (also known as Walker A and Walker B motifs) are structurally located in a NTP-binding pocket formed between the two RecA-like domains and residues from both motifs interact closely with bound NTP (Cheng et al., 2007; Linder and Jankowsky, 2011; Pyle, 2008; Sengoku et al., 2006). Mutations in motif I or II disrupt the NTP-binding and/or hydrolysis rendering the helicases catalytically inactive (Tanner and Linder, 2001; Welker et al., 2010).

The largest subfamily of RNA helicases is termed the DEAD box family due to the conserved amino acids making up motif II and belongs to the SF2 family (Figure 1B) (Fairman-Williams et al., 2010). DEAD box RNA helicases typically display bidirectional unwinding activity and in contrast to other helicases, they are generally considered as non-processive, meaning that they do not translocate along longer stretches of RNA, but instead exert their function through a clamping-mode to facilitate local strand unwinding or complex remodeling of RNA-bound complexes (Jankowsky and Fairman, 2007; Linder and Jankowsky, 2011). The EJC DEAD box RNA helicase eIF4A3 interacts with RNA in a sequence-independent manner and binds upstream of the exon-exon junction on spliced mRNAs (Sauliere et al., 2012; Shibuya et al., 2004; Singh et al., 2012).

In contrast to DEAD box RNA helicases, RNA helicases from the DExH are generally considered to be processive helicases and display directional unwinding activity (Jankowsky and Fairman, 2007; Jankowsky et al., 2000; Kawaoka et al., 2004; Kawaoka and Pyle, 2005; Pang et al., 2002). Evidence suggests that the DExH vaccinia virus RNA helicase NPH-II can track

along the loading strand in a 3' to 5' direction using a so-called wire stripper mechanism to displace away the base paired strand (Jankowsky et al., 2000; Kawaoka et al., 2004; Kawaoka and Pyle, 2005). In addition to processive unwinding NPH-II has been shown to promote *in vitro* protein displacement independent of duplex unwinding (Fairman et al., 2004). UPF1 is a SF1 RNA helicase with directional 5' to 3' unwinding activity and able to unwind a 28 bp duplex (Bhattacharya et al., 2000), suggesting that UPF1 can function as a processive helicase.

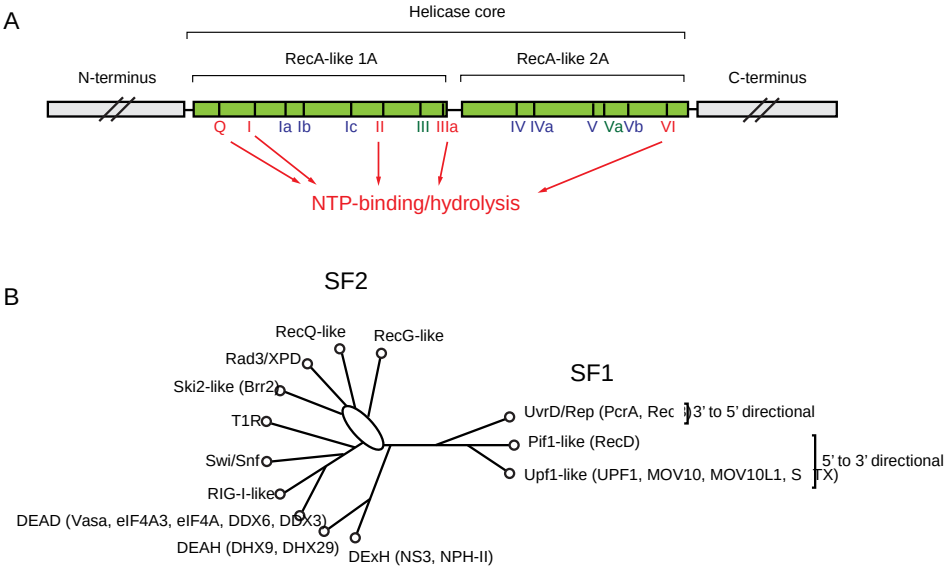

Figure 1. Structural organization of the helicase core and phylogenetic relationship between SF1 and SF2 helicases.
(A) Overall domain structure of SF1 and SF2 helicases, consisting of two RecA-like domains termed 1A and 2A. Conserved helicase motifs are marked throughout the helicase core. Motifs involved in NTP-binding and/or hydrolysis are shown in red, motifs involved in RNA-binding are shown in blue and motifs involved in coordination between NTP- and RNA-binding are shown in green. **(B)** Unrooted cladogram showing the phylogenetic relationship between the different subgroups of SF1 and SF2 helicases. For the SF1 helicases 3' to 5' directional unwinding activity has been observed for all tested members of the UvrD/Rep-like family, while 5' to 3' directional unwinding activity has been observed for tested memebers of the Pif1-like and Upf1-like subfamilies. Examples of proteins belonging to the different subgroups are shown in parenthesis. Adapted from Fairman-Williams et al., 2010.

Structural Clues about RNA Helicase Mechanism of Action

Structural studies of RNA helicases have provided important insights into how NTP-binding and hydrolysis is coupled to binding of RNA as well as how RNA helicases may facilitate RNA unwinding (Pyle, 2008). These studies suggest common structural features of RNA helicases from different subfamilies, but also highlight differences in the mechanism used to destabilize RNA structures and for translocation along their RNA targets (Pyle, 2008).

A common feature of all SF1 and SF2 helicases is that they contain two dual RecA-like domains which come together to form a nucleotide binding site in the cleft between them (Fairman-

Williams et al., 2010). Nucleic acid are usually bound on the surface across the two Rec-A like domains (Fairman-Williams et al., 2010). In most cases, nucleotide binding and hydrolysis induces conformational changes in the degree of interaction between the two RecA-like domains, opening or closing the cleft between them. Interactions between bound nucleic acid in UPF1, Vasa, NS3, PcrA, RecD2 and other helicases involve hydrogen-bonds and salt-bridges to the sugar-phosphate backbone of nucleic acid, explaining the lack of sequence specificity (Appleby et al., 2011; Cheng et al., 2007; Saikrishnan et al., 2009; Sengoku et al., 2006; Singleton et al., 2007; Velankar et al., 1999).

The crystal structure of the *Drosophila melanogaster* (*D. melanogaster*) RNA helicase Vasa (belonging to the DEAD box subfamily) in complex with an ssRNA oligo and an ATP analog showed that bound RNA is sharply bent around a highly conserved alpha-helix (Sengoku et al., 2006). This bent conformation of the RNA is incompatible with a double-stranded structure, suggesting a mechanism where bending of the RNA molecule facilitates unwinding through a wedging mechanism different from translocating helicases that move along the RNA (Sengoku et al., 2006). Similarly to Vasa, the DEAD box RNA helicase eIF4A3 interacts with RNA in a kinked orientation (Andersen et al., 2006; Bono et al., 2006). However, the mechanism of RNA bending is most likely restricted to DEAD box RNA helicases since it involves interdomain interactions that are only found in RNA helicases belonging to this family (Linder and Jankowsky, 2011; Sengoku et al., 2006). In contrast to DEAD box helicases, the DExH box helicases such as the hepatitis C virus RNA helicase NS3 and NPH-II both facilitate directional processive RNA unwinding (Jankowsky et al., 2001; Kim et al., 1998; Tai et al., 1996). Crystal structures of NS3 in complex with ssDNA or ssRNA have provided insights into how NS3 facilitates 3’ to 5’ directional translocation (Appleby et al., 2011; Gu and Rice, 2010). In an ATP-bound state the cleft between helicase domain 1A and 2A of NS3 is closed and the interactions with the 3’ end of bound RNA is reduced (Appleby et al., 2011). However, in the ADP-bound state the affinity for ssRNA is increased and the conformation between the two helicase domains is relaxed, resulting in movement of domain 2A one nucleotide towards the 5’ end of the ssRNA (Appleby et al., 2011). This suggests that hydrolysis of ATP allows the helicase to pull one more nucleotide into the RNA-binding cleft providing the basis for the 3’ to 5’ directional translocation (Appleby et al., 2011). A similar mechanism was also reported for the SF1 DNA helicase PcrA from *Bacillus stearothermophilus*, indicating that the overall mechanism of directional unwinding is related between DExH and SF1 helicases (Velankar et al., 1999). Moreover, crystal structures of the 5’ to 3’ SF1 DNA helicase RecD2 from *Deinococcus radiodurans* in complex with ssDNA reveals that ssDNA is bound in a similar

orientation to NS3, but that the difference in directionality results from movement of domain 1A in the opposite direction upon ATP hydrolysis (Saikrishnan et al., 2009). However, details of the coupling between ATP hydrolysis and nucleic acid binding differ between PcrA and RecD2 and the process is carried out by different residues in PcrA and RecD2 (Saikrishnan et al., 2009). Similarly to the DExH helicase NS3, the SF1 RNA helicase UPF1 has been shown to transition between closed state (nucleotide bound) and open state (nucleotide free), suggesting that UPF1 uses a similar mechanism as NS3, PcrA and RecD2 for its translocation along bound RNA (Appleby et al., 2011; Cheng et al., 2007).

Regulation of RNA Helicase Activity

In addition to the helicase core, most RNA helicases contain additional domains which are thought to provide functional specificity, for instance by facilitating interactions with other protein factors or by influencing the catalytic activity of the RNA helicase (Silverman et al., 2003). As an example the N-terminal cysteine-histidine rich (CH) domain of UPF1 has an inhibitory effect on UPF1's ATPase activity (Figure 2) (Chakrabarti et al., 2011). However, when UPF2 binds the CH domain of UPF1 and distorts the interaction between the CH domain and the helicase core of UPF1, the inhibitory effect of the CH domain is relieved and UPF1's ATPase activity as well as unwinding activity is increased (Chakrabarti et al., 2011). As an additional level of regulation, UPF1 is also regulated by sequential SMG1-mediated phosphorylation and PPP2R4-mediated dephosphorylation, leading to remodeling of the surveillance complex (Ohnishi et al., 2003) In addition to its N-terminal CH domain, UPF1 also contains a C-terminal serine-glutamine rich (SQ) domain which has a inhibitory effect both on UPF1's ATPase and unwinding activity, independently of the N-terminal CH domain (Figure 2) (Fiorini et al., 2013). The helicase activity of the EJC RNA helicase eIF4A3 is also regulated through association with protein factors. Strong clamping of eIF4A3 to its bound RNA targets is partly facilitated through the inhibition of eIF4A3's ATPase activity by MAGOH and Y14 (Andersen et al., 2006; Ballut et al., 2005; Bono et al., 2006). In addition, the spliceosomal RNA helicase Brr2 is inhibited by the spliceosomal protein Prp8 by preventing the interaction of Brr2 with RNA (Mozaffari-Jovin et al., 2012; Mozaffari-Jovin et al., 2013). Thus associated protein factors can promote the formation of stable RNP complexes through the inhibition of RNA helicase's activity or serve to restrict the activity of RNA helicases by preventing their binding to RNA or by inhibiting their ATPase activity (Ballut et al., 2005; Chakrabarti et al., 2011; Fiorini et al., 2013; Mozaffari-Jovin et al., 2013).

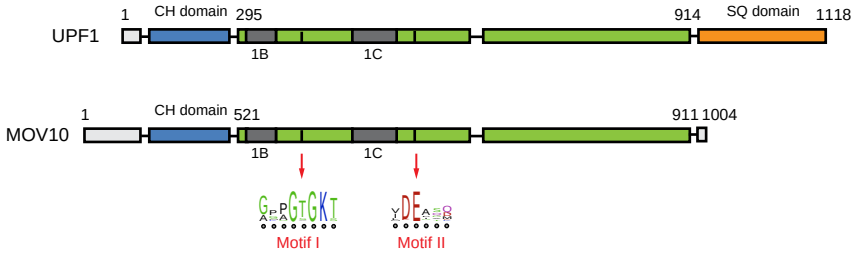

Figure 2. Domain structure of the RNA helicases UPF1 and MOV10.

Both UPF1 and MOV10 contain N-terminal CH domains typically involved in protein-protein interactions. Domain insertions 1B and 1C are specific to the UPF1-like helicase family. In addition UPF1 contain a C-terminal SQ domain. The conservation of helicase motif I and II among SF1 helicases from human *Saccharomyces cerevisiae* and *Escherichia coli* are shown below as LOGO sequences. Based on Fairman-Williams et al., 2010.

RNA Helicases Involved in mRNP Remodeling During Translational Regulation and mRNA Turnover

The assembly of an actively translating mRNP requires the assembly of the translation initiation complex eIF4F (comprised of cap-binding protein eIF4E, the DEAD box RNA helicase eIF4A (also known as DDX2) and eIF4G forming a scaffold for eIF4E and eIF4A) at the 5'cap structure of the mRNA followed. The assembly of the translation initiation complex is then followed by 5' to 3' directional scanning of the 5'UTR by the ribosome until the initiation codon is encountered (Parsyan et al., 2011).

RNA Helicases Involved in mRNA Translational Initiation

eIF4A is a canonical DEAD box helicase with bidirectional ATP-dependent RNA unwinding activity (Cox and Mann, 2008). It removes secondary structures in 5'UTRs prior to assembly of the 43S pre-initiation complex onto the mRNA (Aitken and Lorsch, 2012; Parsyan et al., 2011). In addition to eIF4A, several other RNA helicases have been implicated in translational initiation (Parsyan et al., 2011). One of these helicases is DDX3, which resolves structures immediately in the vicinity of the 5'cap structure prior to 43S ribosomal scanning of selected viral and host transcripts (Soto-Rifo et al., 2012). Another RNA helicase also implicated in translation initiation is the SF2 DEAH box RNA helicase DHX29. DHX29 remodels the 40S subunit and promotes 48S complex formation on 5'UTRs containing stable secondary structures (Pisareva et al., 2008). DHX29 does not display any target specificity but most likely works as a

general translational factor (Pisareva et al., 2008). However, unlike eIF4A, DHX29 is unable to unwind short duplex structures containing either 3' or 5' overhangs *in vitro*, and is therefore unlikely to function as a processive RNA helicase, but may simply work to induce conformational changes of the 40S/mRNA/eIFs complex on 5'UTRs (Pisareva et al., 2008). It remains unknown what determines the specific need for different RNA helicases during translation initiation, but it may depend on the 5'UTR length and the degree of secondary structure within the 5'UTR.

RNA Helicases Involved in Translational Repression and mRNA Turnover

Translationally repressed mRNAs or mRNAs targeted for degradation are highly concentrated in cytoplasmic P-bodies together with numerous proteins involved in translational repression and/or mRNA degradation (Eulalio et al., 2007; Garneau et al., 2007). These proteins include AGO2, involved in miRNA-mediated regulation, the decapping enzyme DCP1, activators of decapping such as the DEAD box RNA helicase DDX6 (also known as RCK/p54) and the 5' to 3' exonuclease XRN1. Strikingly, all proteins involved in 5' to 3' RNA degradation are found in P-bodies, underlining the role of P-bodies as sites for mRNA decapping and subsequent degradation (Eulalio et al., 2007). The yeast homolog of DDX6, Dhh1 interacts with both the decapping and deadenylase complexes, and promotes mRNA decapping as well as subsequent mRNA degradation (Coller et al., 2001). In *Xenopus laevis* (*X. laevis*), the DDX6 homolog, Xp54 represses translation of maternal mRNA (Minshall et al., 2001). In both organisms the phenotypes associated with DDX6 have been suggested to be a manifestation of deadenylation, leading to mRNA decapping in yeast and mRNA storage/translational repression in *X. laevis* until the mRNAs are re-activated by cytoplasmic polyadenylases (Coller et al., 2001). Depletion of DDX6 in human cells leads to a reduction in the number of P-bodies, suggesting that DDX6 might also be involved in mRNA degradation and/or translational repression in human cells (Minshall et al., 2009; Serman et al., 2007). It has been postulated that the decision regarding whether an mRNA is translated or being targeted for translational repression and/or mRNA degradation depends on competition between the assembly of the translation initiation complex and the assembly of a 'P-body mRNP' (Parker and Sheth 2007). In line with this, a recent study found DDX6 to stably bind translationally repressed mRNAs and to induce structural relaxation of mRNAs in an ATP-dependent manner promoting recruitment of mRNAs to P-bodies (Ernoult-Lange et al., 2012). Thus, DDX6 could represent a RNA helicase promoting the formation of P-body mRNPs.

mRNAs can also be targeted to P-bodies based on sequence-specific elements in their 3'UTRs, such as AU-rich elements (AREs) or miRNA-binding sites (Bhattacharyya et al., 2006). AREs are recognized by the tristetraprolin protein (TTP) or Roquin (also known as RC3H1) (Fenger-Gron et al., 2005; Leppek et al., 2013). TTP interacts directly with subunits of the decapping complex DCP1 and DCP2 to promote decapping of its mRNA targets (Fenger-Gron et al., 2005). Roquin on the other hand interacts with the deadenylase complex CCR4-CAF1-NOT to promote deadenylation followed by rapid degradation of its mRNA targets (Leppek et al., 2013). miRNAs loaded onto AGO2 regulate their targets by base-pairing with complementary regions in 3'UTRs and promote both mRNA degradation as well as translational repression (Bartel, 2009).

mRNA surveillance mechanisms such as NMD can also target mRNAs for rapid mRNA degradation in P-bodies (Lykke-Andersen et al., 2000; Sheth and Parker, 2006). The RNA helicase UPF1 is a key component of the NMD pathway and is responsible for targeting PTC-containing mRNA transcripts and mRNAs with long 3'UTRs for rapid decay (Amrani et al., 2004; Behm-Ansmant et al., 2007; Eberle et al., 2008; Hogg and Goff, 2010; Ivanov et al., 2008; Longman et al., 2007; Lykke-Andersen et al., 2000; Mitrovich and Anderson, 2005; Silva et al., 2008; Singh et al., 2008). NMD-mediated decay is enhanced by the presence of an EJC downstream of the PTC (Maquat, 2004), but a downstream EJC is not an absolute requirement for NMD to take place (Buhler et al., 2006; Eberle et al., 2008; LeBlanc and Beemon, 2004; Metze et al., 2013; Singh et al., 2008). In addition, evidence indicates that both translation termination events and mRNP composition of the 3'UTR influences whether an mRNA transcript is targeted for NMD (Amrani et al., 2004; Hogg and Goff, 2010; Kervestin and Jacobson, 2012; Le Hir et al., 2001; Rebbapragada and Lykke-Andersen, 2009). The helicase activity of UPF1 is required for NMD-mediated degradation (Franks et al., 2010). Expression of UPF1 helicase mutants in cells depleted of endogenous UPF1 and XRN1 results in accumulation of a 3' mRNP decay intermediate resulting from SMG6-mediated endonucleotlyic cleavage of NMD targeted transcripts (Franks et al., 2010). Further experiments showed that the lack of UPF1's helicase activity prevented the disassembly of the UPF1 containing surveillance complex on the 3' mRNP decay intermediate resulting in decreased mRNP clearance and mRNA degradation, clearly proving that the helicase activity of UPF1 is required for mRNP remodeling of NMD targeted mRNPs (Franks et al., 2010).

Not all mRNAs targeted to P-bodies are necessarily degraded. Experiments in both human and yeast cells indicate that mRNA targeted to P-bodies can undergo either one of two fates. Either the mRNPs undergo remodeling followed by mRNA degradation or they are released and re-

enter the translational pool of mRNAs (Bhattacharyya et al., 2006; Brengues et al., 2005; Sheth and Parker, 2006). CAT-1 mRNA for example can be relieved of its miR-122 mediated repression in an ELAVL1-dependent (ELAVL1 is also known as HuR) manner and released from P-bodies upon amino acid starvation (Bhattacharyya et al., 2006). Moreover ELAVL1 binding to 3'UTR sites have also been shown to interfere with miRNA-mediated regulation, resulting in stabilization of the mRNA (Kundu et al., 2012). Thus, P-bodies can be viewed as a buffering system for the cells' translating capacity and as mRNP chaperones to resolve stalled defective translation complexes and potential allow them re-enter into a translation state through mRNP remodeling (Parker and Sheth 2007). The studies mentioned above indicate that UPF1 and ELAVL1 can dictate the fate of mRNAs targeted to P-bodies through association with their target mRNAs, with UPF1 promoting rapid mRNA degradation and ELAVL1 promoting release of certain mRNAs from P-bodies.

Methods to Study mRNP Structures

A crucial aspect of studying mRNP structures and transitions is to identify and map the interactions between proteins and mRNAs. A widely used method to identify the RNA targets of RNA-binding proteins is RNA immunoprecipitation (RIP) used in combination with qRT-PCR, microarrays or high-throughput sequencing (Keene et al., 2006). However, one major disadvantage of RIP is that it does not allow the identification of the actual binding sites of the protein within its targets, but only provides the identity of the RNA targets. In addition, high background due to the low stringency washes used to maintain protein-RNA interactions during the RIP procedure often lead to the identification of a large number of false positive RNA targets. A way to overcome this issue is to introduce covalent bonds between proteins and RNA, which can be achieved by irradiation with UV light (Greenberg, 1979; Wagenmakers et al., 1980). Recently, several methods allowing the mapping of protein-RNA interactions *in vivo* based on UV-crosslinking and immunoprecipitation (CLIP) have been published (Chi et al., 2009; Hafner et al., 2010; Konig et al., 2010; Ule et al., 2003).

Identification of Protein-RNA Interactions Using CLIP

CLIP is based on formation of a covalent bound between proteins and their bound RNA targets followed by a stringent purification scheme to isolate RNA co-immunoprecipitated with a specific protein. If used in combination with high-throughput sequencing it allows a genome-

wide identification of RNAs bound by a given RNA-binding protein. Different variations of CLIP methods exist (Chi et al., 2009; Hafner et al., 2010; Konig et al., 2010). They distinguish themselves from each other based on the use of modified ribonucleosides, the method for trimming of RNA fragments and the cloning strategy used for the sequencing library preparation. Photoactivatable-ribonucleoside-enhanced CLIP (PAR-CLIP) is the only method that relies on the incorporation of photoactivatable nucleoside analogs 4-thiouridine (4SU) or 6-thioguanosine (6SG) into nascent RNAs (Hafner et al., 2010). The incorporation of either 4SU or 6SG strongly enhances protein-RNA crosslinking and furthermore results in diagnostics transitions in sequencing reads at the crosslinking sites, thus allowing the identification of protein-RNA-binding sites at nucleotide resolution (Hafner et al., 2010). In contrast individual-nucleotide-resolution CLIP (iCLIP) relies on abrogation of reverse transcription at the crosslinking site to provide nucleotide resolution of the RNA-binding sites (Konig et al., 2010). High-throughput sequencing together with UV-crosslinking and immunoprecipitation (HITS-CLIP) has also been reported to provide nucleotide resolution of binding sites through nucleotide deletions introduced at the crosslinking site during reverse transcription (Zhang and Darnell, 2011). However, the frequency of deletions at the site of crosslinking observed with HITS-CLIP is significantly lower than the frequency of nucleotide transitions or abrogation of reverse transcription observed using PAR-CLIP or iCLIP (Chi et al., 2009; Hafner et al., 2010; Konig et al., 2010). Since iCLIP and HITS-CLIP do not rely on the incorporation of modified ribonucleosides they are suitable for CLIP preformed on animal tissue and biological samples where labeling is not feasible. However, PAR-CLIP was recently applied *in vivo* in *Caenorhabditis elegans* (*C. elegans*) to identify the binding sites of the RNA-binding protein GLD-1 (Jungkamp et al., 2011).

The first comprehensive identification of the targets of an RNA helicase was performed for the yeast RNA helicase Prp43 involved in ribosome biogenesis using a modified CLIP protocol adapted for yeast termed CRAC (cross-linking and analysis of cDNAs) (Bohnsack et al., 2009). More recently CLIP studies of the human RNA helicases UPF1 and Moloney leukemia virus 10 (MOV10) have been published (Hurt et al., 2013; Sievers et al., 2012; Zund et al., 2013). In addition, CLIP studies of eIF4A3 have been used to map EJC binding sites in human cells (Sauliere et al., 2012; Singh et al., 2012). Lastly, the binding sites have been identified for the *D. melanogaster* RNA/DNA helicase MLE, part of the Male-Specific Lethal complex, which mainly binds the two long non-coding RNAs roX1 and roX2 involved in X chromosome activation in male flies (Ilik et al., 2013).

The RNA Helicase MOV10

MOV10 belongs to the UPF1-like subfamily of SF1 helicases (Figure 1B) (Fairman-Williams et al., 2010). In addition to UPF1, this family of helicases also includes SETX, which is involved in resolving RNA-DNA hybrids during transcription (Skourti-Stathaki et al., 2011). The *Mov10* gene was initially discovered as the integration site of the Moloney leukemia virus (M-MuLV) in a mice strain derived from M-MuLV exposed embryos (Jaenisch et al., 1981). The mice stain did not produce infectious virus particles, however further studies concluded that this was not due to *cis*-acting elements, but instead caused by mutations within the M-MuLV locus (Harbers et al., 1982; Schnieke et al., 1983).

MOV10 shares homology with *D. melanogaster* Armitage and *Arabidopsis thaliana* (*A. thaliana*) SDE3 RNA helicases, both of which function in RNAi pathways (Cook et al., 2004; Dalmay et al., 2001). Armitage is essential for primary piRNA (PIWI-interacting RNAs) biogenesis in *D. melanogaster* and SDE3 is required for viral RNAi defense in *A. thaliana* (Cook et al., 2004; Dalmay et al., 2001; Haase et al., 2010; Olivieri et al., 2010; Tomari et al., 2004). In addition MOV10 has a mammalian paralog MOV10L1. While MOV10 is ubiquitously expressed, MOV10L1 is primarily expressed in testis and knockout *Mov10l1* male mice display defects in spermatogenesis due to defects in piRNA-directed retrotransposon silencing (Frost et al., 2010; Zheng et al., 2010). MOV10L1 interacts with both MILI and MIWI proteins, which are involved in piRNA biogenesis (Frost et al., 2010; Zheng et al., 2010). MOV10L1 works either in primary piRNA biogenesis or is required for loading of piRNA into the MILI complex, since piRNAs are absent from the MILI complex in *Mov10l1* knockouts (Zheng et al., 2010). In accordance with MOV10L1's role in piRNA-mediated silencing, endogenous retroviral elements such as long interspersed element 1 (LINE-1) and intracisternal A particles (IAP) were de-repressed in testis from *Mov10l1* knockout mice (Frost et al., 2010; Zheng et al., 2010).

MOV10 has been Implicated in miRNA-mediated Regulation

Human MOV10 has been reported to co-immunoprecipitate (co-IP) and co-localize with AGO2 to P-bodies, suggesting a role for MOV10 in miRNA-mediated regulation (Chendrimada et al., 2007; Landthaler et al., 2008; Meister et al., 2005). However, a later study reported the interaction between AGO2 and MOV10 to be highly dependent on the presence of RNA (Frohn et al., 2012). Moreover, conflicting reports, regarding the effect of MOV10 knockdown on reporters designed to measure the miRNA-mediated repression, indicate that the role of MOV10

in miRNA-mediated regulation still remains to be fully resolved (Arjan-Odedra et al., 2012; Banerjee et al., 2009; Chendrimada et al., 2007; Liu et al., 2012; Meister et al., 2005).

MOV10 Inhibits Infectivity of Retroviral Viruses

MOV10 inhibits the infectivity of human immunodeficiency virus type 1 (HIV-1), simian immunodeficiency virus, Moloney murine leukemia virus, feline immunodeficiency virus and equine infectious anemia virus (Arjan-Odedra et al., 2012; Burdick et al., 2010; Furtak et al., 2010; Izumi et al., 2013; Wang et al., 2010) as well as hepatitis C virus (Schoggins et al., 2011). Retroviruses replicate in host cells by reverse transcription of their RNA genome followed by integration of a cDNA copy into the genome of their host. Retroviruses are partly dependent on host cell proteins for processing of viral RNA products and host cells have developed multiple mechanisms to restrict the replication of retrovirus both post-transcriptionally and post-translationally (Lorgeoux et al., 2012). Members of the protein family APOBEC (apolipoprotein B mRNA-editing enzyme catalytic polypeptide 1-like 3) are cytidine deaminases with potent antiviral activity towards retroviruses, but also restrict the propagation of endogenous retroelements (Koito and Ikeda, 2012). MOV10 has been shown to interact with APOBEC3G and APOBEC3F in an RNA-dependent manner and to co-localize with APOBEC3G to P-bodies, (Gallois-Montbrun et al., 2008; Izumi et al., 2013; Liu et al., 2012).

The mechanism behind MOV10's anti-viral activity remains controversial, but evidence suggests that the reverse transcription step is inhibited by MOV10 over-expression (Arjan-Odedra et al., 2012; Burdick et al., 2010; Furtak et al., 2010; Wang et al., 2010). Some studies have indicated that the presence of all helicase motifs except motif V is required for its anti-viral activity (Abudu et al., 2012; Wang et al., 2010). However, another study reported that only the N-terminal domain of MOV10 is required for MOV10's anti-viral activity (Furtak et al., 2010). Finally, yet another study reported helicase motifs III, IV and VI to be required for MOV10-mediated inhibition of HIV-1 infectivity (Izumi et al., 2013).

Similarly to MOV10, the *A. thaliana* helicase SDE3 also restricts viral activity (Dalmay et al., 2001). SDE3 has been suggested to work together with the RNA polymerase RDR6 to produce double-stranded RNA (dsRNA) from transgenic or viral genomic RNA templates to enhance siRNA-mediated silencing in plants (Garcia et al., 2012). It has been proposed that SDE3 unwinds dsRNA products to create additional single stranded RNA templates for RDR6 (Garcia et al., 2012). In addition, mutations of SDE3 were found to increase levels of endogenous transposable elements (Garcia et al., 2012). The later function is similar to the function of

Armitage in *D. melanogaster* and the MOV10 paralog MOV10L1 required for piRNA-mediated repression of endogenous retroelements in the germline.

MOV10 Inhibits Endogenous Retrotransposable Elements in Somatic Cells

Recently, MOV10 was found to inhibit retrotransposition of LINE-1, short interspersed elements, IAP and long-terminal repeats (Arjan-Odedra et al., 2012; Goodier et al., 2012; Li et al., 2013; Lu et al., 2012). Almost all interspersed repeats in the human genome are derived for transposable elements and make up close to 45% of the human genome (Lander et al., 2001). Retrotransposons are mobile elements that can move around in the genome through a RNA intermediate by using reverse transcription to generate cDNA copies of their RNA transcripts. The largest group of retrotransposons is LINE-1 elements comprises 17% percent of the human genome (Lander et al., 2001). However, most LINE-1 elements are inactive and it is estimated that only 80-100 are active on average (Brouha et al., 2003). LINE-1 elements are around 6 kb long and contain two open reading frames encoding an RNA-binding protein and a protein with both endonuclease and reverse transcriptase activity. Both proteins interact with LINE-1 RNA to promote its processing (Doucet et al., 2010). MOV10 as well as the RNA helicases DDX5, DHX9, DDX17, DDX21, and DDX39A have been found to associate with LINE-1 mRNPs (Goodier et al., 2012; Li et al., 2013). Of those helicases both DDX39A and MOV10 were able to inhibits LINE-1 retrotransposition in HEK293 cells, but only MOV10 was able to inhibit LINE-1 retrotransposition in multiple cell lines (Goodier et al., 2012). Over-expression of MOV10 inhibits LINE-1 retrotransposition in a dose-dependent manner, whereas MOV10 knockdown results in higher levels of LINE-1 RNA and an increased in the number retrotransposition events (Goodier et al., 2012; Li et al., 2013). Mutations of helicase motifs I, II, III, IV, and VI suppressed MOV10's ability to inhibit LINE-1 retrotransposition (Goodier et al., 2012), indicating that MOV10's potential helicase activity is required for its inhibition of retrotransposition. Although the precise mechanism behind MOV10's inhibition of retrotransposition remains undetermined, it has been speculated that MOV10 disrupts the organization of LINE-1 mRNPs localized in P-bodies thereby making the RNA susceptible for degradation (Li et al., 2013). Knockdown of AGO2 did not have any effect on MOV10's ability to inhibit LINE-1 activity, indicating that MOV10's potential role in mRNA degradation of LINE-1 RNA works independently of the miRNA-mediated pathway (Li et al., 2013). Previously LINE-1 elements were considered to be expressed primarily in the germ line, however a recent report showed that LINE-1 elements are also expressed in somatic and

transformed cells (Belancio et al., 2010). Taken together, this indicates that MOV10 functions in a similar manner as MOV10L1 to restrict transposable elements, but whereas MOV10L1 works in the germline to silence transposons through the piRNA pathway, MOV10 works in somatic cells to restrict a diverse range of transposable elements using a yet to be defined mechanism.

MOV10 and its Implication in Chromatin Remodeling

MOV10 has also been reported to associate with the polycomb repressive complex (PRC) 1 component CBX7 (El Messaoudi-Aubert et al., 2010). The PRC1 complex recognizes the PRC2 trimethylation on histione 3 Lys27 (H3K27me3), and catalyzes a monoubiquitination of histone H2A on Lys119 (H2AK119ub) resulting in gene silencing (Schwartz and Pirrotta, 2007). A major question regarding polycomb-mediated gene silencing is how PRC1 and PRC2 complexes are recruited to their targets genes. Recently, long non-coding RNAs such as HOTAIR have been shown to mediate the recruitment of PRC2 to its targets genes (Gupta et al., 2010; Rinn et al., 2007; Tsai et al., 2010). Since none of the protein components of the PRC1 or PRC2 complexes contain canonical RNA-binding domains, MOV10 may represent the RNA-binding component of the PRC1 complex. In line with this, knockdown of MOV10 was found to decrease binding of CBX7 to the *INK4A* locus, a locus known to be repressed by PRC1 (El Messaoudi-Aubert et al., 2010). Almost at the same time the long non-coding RNA *ANRIL*, which is encoded antisense to the *INK4b/ARF/INK4a* locus, was reported to associate directly with CBX7 to promote silencing of the *INK4A* locus (Yap et al., 2010). By mutations of amino acid residues in a CBX7 binding pocket that showed changes in NMR resonance upon RNA binding, Yap and colleagues were able to generate a CBX7 mutant unable to interact with RNA (Yap et al., 2010). In addition to CBX7, ANRIL also interacts with the PRC2 component SUZ12 to direct silencing of the *INK4B* locus (Kotake et al., 2011). Identification of nuclear MOV10 targets failed to identify ANRIL or other long ncRNAs as a MOV10 target (Sievers et al., 2012). Thus, direct evidence that MOV10 can interact with long non-coding RNAs is still missing.

AIMS OF THESIS

Despite evidence that MOV10 plays a role in miRNA-mediated regulation, retroviral defense, retrotransposition as well as chromatin remodeling, its molecular function remains unknown. In particular, the function of MOV10's putative helicase domain remains unexplored.

The aims of my PhD project were to address the molecular function of MOV10 and investigate the importance of its putative helicase activity. To achieve this, I have experimentally addressed the questions below.

- **Does MOV10 have *in vitro* helicase activity?**
- **How does the transcriptome-wide binding pattern of wild-type MOV10 compare to the binding pattern of its helicase mutants?**
- **Which proteins do MOV10 interact with? And which proteins are bound to RNA in the proximity of MOV10?**
- **What is the molecular function of MOV10 on its RNA targets?**

An overview of the experimental setup used in this study is outlined in Figure 3.

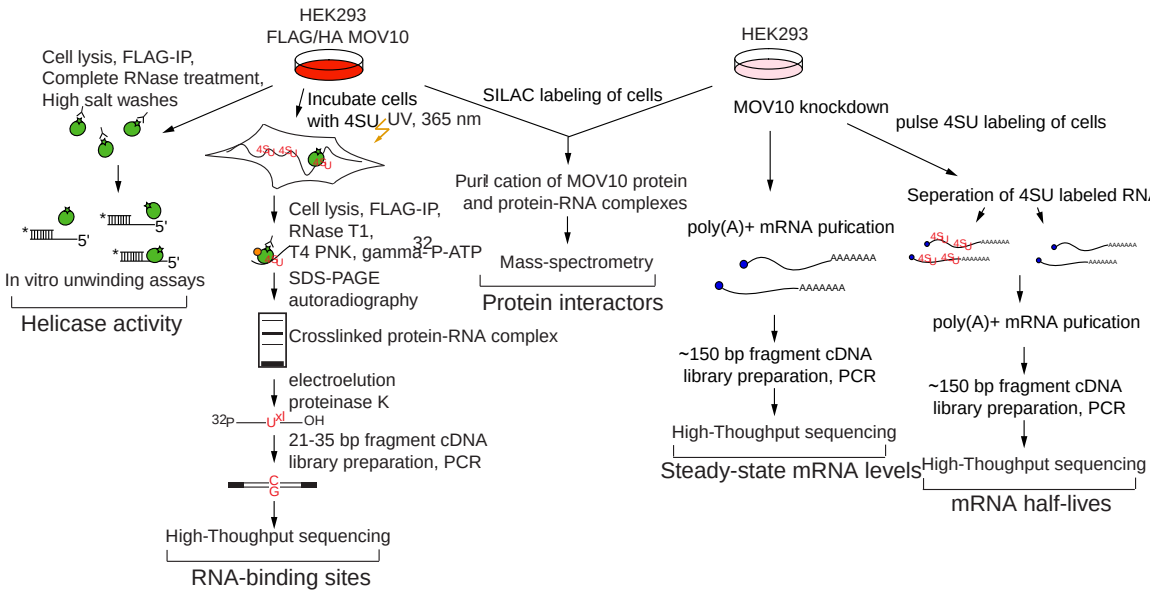

Figure 3. Overview of experiments used to study the functional role of MOV10.

HEK293 cells stably expressing FLAG/HA-tagged MOV10 WT or MOV10 helicase mutants was used to purify MOV10 proteins for in vitro unwinding assay and for purification of protein-RNA complexes followed by cloning of 25-30 nt RNA fragments crosslinked to MOV10 using the PAR-CLIP method (Hafner et al., 2010). For the identification of protein complexes or protein-RNA complexes associated with MOV10 WT, HEK293 cells stably expressing FLAG/HA-tagged MOV10 WT and parental HEK293 cells were

grown in SILAC (stable isotope labeling by amino acid in cell culture) media, used for MOV10 immunoprecipitation (IP) and analyzed by mass-spectrometry (for details see Figure 11). Parental HEK293 were used for siRNA-mediated MOV10 knockdown, followed by poly(A)+ mRNA purification and RNA-Seq used for calculation of mRNA steady state expression levels or pulse 4SU labeling, followed by poly(A)+ mRNA purification and RNA-Seq and calculation of mRNA half-lives.

MATERIAL AND METHODS

Cell Lines and Plasmids

Unless otherwise stated, Flp-In T-REx HEK293 cells (Invitrogen) and stable cell lines derived from these cells were grown in high glucose DMEM media (Invitrogen) supplemented with 10 % (v/v) fetal bovine serum (Sigma-Aldrich), 1 % (v/v) 2 mM L-glutamine (Invitrogen), 1 % (v/v) 10,000 U/mL penicillin and 10,000 µg/mL streptomycin (Invitrogen).

pENTR4 carrying the coding sequence of MOV10 (hereafter termed pENTR4 MOV10) has been previously described (Meister et al., 2005). The helicase motifs, motif I and II, in pENTR4 MOV10 were mutated using the QuikChange site-directed mutagenesis kit (Agilent Technologies, Stratagene) according to the manufacturer's protocol, resulting in single amino acid changes K530A (motif I) and D645N (motif II). Mutagenesis primers used are listed in Table S1. Mutations were confirmed by sequencing.

The coding sequences of UPF1 and XPO5 were amplified from HEK293 cDNA generated using the SMARTer PCR cDNA synthesis kit (Clontech) according to the manufacturer's protocol and inserted into the XmnI/NotI or SalI/NotI sites of pENTR4, respectively. Primers used for the amplification of the coding regions are listed in Table S1. To generate stable cell lines expressing FLAG/HA-tagged proteins, the pENTR4 vectors containing either the WT or mutated versions (K520A and D645N) of the MOV10 coding sequence were recombined into the pFRT/FLAG/HA-DEST (Addgene ID: 26360) destination vector using Gateway LR recombinase according to the manufacturer's protocol (Invitrogen) and co-transfected with the pOG44 vector (Invitrogen) into Flp-In T-REx HEK293 cells (Invitrogen). Cells were selected with 100 µg/mL hygromycin (InvivoGen) and 15 µg/mL blasticidin (InvivoGen) for two weeks where after single colonies were expanded to generate monoclonal cell lines. Plasmids pENTR4 AGO2, pENTR4 TNRC6B and pENTR4 DICER1 have been previously described (Landthaler et al., 2008; Meister et al., 2005). Cell lines expressing GFP-tagged AGO2 and GFP-tagged TNRC6B were generated by recombination of pENTR4 AGO2 and pENTR4 TNRC6B into pFRT/TO/GFP-DEST (Addgene ID: 26362) followed by transfection into Flp-In T-REx HEK293 cells (Invitrogen) as described above. To generate constructs expressing RFP- and MYC-tagged MOV10, pENTR4 MOV10 was recombined into pFRT/TO/RFP-DEST or pDEST26-MYC vectors as described above (Landthaler et al., 2008). To generate constructs expressing MYC-tagged AGO2, MYC-tagged TNRC6B and MYC-tagged DICER1, the

appropriate pENTR4 vectors were recombined into pDEST26-MYC vectors also as described above.

PAR-CLIP Experiments

Flp-In T-REx HEK293 cells expressing FLAG/HA-tagged MOV10 WT, K530A and D645N were grown in high glucose SILAC (stable isotope labeling by amino acid in cell culture) DMEM (PAA) supplemented with 10 % (v/v) dialyzed fetal bovine serum (Sigma-Aldrich), 4 mM Glutamine (PAA), 0.05 mg/mL Lysine (Sigma-Aldrich) and 0.03 mg/mL Arginine (Sigma-Aldrich). Cells were incubated with 100 µM 4SU (ChemGenes) or 100 µM 6SG (Sigma-Aldrich) nucleoside analogs for 16 hours (hrs), UV-crosslinked as previously described (Hafner et al., 2010), frozen in liquid nitrogen and stored at -80 ^{o}C. Cell pellets were lysed in 3 times the cell pellet volume of high salt NP-40 lysis buffer (50 mM Tris [pH 7.2], 500 mM NaCl, 1 % (v/v) NP-40, 1 mM DTT, complete EDTA-free protease inhibitor cocktail (Roche)), incubated 30 min on ice followed by 45 sec sonication (80 % amplitude). IP and RNA library generation was performed as previously described (Hafner et al., 2010) with the following modifications. The second ribonuclease digestion was performed with a final concentration of 20 U/µL RNaseT1 (Fermentas) for MOV10 WT and K530A IPs, for MOV10 D645N the second ribonuclease digestion was performed with a final concentration of 10 U/µL RNaseT1 (Fermentas). Proteinase K (Roche) digestion was performed with a final concentration of 2 mg/mL for 1 hr at 55 ^{o}C. cDNA libraries were amplified using the Phusion High-Fidelity DNA polymerase (Finnzymes) and gel purified using the QIAquick gel extraction kit (Qiagen).

RNA Unwinding Assays

MOV10 proteins were purified from Flp-In T-REx HEK293 cells expressing FLAG/HA-tagged MOV10 WT, K530A or D645N. Cells were lysed in high salt NP-40 lysis buffer (50 mM Tris [pH 7.2], 500 mM NaCl, 1 % (v/v) NP-40, 1 mM DTT, complete EDTA-free protease inhibitor cocktail (Roche)), incubated 30 min on ice followed by 45 sec sonication (80 % amplitude). Lysates were cleared by centrifugation at 20,000 g for 20 min and treated with 20 U/µL of RNaseT1 (Fermentas) for 5 min at 37 ^{o}C. 50 µL of Dynabeads ProteinG magnetic beads (Invitrogen) per sample were washed twice in PBS-T buffer (PBS (Phosphate buffered saline), 0.1 % Tween20) and resuspended in twice the volume of PBS-T relative to the original volume of bead suspension. Anti-FLAG M2 monoclonal antibody (F3165, Sigma-Aldrich) was added to

a final concentration of 0.25 µg/µL and the beads were incubated at room temperature for 40 min. Following conjugation of anti-FLAG, the beads were washed twice in PBS-T, resuspended in the original volume of the bead suspension, added to RNaseT1 treated lysates and incubated for 1 hr at 4 ^{o}C. Beads were washed 5 times in high salt NP-40 lysis buffer followed by one wash in FLAG elution buffer (100 mM NaCl, 20 mM TRIS-HCl [pH 7.5], 5 mM $MgCl_2$ and 10 % glycerol) and resuspended in 60 µL FLAG elution buffer. FLAG peptide was added to a final concentration of 0.5 µg/µL and incubated 1 hr at 4 ^{o}C on rotation. Supernatant containing FLAG eluted MOV10 proteins were collected and the concentration of the FLAG eluted proteins was estimated by coomassie staining using SimplyBlue SafeStain (Invitrogen) with known concentrations of BSA as a standard (Fermentas).

RNA oligonucleotides as indicated below were purchased from Eurofins MWG Operon, and duplex substrates were prepared as previously described (Yang and Jankowsky, 2006). Duplex regions are underlined.

3T1 5‘-AGCACCGUAAAGACGC-3‘,

3B1 5‘-GCGUCUUUACGGUGCUUAAAACAAAACAAAACAAAACAAA-3‘

5B1 5‘-AAACAAAACAAAACAAAACAAAAUAGCACCGUAAAGACGC-3‘

5T1 5‘-GCGUCUUUACGGUGCU-3‘

Briefly, top strand oligonucleotides 3T1 and 5T1 were radioactively end-labeled with (γ-^{32}P)-ATP (Perkin Elmer). 10 µM of each strand was incubated with 15 µCi ATP in T4 PNK buffer (NEB) and 15 U of T4 PNK (NEB) for 1 hr at 37 ^{o}C, 800 rpm in a final volume of 10 µL and purified by denaturing gel electrophoresis.

RNA duplexes were annealed by combining the bottom strand (3B1 or 5B1) with a five-fold molar excess of radiolabled top strand (3T1 or 5T1) in 10 mM MOPS [pH 6.5], 1 mM EDTA and 50 mM KCl. The solution was heated to 95 °C for 5 min followed by 1 hr incubation at 37 ^{o}C. Duplexes were separated from single-strand oligonucleotides on non-denaturing 15 % TBE polyacrylamide (acrylamide: bis 19:1) gels, excised from the gels, eluted by overnight incubation in 0.3 M NaCl at 4 ^{o}C, 800 rpm, ethanol precipitated and dissolved in 50 mM MOPS [pH 6.0], 50 mM KCl.

In vitro unwinding assays were performed in 30 µL reaction mixtures containing 40 mM Tris-HCl [pH 7.5], 50 mM NaCl, 0.5 mM $MgCl_2$, 1.5 mM DTT, 8 % glycerol and 200 ng BSA, annealed RNA duplexes and approximately 250 ng FLAG purified MOV10 proteins. Unwinding reactions were initiated by adding ATP (NEB) to a final concentration of 1 mM. All reactions were incubated at 37 °C for 10 min prior to addition of ATP. Reactions containing 450 ng BSA (Fermentas) instead of MOV10 proteins served as a negative control. Unless otherwise stated,

reactions were incubated for 1 hr. Reactions were stopped by the addition of loading buffer containing 1 % SDS, 50 mM EDTA, 0.1 % xylene cyanol, 0.1 % bromophenol blue, and 20 % glycerol and placed on ice. RNA was separated on non-denaturing 15 % TBE polyacrylamide (acrylamide: bis 19:1) gels in 4 °C 0.5x TBE running buffer (44.5 mM Tris-borate, 44.5 mM boric acid, 1 mM EDTA) and exposed to phosphoimager screens for visualization.

siRNA-mediated Knockdown

siRNAs with oligo dT overhangs were purchased from Sigma-Aldrich. The sense strands of the siRNAs are as follows:
MOV10 siRNA #1: 5'- GUUUGGUGAUGCAGUAACG[dT][dT]-3',
MOV10 siRNA #2: 5'- UUGCAGUAAAUUCUGUCCC[dT][dT]-3',
UPF1 siRNA: 5'- AAGAUGCAGUUCCGCUCCA[dT][dT]-3'.
$2.5 \cdot 10^5$ Flp-In T-REx HEK293 cells/well were seeded in 6-well plates and transfected with siRNA duplexes to a final concentration of 50 nM the following two days using 5 µl/well Lipofectamine RNAiMAX (Invitrogen). Cells were harvested 48 hrs post-transfection and the knockdown efficiency was evaluated on protein level by Western blotting and on RNA level by quantitative real-time PCR (qRT-PCR). For mRNA half-life determination, cells were treated with 5 µg/mL Actinomycin D (Sigma-Aldrich) and harvested at the indicated time points by addition of 1 mL TRIZOL (Invitrogen) directly to the cells.

RNA Isolation and Quantitative Real-Time-PCR

Total RNA was isolated with TRIZOL (Invitrogen) following the instructions of the manufacturer and treated with DNaseI (Ambion). Reverse transcription was performed using oligo dT_{18-20} primers and SuperScriptIII reverse transcriptase (Invitrogen). cDNA was amplified using SYBR Green 2x PCR Master Mix (Applied Biosystems) with 30 cycles of 15 sec denaturation at 94 ^{o}C, 15 sec annealing at 60 ^{o}C, and 20 sec extension at 72 ^{o}C. RPL18A was used as normalization control. Primer sequences are listed in Table S1. The PANK2 primer set is previously described (Tarpey et al., 2007).

Quantitative Mass Spectrometry of MOV10 and UPF1 IPs

For the MOV10 experiments Flp-In T-REx HEK293 cells or Flp-In T-REx HEK293 cells expressing FLAG/HA-tagged MOV10 were grown in light SILAC media containing non-labeled

amino acids ($^{12}C_6{}^{14}N_4$ L- arginine and $^{12}C_6{}^{14}N_2$ L-lysine (Sigma-Aldrich)) and heavy-heavy SILAC media containing ($^{13}C_6{}^{15}N_4$ L- arginine and $^{13}C_6{}^{15}N_2$ L-lysine (Cambridge Isotope Laboratories)). For the UPF1 experiments, either non-induced or doxycycline (Sigma-Aldrich) induced Flp-In T-REx HEK293 cells expressing FLAG/HA-tagged UPF1 were grown in light SILAC media containing non-labeled amino acids ($^{12}C_6{}^{14}N_4$ L- arginine and $^{12}C_6{}^{14}N_2$ L-lysine (Sigma-Aldrich)) and heavy-heavy SILAC media containing ($^{13}C_6{}^{15}N_4$ L- arginine and $^{13}C_6{}^{15}N_2$ L-lysine (Cambridge Isotope Laboratories)). For the identification of proteins bound in the proximity of MOV10 or UPF1, cells were incubated overnight with a final concentration of 200 µM 4SU (ChemGenes) and UV-crosslinked as previously described (Hafner et al., 2010). Control cells not expressing any FLAG/HA-tagged bait protein were mixed 1:1 with cells expressing FLAG/HA-tagged MOV10. For each experiment, approximately $1 \cdot 10^{16}$ cells were used. Cells were lysed in 3 times the cell pellet volume of low salt NP-40 lysis buffer (50 mM Tris-HCl [pH 7.5], 150 mM KCl, 2 mM EDTA, 0.5 % (v/v) NP-40, 1 mM NaF, 1 mM DTT, complete EDTA-free protease inhibitor cocktail (Roche)) and incubated for 30 min on ice. Lysates were cleared by centrifugation at 15,000 g for 20 min. For identification of proteins bound in the proximity of MOV10 or UPF1, cell lysates were treated with 10 U/µL RNaseT1 (Fermentas) for 5 min at 22 ^{o}C to generate RNA fragments of 200 - 500 nt of length. For the identification of RNA-independent interaction partners, cell lysates were treated with 50 U/µL RNaseT1 (Fermentas) for 5 min at 37 ^{o}C. RNaseT1 (Fermentas) treated lysates were mixed with 50 µL FLAG-conjugated Protein G Dynabeads (Invitrogen) per mL lysate, prepared as described above and incubated for 1 hr at 4 ^{o}C. Dynabeads were washed 4 times in 250 mM salt wash buffer (50 mM Tris-HCl [pH 7.5], 250 mM KCl, 0.5 % NP-40, 0.5 mM DTT, complete EDTA-free protease inhibitor cocktail (Roche)) and once in FLAG elution buffer (100 mM NaCl, 20 mM Tris-HCl [pH 7.5], 5 mM $MgCl_2$, 10% glycerol). Proteins were eluted by incubation with FLAG peptide (Sigma-Aldrich) at a final concentration of 0.5 mg/mL for 1 hr at 4 ^{o}C, the supernatant collected and used for HA affinity purification. An equal volume of µMACS HA magnetic beads (Miltenyi Biotec) as the original volume of Dynabeads were added to the FLAG eluates and incubated on ice for 30 min. Meanwhile µMACS columns (Miltenyi Biotec) were equilibrated with 1.5 mL FLAG elution buffer. µMACS HA beads were added to the column and washed 3 times with 800 µL ice-cold wash buffer I (150 mM NaCl, 50 mM Tris-HCl [pH 7.5], 5 % glycerol, 0.05 % NP-40) and 2 times with 500 µL ice-cold wash buffer II (50 mM NaCl, 50 mM Tris-HCl [pH 7.5], 5 % glycerol). For analysis of FLAG/HA MOV10 IPs on gels, proteins were eluted from µMACS columns by addition of 50 µL pre-boiled SDS-containing loading buffer (Miltenyi Biotec). For mass-spectrometry analysis, an on-column trypsin

digestion was performed as previously described (Hubner and Mann, 2011) by adding 25 µL 2 M urea in 100 mM Tris-HCl [pH 7.5], 1 mM DTT containing 150 ng trypsin (Promega). After on-column digestion for 30 min at RT, proteins were eluted by adding two times 50 µL 2 M urea in 100 mM Tris-HCl [pH 7.5] containing 5 mM iodoacetamide. Samples were allowed to digest overnight at RT protected from light and stopped the next morning by acidification with 10 µL of trifluoroacetic acid. Digested peptides were desalted on STAGE tips, dried and reconstituted to 15 µL of 0.5 % acetic acid in water (Rappsilber et al., 2003). Two times 5 µL were injected in duplicate on an LC-MS/MS system (NanoLC-Ultra [Eksigent] coupled to LTQ-Orbitrap Velos [Thermo]), using a 240 min gradient ranging from 5 % to 40 % of solvent B (80 % acetonitrile, 0.1 % formic acid; solvent A= 5 % acetonitrile, 0.1 % formic acid). For the chromatographic separation ~20 cm long capillary (75 µm inner diameter) was packed with 1.8 µm C18 beads (Reprosil-AQ, Dr. Maisch). On one end of the capillary a nanospray tip was generated using a laser puller (P-2000 Laser Based Micropipette Puller, Sutter Instruments), allowing fretless packing. Raw data were analyzed using the MaxQuant proteomics pipeline (v1.2.2.5) and the built in the Andromeda search engine (Cox et al., 2011) with the International Protein Index Human (v3.71) database. Carbamidomethylation of cysteines was chosen as fixed modification, oxidation of methionine and acetylation of the N-terminus were chosen as variable modifications. The search engine peptide assignments were filtered at 0.01 false discovery rates. Only proteins with a minimum ratio count of 3 were considered for quantification. Proteins with log2-transformed ratios above 1.5 for MOV10 IPs and above 1 for UPF1 IPs in both labeling-swap experiments for the high RNaseT1 experiment were considered to be direct interaction partners. Proteins with log2-transformed ratios above 1.5 for MOV10 IPs and above 1 for UPF1 IPs in both labeling-swap experiments for the low RNaseT1 experiments were considered to be either protein-protein interaction partners or proteins bound in the proximity of MOV10 or UPF1. Proteins were considered RNA-binding if they were annotated as RNA-binding based on their associated Gene Ontology terms or experimentally identified to bind poly(A) purified mRNAs (Baltz et al., 2012; Castello et al., 2012). Proteins with the Gene Ontology term nucleic binding were considered as nucleic binding and the remaining proteins were classified as 'not annotated'. Functional enrichment of Gene Ontology pathway terms among the proteins bound in the proximity of MOV10 were identified using the DAVID online tool (Huang da et al., 2009).

Western Blotting and Co-Immunoprecipitations

For Western blotting, cells were lysed in low salt NP-40 lysis buffer (50 mM Tris-HCl [pH 7.5], 150 mM KCl, 2 mM EDTA, 0.5 % (v/v) NP-40, 0.5 mM DTT, complete EDTA-free protease inhibitor cocktail (Roche)). After 20 min incubation on ice, lysates were cleared by centrifugation at 20,000 g for 20 min and supernatants transferred to a new tube. 50 µg protein per lane was separated on SDS polyacrylamide gels and transferred to nitrocellulose membranes (GE Healtcare Life Sciences). Membranes were blocked in 5 % skim milk in TBS-T buffer and incubated with antibodies against the HA-tag (1:1,000, HA.11 16B12, Covance), MOV10 (1:700, 10370-1-AP, ProteinTech), UPF1 (1:1,000, A300-036A, Bethyl), TBP (1:1,000, ab818, Abcam), H3K36me3 (1:1,000, ab9050, Abcam) or tubulin serving as a loading control (1:2,000, Clone AA2 T8328, Sigma-Aldrich). For co-IP experiments, non-inducible Flp-In T-REx HEK293 cells lines expressing FLAG/HA-tagged MOV10, UPF1 or AGO2 were transfected with 10 µg of indicated pDEST26-MYC expression vectors in a 10 cm dish format using 60 µL/dish of Lipofectamine2000 (Invitrogen). Cells were harvested 18 hrs post-transfection, pelleted and resuspended in 400 µL low salt NP-40 lysis buffer, incubated on ice for 30 min and cleared by centrifugation at 20,000 g for 15 min. 50 µL Protein G Dynabeads (Invitrogen) were prepared as described above and added to the cleared lysate. Following 1.5 hrs incubation at 4 ^{o}C on rotation, the beads were washed three times with 150 mM KCl wash buffer (50 mM Tris-HCl [pH 7.5], 150 mM KCl, 0.05 % NP-40, 0.5 mM DTT, complete EDTA-free protease inhibitor cocktail (Roche)). Proteins were eluted by the addition of SDS loading buffer (50 mM Tris-HCl, [pH 6.8], 2 mM EDTA-NaOH [pH 8.0], 10 % glycerol, 2 % SDS, 100 mM DTT, 0.1 % (w/v) bromophenol blue) directly to the washed beads and boiled for 5 min at 95 ^{o}C. Input and bead eluted supernatants were separated on SDS polyacrylamide gels and used for Western blotting as described above with antibodies recognizing the HA-tag (1:1,000, HA.11 16B12, Covance) or MYC-tag (1:1,000, 05-419, Millipore).

mRNA Decay Assays

mRNA decay assays were performed in HEK293 Tet-off cells (Clontech) transfected with βWT (WT β-globin transcript) or β39 (β-globin transcript with a PTC at position 39) reporter plasmids together with the internal control plasmid β-UAC-GAP as described (Lykke-Andersen et al., 2000; Lykke-Andersen and Wagner, 2005). $2.5 \cdot 10^5$ HEK293 Tet-off cells/well were seeded in 6-well plates in doxycycline-containing media (50 ng/mL, Sigma-Aldrich) and transfected on the two consecutive days with 25 nM siRNA duplexes using 4.5 µL/well Lipofectamine RNAiMAX

(Invitrogen). 48 hrs after the first siRNA transfection, cells were transfected with 0.5 µg/well βWT or β39 reporter plasmids together with 25 ng of the internal control plasmid β-UAC-GAP using 10 µL/well Lipofectamine2000 (Invitrogen) in the presence of 50 ng/µL doxycycline (Sigma-Aldrich). 24 hrs after plasmid transfection, transcription was induced by removal of doxycycline from the media by repeated washes with PBS followed by the addition of fresh high glucose DMEM media (Invitrogen) supplemented with 10 % (v/v) tetracycline-free fetal bovine serum (Lonza), 1 % (v/v) 2 mM L-glutamine (Invitrogen). 12 hrs later transcription was stopped by addition of doxycycline (Sigma-Aldrich) to a final concentration of 1 µg/µl. Cells were harvested by addition of 1 mL TRIZOL (Invitrogen) directly to the wells at indicated time points and total RNA was extracted following the instructions of the manufacturer. 5 µg total RNA per sample were denatured by addition of glyxoal-based NorthernMax-Gly Sample Loading Dye (Ambion) and incubated at 50 ^{o}C for 30 min. Denatured RNA samples were separated on 1.2 % SeaKem LE agarose (Lonza) gels in 10 mM $NaPO_4$ [pH 7.0] buffer at 100 V for 5 hrs. RNA was transferred to Hybond-N+ nylon membranes (GE Healtcare Life Sciences) in 1x TBE buffer (89 mM Tris-borate, 89 mM boric acid, 2 mM EDTA) by electroblotting in a semi-dry blotting chamber (BioRad) for 1.5 hrs at 15 V. RNA was crosslinked to membrane by UV irradiation at 265 nm at 2,000 µJ. Prior to hybridization membranes were incubated with 50 mM Tris-HCl [pH 8.0] at 45 ^{o}C for 10 min followed by 30 min incubation with NorthernMax Prehybridization/Hybridization Buffer (Ambion) at 68 ^{o}C. An internally radiolabeled RNA probe spanning the entire β-globin coding sequence was generated by T7 *in vitro* transcription. The coding sequence of β-globin was amplified from a β-globin containing plasmid from the ORFeome library (clone id: 100005789) and cloned into the XbaI/HindIII site of pcDNA3.1 plasmid (Invitrogen). The coding sequence of β-globin including the T7 promoter region was amplified from pcDNA3.1 β-globin inverted plasmid using a CMV FW primer and β-globin HindIII primer. Primer sequences used for cloning and PCR are listed in Table S1. The PCR product was purified using the QIAquick PCR purification kit (Qiagen) and used for T7 *in vitro* transcription using the MAXIscript T7 kit (Ambion) with (α-^{32}P)-UTP (Perkin Elmer). Unincorporated nucleotides were removed from the *in vitro* transcription product using illustra MicroSpin G-25 Columns (GE Healtcare Life Sciences). The probe was denatured by 2 min incubation at 95 ^{o}C and then hybridized to the membrane in NorthernMax Prehybridization/Hybridization Buffer (Ambion) overnight at 68 ^{o}C. The following day, the membrane was washed in 2 X SSC (300 mM NaCl, 30 mM sodium citrate), 0.1 % SDS once for 1 min and twice for 30 min at 68 ^{o}C, followed by washes in 0.2 X SSC, 0.1 % SDS once for 30 min and once for 60 min at 68 ^{o}C. Northern blot was visualized by exposure to phosphoimager

screens. Bands were quantified using the Multi Gauge v. 3.2 software (FujiFilm).

Pulse 4SU Labeling of RNA

For measurements of 4SU incorporation rates, Flp-In T-REx HEK293 cells were labeled with 500 µM of 4SU (ChemGenes) for 10 and 45 min, or with 100 µM of 4SU (ChemGenes) for 16 hrs. Cells were harvested by addition of TRIZOL (Invitrogen) directly to the plates and RNA was extracted following the instructions of the manufacturer. *Saccharomyces cerevisiae (S. cerevisiae)* strain BY4741 *MATa, his3D1, leu2D0, met15D0, ura3D0* (Euroscarf) was labeled with 4-thiouracil (4TU) as previously described (Sun et al., 2012). *S. cerevisiae* cells were grown in YPD medium overnight, diluted to an OD_{600} of 0.1, and grown to mid-log phase. OD_{600} of 0.8 corresponded to $1.75 \cdot 10^7$ cells per mL. 4TU (Sigma, dissolved in DMSO) or DMSO alone as control was added to the media at a final concentration of 5 mM, and cells were harvested after 6 min of labeling by centrifugation at 2,000 g and 4 °C for 5 min. Total RNA was extracted using the GeneMATRIX Universal RNA Purification Kit (Roboklon) following the protocol for yeast RNA.

Measurement of 4SU Incorporation Rates

For dot blot, 12 µg total RNA was biotinylated by 3 hrs incubation in the dark with 50 µL solution of EZ-Link HPDP-Biotin (Thermo Scientific, dissolved to 1mg/mL in DMF) in buffer containing 100 mM TRIS-HCl [pH 7.4] and 50 mM EDTA. RNA was separated from free HPDP-Biotin by extraction of RNA using phase lock tubes (5PRIME). Labeled RNA was then blotted onto a Hybond-N+ nylon membrane (GE Healtcare Life Sciences) in a dot blot apparatus. Membranes were blocked in blocking solution (PBS, 10 % SDS and 1mM EDTA) for 20 min and then incubated with HRP-Conjugated Streptavidin (Thermo Scientific, 1:10,000) in blocking solution for 15 min. Membrane was washed twice in blocking solution for 10 min each, twice in wash buffer I (PBS, 1 % SDS) for 10 min each, twice in wash buffer II (PBS, 0.1 % SDS) for 10 min each and developed using ECL reagent (GE Healtcare Life Sciences). To control for loading, membranes were stained for 2 min with a 0.5 M NaOAc, 0.5 % methylene blue solution followed by several washes with water. For the measurement of 4SU incorporation by LC-MS, total RNA was digested and dephosphorylated to single nucleosides using a modified protocol described by Andrus and Kuimelis (Schwalb et al., 2012). In brief, 60 µg total RNA was incubated 16 hrs at 37 ^{o}C with 0.9 U bacterial alkaline phosphatase (Worthington Biochemicals) and snake venom phosphodiesterase (Worthington Biochemicals) in 60 µL

reactions containing 13 mM $MgCl_2$, 3 mM $ZnCl_2$ and 63mM TRIS-HCl [pH 8.5]. To separate the nucleosides from residual salts and enzyme 8 µL 3 M sodium acetate [pH 5.5] and 200 µL 100 % ethanol was added to the reactions, chilled on dry ice for 10 min and centrifuged for 5 min at 20,000 g. The supernatant was transferred to new tubes and used for a second round of precipitation by addition of 600 µL 100 % ethanol, chilled on dry ice for 10 min and centrifuged for 5 min at 20,000 g. The supernatant was then dried completely under vacuum and samples were dissolved in 10 µL water. LC-MS analysis was carried out as previously described (Jungkamp et al., 2011).

RNA-Seq Library Preparation for Measurement of Steady-state mRNA Levels

HEK293 total RNA was extracted using the miRNeasy kit (Qiagen) following the instructions of the manufacture. *S. cerevisiae* strain BY4741 (Euroscarf) were grown in YPD medium overnight, diluted to an OD_{600} of 0.1, and grown to mid-log phase. OD_{600} of 0.8 corresponded to $1.75 \cdot 10^7$ cells per mL. Total RNA was extracted using the GeneMATRIX Universal RNA Purification Kit (Roboklon) following the protocol for yeast RNA. For quantification of changes in steady-state mRNA levels, 4 µg of HEK293 total RNA was spiked-in with 1/200 of *Sc* BY4741 total RNA and used for poly(A)+ mRNA library preparation following the TruSeq RNA sample Prep v2 LS protocol (Illumina). The libraries were sequenced on an Illumina Genome Analyzer GAII or Illumina HiSeq for 100 cycles (multiplexed 1× 101 + 7 index).

Nanostring nCounter Assay

Equal amounts (100 ng) of total RNA isolated from mock and MOV10-depleted cells were analyzed in parallel with the nCounter Human Cancer Reference Kit (GXA-CR1-12, NanoString Technologies). The nCounter assay was performed at the nCounter Core Facility at University Hospital Heidelberg. The counts for the positive spike-ins were summed up for each lane and the mean across all lanes was used to calculate a normalization reference. The normalization factor was calculated for each lane as the sum of the positive spike-ins divided by the normalization reference. All remaining code counts were multiplied by this normalization factor to take into account difference in hybridization efficiency between lanes. Next counts were further normalized to internal housekeeping controls *GAPDH*, *GUSB*, *PGK1* and *TUBB* similarly to the spike-in normalization. Finally, normalized counts were log2-transformed. Only genes with an mRNA expression count above 4 in all samples were considered for the downstream analysis.

Global mRNA Half-life Determination

For preparation of RNA for half-life determination, MOV10-depleted cells or mock transfected cells were labeled with 700 µM 4SU for 60 min, 48 hrs post-transfection. Total RNA was extracted using the miRNeasy kit (Qiagen) following the instructions of the manufacture. As a control of equal sample preparation we spiked-in a small amount of *S. cerevisiae*. RNA from *S. cerevisiae* treated with 4TU was prepared as described above for pulse 4SU labeling of RNA. For purification of 4SU-labeled RNA, 70 µg HEK293 4SU-labeled RNA was spiked-in 1/200 of 4TU-labeled *S. cerevisiae* BY4741 total RNA. 5 µg of total RNA was removed as input material and the remaining RNA was used for biotinylation. Biotinylation reactions were carried out in a total volume of 250 µL, containing 10 mM Tris-HCl [pH 7.4], 1 mM EDTA and 50 mg EZ-Link biotin-HPDP (Thermo Fisher Scientific, dissolved in DMF). Reactions were incubated at room temperature for 3 hrs in the dark. Following biotinylation, excess of free biotin was removed by phenol:chloroform extraction of the RNA using Phase-Lock-Gel tubes (5PRIME). Purified RNA was dissolved in 50 µL RNase-free water and denatured at 65 ^{o}C for 10 min followed by rapid cooling on ice for 5 min. Biotinylated RNA was separated from non-labeled RNA using µMACS Streptavidin MicroBeads (Miltenyi). 200 µL beads were added to each sample and incubated for 15 min at room temperature. In the meantime, µColumns placed in the magnetic field of the µMACS separator were equilibrated with nucleic acid wash buffer supplied with the beads (Miltenyi). Reactions were applied to the µColumns and flow-through was collected as a non-labeled fraction. µColumns were washed twice with 500 µL pre-warmed high salt wash buffer (100 mM Tris-HCl [pH = 7.4], 10 mM EDTA, 1 M NaCl and 0.1 % Tween20). 4SU-labeled RNA was eluted from µColumns by addition of 100 µL freshly prepared 100 mM DTT followed by a second elution with additional 100 µL 100 mM DTT 5 min later. RNA was recovered from the flow-through fraction and labeled RNA fraction using the MinElute Spin columns (Qiagen) according to the instructions of the manufacture. RNA concentrations were determined using the Qubit RNA Assay Kit (Invitrogen) and measured on a Qubit® 2.0 Fluorometer (Q32866, Invitrogen). Final amounts of 4SU-labeled RNA were in the range of 700-800 ng per sample. 5 µg of input (total), flow-through (non-labeled RNA) and eluate (4SU-labeled RNA) fractions were used for poly(A)+ mRNA library preparation following the TruSeq RNA sample Prep v2 LS protocol (Illumina). The libraries were sequenced on an Illumina Genome Analyzer GAII or Illumina HiSeq for 100 cycles (multiplexed 1× 101 + 7 index). mRNA half-lives were computed as previously described (Schwanhausser et al., 2011). Functional enrichment of Gene Ontology pathway terms among short-lived and long-lived mRNAs were identified using the DAVID online tool (Huang da et al., 2009).

Cellular Fractionation

Flp-In T-REx HEK293 cells were collected by centrifugation, washed in PBS and resuspended in 5 times the cell pellet volumes of isotonic swelling buffer (20 mM Tris [pH 7.7], 3 mM $CaCl_2$, 2 mM $MgCl_2$, 0.3 M sucrose, 10 mM DTT, complete EDTA-free protease inhibitor cocktail (Roche)). Cells were allowed to swell 10 min on ice before digitonin (Sigma-Aldrich) was added to a final concentration of 70 ng/µL followed by another 10 min incubation on ice. Lysates were homogenized by performing 2 strokes with a douncer followed by additional 5 min incubation on ice. Cell nuclei were pelleted by centrifugation at 1,000 g for 5 min at 4 ^{o}C and the cytoplasmic fraction was collected as the supernatant. To remove any remaining cytoplasmic proteins, the nuclear pellet was resuspended in 5 pellet volumes of isotonic swelling buffer, incubated on ice for 10 min, followed by addition of Triton X-100 to 0.1 % (v/v), vortexed for 10 sec and centrifuged immediately at 1,000 g for 5 min at 4 ^{o}C. Supernatant was removed. The pellet was washed twice in 5 pellet volumes of isotonic selling buffer without any detergent. To lyse the nuclei, the pellet was resuspended in 5 pellet volumes nuclear extraction buffer (100mM Tris [pH 7.5], 500 mM LiCl, 10mM EDTA [pH 8.0], 1 % LiDS, 5 mM DTT, complete EDTA-free protease inhibitor cocktail (Roche)) and incubated on ice for 30 min with vortexing every 5-10 min. Samples were centrifuged at 20,000 g for 30 min at 4 ^{o}C and supernatant was collected as the nuclear fraction.

Microscopy

Doxycycline-inducible Flp-In T-REx HEK293 cells expressing GFP-tagged AGO2 were transfected with 4 µg pFRT/TO/RFP/MOV10-DEST expression vector in a 6-well format using 10 µL/well Lipofectamine2000 (Invitrogen). Cells were seeded onto 0.2 % gelatin coated coverslips 24 hrs post-transfection in media containing 1 µg/µL doxycycline (Sigma-Aldrich) and allowed to attach for 48 hrs. The cells were fixed with 37 ^{o}C pre-warmed 4 % formaldehyde in PBS for 15 min and washed twice in PBS. Nuclei were stained with TO-PRO3 (Invitrogen) by 5 min incubation using a 1:1,000 dilution in PBS followed by two washes in PBS. Coverslips were mounted onto a glass slides using ProLong Gold Antifade Reagent (Invitrogen). Cells were visualized with an LSM510 Zeiss confocal microscope.

Computational Analysis of PAR-CLIP Libraries

The bioinformatic analysis of PAR-CLIP experiments was conducted by Dr. Markus Schueler from the laboratory of Dr. Christoph Dieterich using scripts written in Perl and R. In addition, several freely available Unix tools were used to filter, process and manipulate mapped PAR-CLIP reads including the Samtools library (Gupta et al., 2010) for working with SAM/BAM file data and the Bedtools libraries (Rinn et al., 2007) for working with BED files. Differential expression was determined using the Cuffdiff and cummeRbund analysis pipeline (Dolken et al., 2008). Position-specific T-C transition event counts from PAR-CLIP experiments were calculated using all mapped reads determining the number of reads for each position that showed a T-C transition from the reference DNA. Clusters of MOV10 and UPF1 binding sites for each replicate were generated as previously described (Lebedeva et al., 2011). In short, adapters were removed with FAR 2.0 (the flexible adapter remover: http://sourceforge.net/projects/flexbar/) aligned to hg18 and a set of RefSeq pre-mRNA sequences with BWA 0.6.2. Unique alignments were converted to pileups and read clusters scored for characteristic conversions and read variability with a custom script. After stringent-false positive filtering (using antisense clusters as a decoy database and a false discovery rate of 0.05) remaining clusters were outputted as bed files. Ee defined the position inside each cluster, which had the most T-C transition events, as the preferred crosslinking site. RefSeq gene models used to associate both clusters as well as individual T-C transition positions to genes and transcript compartments were downloaded for hg18 from the UCSC genome browser (Colak et al., 2013). Conservation information was also retrieved from UCSC in a per-position format. Positional accessibility in a window around preferred crosslinking sites was computed using the LocalFold algorithm (Lange et al., 2012) with default parameters and the "-nodot" switch. Conservative MOV10 consensus sets were defined by only retaining overlapping reads with T-C transitions in both biological libraries.

RESULTS

MOV10 has in Vitro 5' to 3' Directional Unwinding Activity

To address the putative helicase function of MOV10, I generated cell lines stably expressing MOV10 WT and helicase deficient mutants, K530A and D645N, by replacing single amino acid residues in the conserved helicase motif I or motif II (Figure 2). The mutations do not seem to affect RNA-binding, as indicated by UV-crosslinking of these proteins to cellular RNA (Figure 4A).

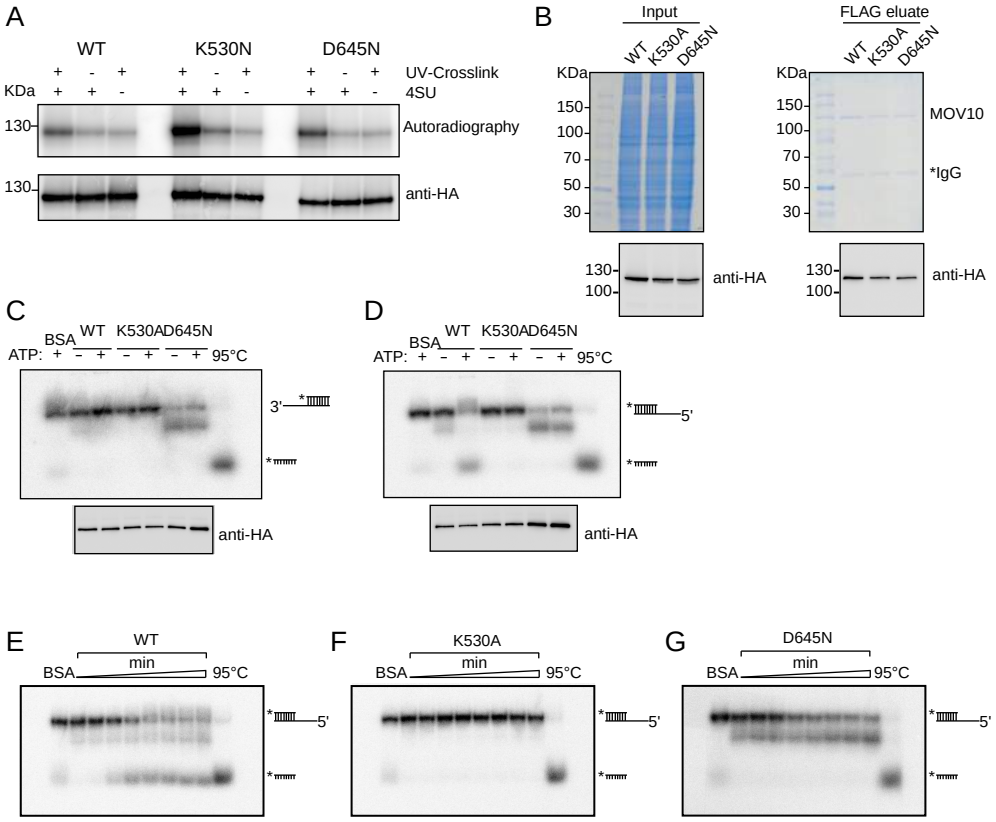

Figure 4. MOV10 has 5' to 3' directional unwinding activity *in vitro*.

(A) Analysis of UV-crosslinked MOV10–RNA complexes using SDS-page and Western blotting. Flp-In T-REx HEK293 cells expressing FLAG/HA-tagged MOV10 WT, K530A or D645N were labeled with 100 µM 4SU and UV-crosslinked as indicated and affinity purified using anti-FLAG antibody. RNA co-IPed with MOV10 was trimmed and radiolabeled to allow visualization. IPs were separated by SDS-page, transferred to a nitrocellulose membrane, exposed to phosphoimager screen (upper panel) and used for anti-HA Western blotting (lower panel). **(B)** Coomassie stain (upper panel) and Western blotting (lower panel) of total cellular extracts (input samples) and FLAG purified MOV10 WT, MOV10 K530A and MOV10 D645N used for *in vitro* unwinding assays. Asterisk marks heavy IgG immunoglobin chain. **(C)** *In vitro* unwinding assays of an RNA duplex containing a 3' overhang. Radiolabeled duplex was incubated with FLAG purified proteins in the presence or absence of ATP. Reactions were incubated for 1

hr and the RNA separated on non-denaturing TBE polyacrylamide gels followed by visualization using a phosphorimager screen (upper panel). Incubation with bovine serum albumin (BSA) served as a negative control and 30 sec incubation at 95 ^{o}C served as a positive control to completely denature the RNA duplex. Motilities of duplex and single-stranded RNAs are indicated on the left. Asterisk indicates the radiolabel. Western blotting using anti-HA antibody confirmed equal loading of epitope-tagged MOV10 proteins (lower panel) **(D)** Same as **(C)**, but with a RNA duplex containing a 5' overhang. **(E, F, G)** Time-dependent *in vitro* unwinding assays for MOV10 WT, K530A and D645N proteins. RNA duplexes containing 5'overhangs were incubated with purified MOV10 WT, K530A or D645N in the presence of ATP. Reactions were stopped at 0, 1, 2.5, 5, 10, 15, 20 and 30 min after addition of ATP, and the RNA separated on non-denaturing TBE polyacrylamide gels followed by visualization using a phosphorimager screen. Incubation with BSA for 30 min served as a negative control while 30 sec incubation at 95 ^{o}C served as a positive control to completely denature the RNA duplex.

Next, I examined whether MOV10 can function as an RNA helicase by performing *in vitro* unwinding assays using partially double-stranded RNA duplexes containing either 3' or 5' single stranded overhangs as substrates. When radiolabeled RNA duplexes containing a 5' overhang were incubated with FLAG-purified MOV10 WT in the presence of ATP, a lower band corresponding to the released single stranded radiolabeled oligoribonucleotide appeared (Figure 4C-E). MOV10 WT was unable to unwind the corresponding duplex containing a 3' overhang, demonstrating that MOV10 has 5' to 3' directional unwinding activity *in vitro* (Figure 4C). Both helicase mutants failed to unwind either of the two RNA substrates containing 3' or 5' overhangs, indicating that both mutants are indeed catalytically inactive (Figure 4C, 4D, 4F and 4G). A lower band appears for MOV10 D645N both in the presence and absence of ATP, which I speculate represents an unwinding intermediate (Figure 4C, 4C and 4G). Alternatively, this band could originate from RNaseT1 activity carried over from the purification step of FLAG purified MOV10 D645N.

Identification of MOV10 RNA Targets Using PAR-CLIP

To identify RNA targets of MOV10 and to map the position of MOV10's binding sites to its endogenous RNA targets, I generated PAR-CLIP libraries of MOV10 and its helicase deficient variants. I found MOV10 to be located predominantly in the cytoplasm and AGO2-containing cytoplasmic foci (Figure 5A and 5B). This is in agreement with published results from HEK293 and HeLa cell lines (Burdick et al., 2010; Gallois-Montbrun et al., 2007; Goodier et al., 2012; Lu et al., 2012; Meister et al., 2005). But since two studies have also reported a nuclear localization of MOV10 (El Messaoudi-Aubert et al., 2010; Sievers et al., 2012), I employed a high salt lysis protocol followed by sonication to capture both cytoplasmic as well as any nuclear and chromatin associated MOV10 by immunoprecipitation (IP) (see Materials and Methods).

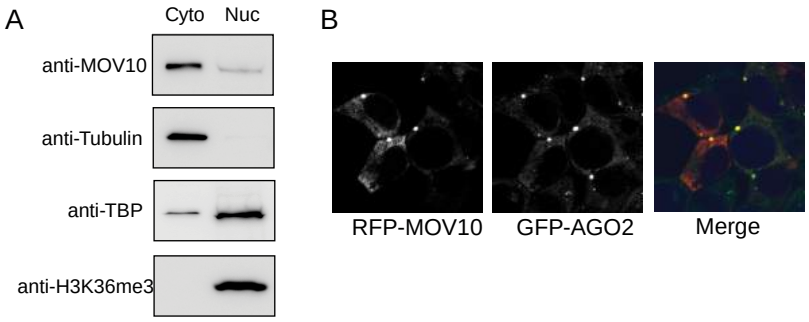

Figure 5. MOV10 is predominantly cytoplasmic and co-localizes with AGO2 to cytoplasmic foci in HEK239 cells.
(A) Cellular fractionation of Flp-In T-REx HEK293 into cytoplasmic (cyto) and nuclear fractions (nuc) followed by Western blotting against endogenous MOV10. Tubulin serves as a cytoplasmic marker, TBP as a nuclear marker and H3K36 serves as nuclear/chromatin marker. **(B)** Confocal microscopy of Flp-In T-REx HEK293 cells stably expressing GFP-tagged AGO2 transiently transfected with RFP-tagged MOV10 expression constructs.

PAR-CLIP is based on the incorporation of photoactivatable nucleoside analogs 4SU or 6SG into nascent RNAs followed by UV-crosslinking at 365 nm, which allows the identification of protein-RNA-binding sites at nucleotide resolution due to diagnostic T-C or G-A transitions observed in the cDNA reverse transcribed from UV-crosslinked RNA (Hafner et al., 2010). Co-IP of RNA with MOV10 and its helicase mutants was greatly enhanced by the incorporation of 4SU into nascent RNAs followed by UV-crosslinking at 365 nm (Figure 4A). I generated two biological replicate 4SU based PAR-CLIP sequencing libraries for MOV10 WT as well as for each of the helicase mutant proteins, K530A and D645N. As an example MOV10 protein-RNA crosslinked complexes used for library generation are shown in Figure S1. The statistics of sequencing reads are summarized in Table S2. I repeatedly observed an over-digestion of RNA crosslinked to MOV10 D645N compared with MOV10 WT and MOV10 K530 after ribonuclease (RNase) T1 treatment (data not shown). This could be due to a more open conformation of the RNA-binding cleft in the MOV10 D645N protein that renders the crosslinked RNA more accessible to RNase digestion. However, by reducing the RNaseT1 concentration for MOV10 D645N, I was able to generate RNA fragments with the same size distribution as MOV10 WT and MOV10 K530A (Figure S1B). Following cDNA library generation and sequencing, the mean length of uniquely mapping adapter-trimmed reads from pooled libraries of two biological replicates were 24.01 nt, 23.75 nt and 23.93 nt for MOV10 WT, K530A and D645N, respectively. As expected when aligning the PAR-CLIP sequencing reads to the reference transcriptome we observed a high enrichment of T-C transitions in reads compared to all other nucleotide changes, deletions or insertions (Figure S1C-H).

MOV10 and its Helicase Mutants Bind a Largely Overlapping Set of Targets, but with Distinct Positional Binding Patterns Throughout 3'UTRs.

To access the reproducibility of the PAR-CLIP libraries, we computed the correlation of the T-C transition counts at a specific position found in a least two of the six individual PAR-CLIP libraries and observed a high correlation between PAR-CLIP libraries of the same protein variant (Figure 6A). Using a previously described approach to define PAR-CLIP binding clusters (Lebedeva et al., 2011), we identified 434,221 and 437,370 putative mRNA-binding clusters of MOV10 WT in the two biological replicate 4SU libraries, demonstrating widespread RNA-binding of MOV10. Similarly, we identified 300,283 and 405,823 mRNA-binding sites for MOV10 K530A, and 297,114 and 321,293 mRNA-binding sites for MOV10 D645N. In all cases the binding sites mapped to more than 12,500 genes.

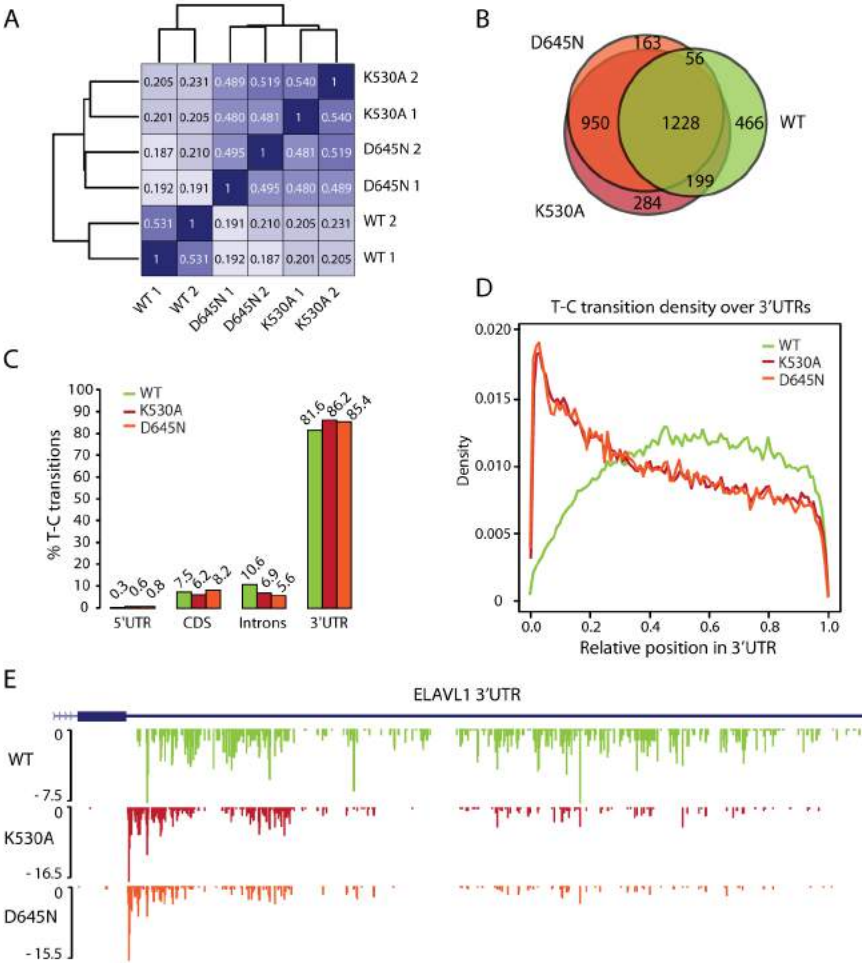

Figure 6. MOV10 WT and its helicase mutants bind a largely overlapping set of targets, but with distinct positional binding pattern throughout 3'UTRs.

(A) Correlation coefficients of T-C transition counts per position between individual MOV10 PAR-CLIP libraries. All T-C transitions with at least two transitions in more than one library were taken into account. **(B)** Venn diagram displaying the overlap

between mRNA targets containing the top 5,000 consensus PAR-CLIP clusters from MOV10 WT, K530A and D645N. **(C)** Location of MOV10 binding sites identified by PAR-CLIP. Barplot depicting the percentage of T-C transitions located in 5'UTRs, coding regions (CDS), introns and 3'UTRs. All T-C transitions with one or more counts in both biological replicates were considered. Total numbers of T-C transitions for MOV10 WT were 4,025 in 5'UTRs, 106,353 in coding regions, 150,011 in introns and 1,155,566 in 3'UTRs. Total numbers of consensus T-C transitions for MOV10 K530A were 6,647 in 5'UTRs, 65,339 in coding regions, 72,683 in introns and 904,550 in 3'UTRs. Total numbers of T-C transitions for MOV10 D645N were 5,334 in 5'UTRs, 55,758 in coding regions, 38,143 in introns and 581,815 in 3'UTRs. **(D)** Relative position of T-C transitions of MOV10 WT, K530A and D645N throughout 3'UTRs of mRNA target transcripts. Y-axis shows density of the median relative coverage over all 3'UTRs of target genes. Only T-C transitions with one or more counts in both biological replicates were considered. **(E)** Example of MOV10 WT, K530A and D645N T-C transition counts found in the 3'UTR of ELAVL1 (also known as HuR) transcript.

To obtain a consensus set of putative RNA-binding sites for MOV10 WT, K530A and D645N proteins we only retained sequence clusters supported by T-C transition containing reads from both replicate PAR-CLIP libraries. Looking at the mRNA targets containing the top 5,000 PAR-CLIP consensus clusters, more than half were overlapping between MOV10 WT, K530A and D645N, demonstrating that MOV10 and its helicase mutants are largely interacting with the same set of mRNA transcripts (Figure 6B). Moreover, the fraction of T-C transitions found in 5'UTRs, coding regions, introns and 3'UTRs were similar for MOV10 and its helicase mutants (Figure 6C). The vast majority (more than 80 %) of T-C transitions were found in 3'UTRs (Figure 6C), suggesting that the MOV10 and its helicase mutants bind a similar set of mRNAs largely by 3'UTR interactions.

Despite the large overlap of mRNA target transcripts, we observed only a low correlation in position-specific T-C transition counts between MOV10 and the mutant proteins, suggesting that the proteins contact different 3'UTR regions on common mRNA targets (Figure 6A). To investigate the differences in RNA-binding, we computed the relative distribution of MOV10 binding sites throughout 3'UTRs. Strikingly, we observed a clear distinction between the distribution of MOV10 and helicase mutant protein-RNA crosslinking sites along 3'UTRs (Figure 6D). Whereas T-C transitions from the helicase mutants were preferentially located at the 5' end of 3'UTRs, the crosslinking sites of the wild-type protein were distributed more towards the 3' end (Figure 6D). As an example, T-C transitions mapping to the 3'UTR of the ELAVL1 mRNA transcript are shown in Figure 6E. An additional PAR-CLIP library for MOV10 WT generated using the photoactivatable nucleoside 6SG, also showed a similar binding pattern as the 4SU MOV10 WT PAR-CLIP libraries, indicating the observed RNA target are not due to a crosslinking bias originating from the use of 4SU (Figure S2). Notably, we observe less G-A transitions in our 6SG library, than T-C transitions in our 4SU libraries, likely due to less efficient crosslinking of 6SG-labeled RNA to MOV10 (Figure S2A and S2B).

Binding of MOV10 Helicase Mutants Peak 30 nt Downstream of Stop Codons

Since the helicase mutants show a strong binding peak in the beginning of the 3'UTR, we wondered whether MOV10 might be recruited to 3'UTRs through interaction with the terminating ribosome. To look more closely at the distribution of binding sites over the termination (stop) codon, we computed the density profile for each individual library. We observed a clear binding peak of the helicase mutants 30 nt downstream of the stop codon (Figure 7). Interestingly, the terminating ribosome has been reported to protect RNA fragments of approximately 30 nt, with the 3' end of the protected fragment ending 12 nt downstream of the stop codon (Ingolia et al., 2009). This suggests that MOV10 binding takes place at the accessible region at the very beginning of the 3'UTR around 18 nt downstream of the termination ribosome, either as a result of direct interactions with the terminating ribosome or as an indirect effect due to accessibility of this regions. Since the MOV10 protein itself protects at least 10 nt (based on RNase digestion of RNA co-IPed with MOV10) this places the helicase mutants into close proximity of the terminating ribosome. For the MOV10 WT binding site we also observed increased binding 30 nt downstream of the stop codon, however the majority of the binding sites are found even further downstream (Figure 7).

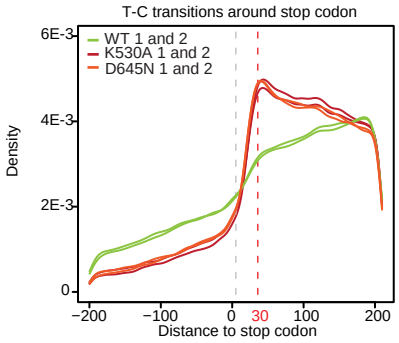

Figure 7.MOV10 helicase mutants bind strongly to regions 30 nt downstream of stop codons.

Density distribution of distances between preferred T-C transitions positions and the stop codon for MOV10 WT, K530A and D645N. Densities are shown for individual PAR-CLIP libraries.

RNA-binding Patterns of MOV10 Helicase Mutants Indicate Impaired Directional Translocation along RNA

To obtain a more detailed picture of the differences in the RNA-binding pattern between MOV10 WT and its helicase mutants we compared the positions of T-C transitions within overlapping binding clusters. Since the helicase mutant proteins lack RNA unwinding activity,

their translocation along RNA is expected to be impaired if MOV10 uses a partially processive mechanism to translocate along its RNA targets. Using the preferred T-C transitions in the top 5,000 PAR-CLIP clusters from one of the MOV10 mutant PAR-CLIP libraries as anchors, we computed the distances to the preferred T-C transition positions in overlapping clusters from all of the other individual PAR-CLIP libraries (Figure 8A). The preferred T-C transition positions were selected as the T-C transitions positions within the top PAR-CLIP clusters with highest number of count for each individual library. Interestingly, we observed a shift of MOV10 WT sites 3' (downstream) of the MOV10 K530A library 1 anchoring sites. This was not the case for any of the three other mutants libraries, which showed an almost identical profile centered on the anchor sites (Figure 8A). These observations are in agreement with the *in vitro* 5' to 3' directionality of MOV10 unwinding activity and indicate that the observed differences in the T-C transition patterns between MOV10 WT and its helicase mutants are likely to be caused by the translocation of MOV10 WT on its RNA targets. If the translocation of the helicase mutants is impaired, we would expect the binding clusters formed from overlapping PAR-CLIP reads for to be longer for WT MOV10 than the helicase mutants. Indeed, we observed a clear difference in the length of the top 5,000 PAR-CLIP clusters between MOV10 WT and mutants (Figure 8B). The median length of MOV10 WT clusters was 613 nt, while the median lengths were 363 nt and 295 nt for MOV10 K530A and MOV10 D645N clusters, respectively (Figure 8B).

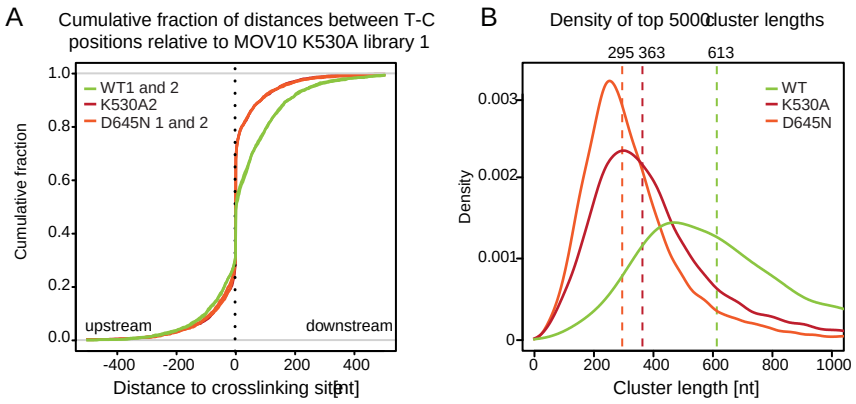

Figure 8. The RNA-binding pattern of MOV10 WT compared to helicase mutants suggests that helicase mutants are impaired in their ability to translocate along 3'UTRs.

(A) Cumulative fraction plot of distances between preferred T-C transition positions in top 5,000 top PAR-CLIP clusters of all libraries relative to the MOV10 K530A PAR-CLIP library 1. Preferred T-C transition positions were selected from the top 5,000 clusters for each consensus set as the positions within each cluster with the highest number of T-C transition counts. **(B)** Density plot of the top 5,000 MOV10 WT, K530A and D645N PAR-CLIP cluster lengths. Median cluster lengths are shown above the graph.

To ensure that this observation was not due to a difference in the number of reads present in the individual libraries, we generated PAR-CLIP clusters from the exact same number of sequencing

reads by 10 rounds of down-scaling the total read number for all libraries to that of the smallest library by choosing reads randomly. In all 10 cases we found the same difference between the cluster lengths as described above (data not shown). In summary the helicase mutants, while still being able to recognize the same targets as the MOV10 WT, seem to be impaired in their ability to directionally translocate 5' to 3' along their mRNA targets, confirming our *in vitro* results.

MOV10 Binds to Conserved Regions in 3'UTRs Immediately Upstream of Regions Predicted to Form Local Secondary Structures

To investigate features characterizing MOV10 binding sites, we analyzed the PhastCons conservation score, positional accessibility and presence of sequence motifs around preferred crosslinking sites. Interestingly, we found that the conservation upstream of MOV10 crosslinking sites located in 3'UTRs is lower compared to control regions (Figure 9A). This was irrespective of whether the crosslinking sites were found in the beginning or the end of 3'UTRs (Figure S3).

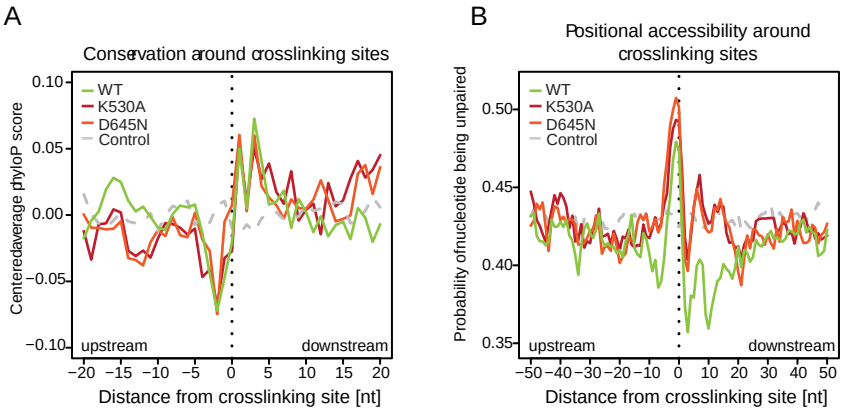

Figure 9. Conservation and positional accessibility around MOV10 binding sites indicate that we capture MOV10 WT immediately upstream of local secondary structures.

(A) Average centered PhastCons conservation scores around MOV10 WT, K530A and D645N preferred crosslinking sites in 3'UTRs. For comparison PhastCons conservation scores were computed for sites shifted 100 nt relative to the preferred crosslinking site, but still located within annotated 3'UTRs (grey dashed line). **(B)** Positional accessibility around MOV10 WT, K530A and D645N preferred crosslinking sites calculated using mfold. Preferred T-C transition positions were selected from the top 1,000 clusters for each consensus set as the positions within each cluster with the most T-C transition counts. Positional accessibility of shuffled regions is shown in grey.

On the other hand conservation downstream of MOV10 binding sites was increased compared to control regions, indicating a distinct conservation pattern around MOV10 binding sites. To investigate whether bound regions are likely to form local secondary structures we computed the positional accessibility around crosslinking sites. The positional accessibility around binding

sites is higher immediately upstream of MOV10 crosslinking sites, indicating that this region is likely to be single stranded (Figure 9B). In contrast, regions downstream of MOV10 WT crosslinking sites are less accessible than the surroundings, indicating that MOV10 WT is occupying sites located immediately upstream of regions likely to form local secondary structures (Figure 9B). Interestingly, this was not the case for the helicase mutants (Figure 9B). To assess whether this difference in accessibility around MOV10 WT and mutants sites could be explained by the different localization of MOV10 WT and mutants in 3'UTRs, we computed the accessibility separately for sites found in the beginning of the 3'UTRs as wells as sites located in the end of the 3'UTRs. However in both cases we only observed a lower accessibility downstream of MOV10 WT crosslinking sites (Figure S3). To determine if any sequence motifs were enriched in the vicinity of MOV10 binding sites, we counted the occurrences of 7mers in a 40 nt region around the preferred crosslinking sites. For both helicase mutants we observed a minor enrichment of AT-rich 7mers (Figure 10B and 10C). This is most likely due to the higher positional accessibility around MOV10 helicase mutants that are typically associated with AT-rich regions. For MOV10 WT we observed more GC-containing 7mers than for the helicase mutants (Figure 10A). Among the motifs found more frequently around MOV10 WT binding sites were TTTCCTT, TGTGAAA, ATTGAGA and TTCAGAA, however the occurrences of all of the mentioned motifs were relatively low, with less than 80 occurrences in the regions around the preferred T-C transition sites (Figure 10A). The increased in GC content relative to the helicase mutants are likely due to the fact that we capture MOV10 WT located next to structured regions which typically have a higher GC content. Taken together, our observations indicate that MOV10 binds to highly accessible regions with MOV10 WT captured immediately upstream of predicted local secondary structures.

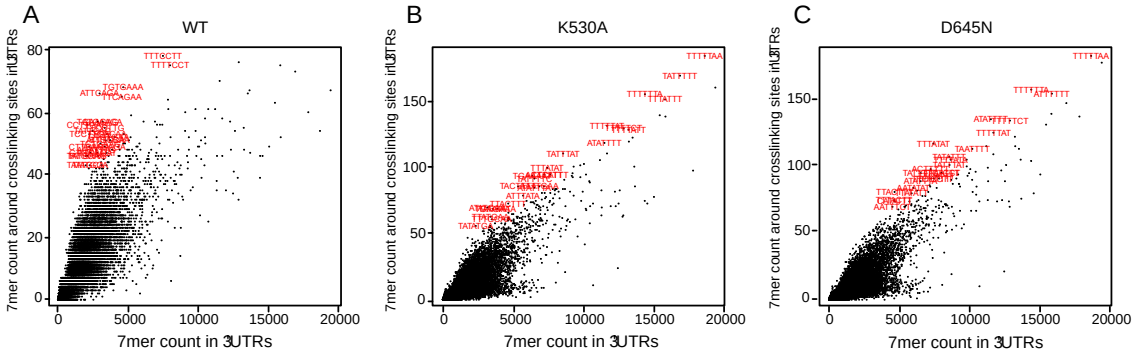

Figure 10. Helicase mutants display a slight binding preference for AT-rich regions likely reflecting the binding preference for structurally accessible regions.

Occurrences of 7mer motifs in 40 nt regions around preferred crosslinking sites compared to the occurrences of motifs in 3'UTRs. 7mer consisting of 7xAs or 7xTs were removed.

MOV10 Interacts with UPF1

To further investigate the molecular function of MOV10, I set out to identify protein interactors and protein complexes associated with MOV10 using a SILAC (Stable isotope labeling by amino acid in cell culture) based quantitative proteomics approach (Figure 11A). Control cells not expressing any FLAG/HA-tagged bait protein and cells expressing FLAG/HA-tagged MOV10 were grown in lysine and arginine isotope labeled media. Cells were mixed and subsequent lysis and IP was carried out using mixed cell populations. This allows the subtraction of proteins enriched in control cells that would otherwise have been identified as false positives (Ong et al., 2002). To obtain RNA-independent protein interactions, I treated cellular extracts with high RNaseT1 concentrations prior to double affinity purification of MOV10 (Figure 11B and 11C). As a biological replicate, I performed a crossover label-swap experiment where the light/heavy isotope labeling was reversed between the control and MOV10 expressing cells (Ong et al., 2002). Mass-spectrometry analysis of the MOV10 eluates revealed 9 proteins that were enriched (log2-transformed SILAC ratios above 1.5) in both MOV10 IP experiments (Figure 3A and Table S3). Among those were UPF1, eIF4A3 as well as the poly(A)-binding proteins PABPC1 and PABPC4. However, while we identified 22 unique peptides for UPF1, we only detected 1 unique peptide from eIF4A3, suggesting that eIF4A3 might be associated only with a subset of MOV10 proteins or a weak interaction between MOV10 and eIF4A3 (Table S3). As additionally enriched proteins, we detected RNF166 belonging to a subfamily of RING ubiquitin ligases (Giannini et al., 2008), RNA-binding protein FAM120A (Tanaka et al., 2009), the inhibitor of Moloney murine and HIV-1 viruses ZC3HAV1 (also known as ZAP) (Zhu et al., 2011), the uncharacterized zinc-finger CCHC domain containing protein ZCCHC3 and the poly(C)-binding protein PCBP1.

MOV10 Interacts in a RNA-Dependent Manner with Numerous RNA-Binding Proteins Involved in Post-Transcriptional Regulation

Because RNA helicases have been shown to have RNPase activity, it is possible that MOV10 is also able to displace proteins from its RNA targets as a result of its 5’ to 3’ translocation along 3’UTRs. To address which proteins that MOV10 could potentially displace from its RNA targets we used a modified IP protocol to identify proteins bound to RNA in the proximity of MOV10. To ensure stringent capture of protein complexes bound to RNA transcripts in the proximity of MOV10, covalent bounds between protein and RNA were created by treatment of cells with 4SU followed by UV-crosslinking prior to the preparation of cellular extracts (Figure 11A).

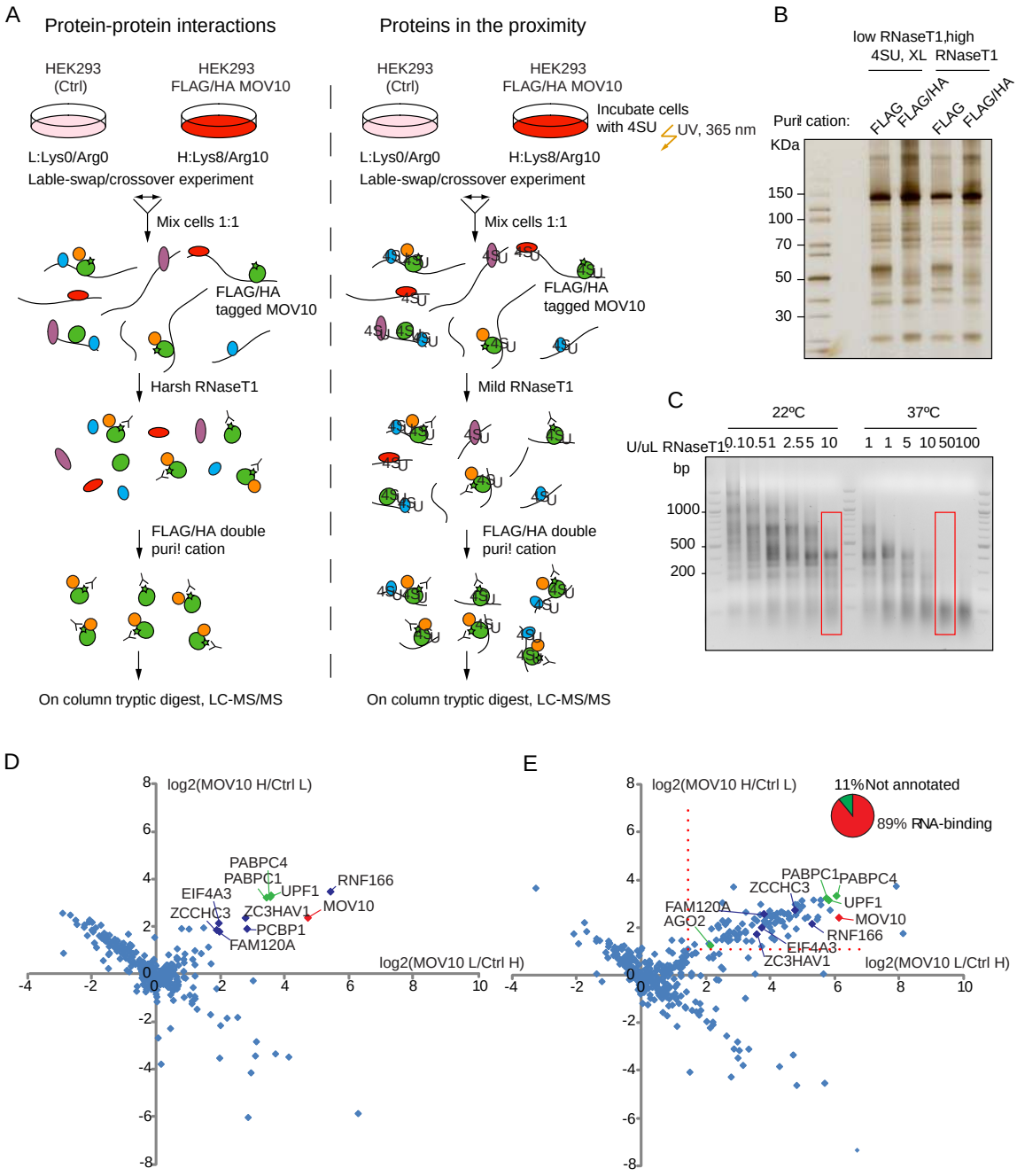

Figure 11. MOV10 is associated with UPF1 and binds RNA in the proximity of AGO2 as well as a number of proteins involved in post-transcriptional regulation.

(A) Outline of the SILAC based proteomics approach used to identify RNA-independent MOV10 protein interaction partners and proteins bound in the proximity of MOV10. Flp-In T-REx HEK293 cells either expressing FLAG/HA-tagged MOV10 or no bait protein were grown in SILAC media with 'light' non-labeled arginine and lysine amino acids (L: Lys0/Arg0 = $^{12}C_6{}^{14}N_4$ L-Arginine and $^{12}C_6{}^{14}N_2$ L-Lysine) or 'heavy' arginine and lysine amino acids (H: Lys8/Arg10 = $^{13}C_6{}^{15}N_4$ L-Arginine and $^{13}C_6{}^{15}N_2$ L-Lysine), respectively. Cells from different labeling states were mixed prior to cell lysis, treated with harsh or mild RNase conditions to allow identification of either RNA-independent or RNA-dependent protein interactions. In the case of RNA-dependent interaction partners, nascent RNA was labeled with 4SU for 16 hrs and UV-crosslinked at 365 nm to stabilize RNA-protein interactions. FLAG/HA-

tagged MOV10 complexes were double affinity purified, eluted by an on-column trypsin digestion and analyzed by mass-spectrometry. **(B)** Silver stain of FLAG IPs and FLAG/HA IPs from mixed cell population of parental HEK293 cells and cells expressing FLAG/HA-tagged MOV10. IPs were eluted from ProteinG Dynabeads using FLAG peptide and FLAG/HA IPs were eluted from μMACS columns using SDS containing loading buffer. **(C)** Optimization of RNase conditions used for MOV10 IPs. Flp-In T-REx HEK293 cells were lysed as described in the experimental procedures for SILAC IP of MOV10. RNaseT1 were added to the lysates to the indicated final concentrations and incubated either at 22°C or 37 °C for the indicated time point. The RNase digestion using 1 U/μL of RNaseT1 at 37 °C was repeated on independently lysed cells at a different day and compared to ensure reproducibility. RNA was isolated and separated on an agarose gel. **(D)** Plot of log2-transformed SILAC ratios from the two label-swap experiments for the identification of RNA-independent MOV10 interaction partners. **(E)** Plot of log2-transformed SILAC ratios from the two label-swap experiments for the identification of proteins bound in the proximity of MOV10 (RNA-dependent interactions). The pie chart indicates the fraction of proteins found to bind to RNA in the proximity of MOV10, which were annotated or experimentally verified as RNA-binding (Baltz et al., 2012; Castello et al., 2012). Red dotted lines indicate the cut-off of 1.5, which was set as the threshold for enrichment.

Mixed cellular extracts were then treated mildy with RNaseT1 to produce RNA fragments ranging from approximately 200 to 500 nt of length (Figure 11A and 11C). As described above, a crossover label-swap experiment was performed as a biological replicate. In total, we identified 91 proteins with log2-transformed SILAC ratios above 1.5 in both label-swap experiments (Figure 11E and Table S4). All 9 proteins identified as RNA-independent interactors were also identified under these conditions (Figure 11D, 11E and Table S4). Notably, UPF1, PABPC1 and PABPC4 were among the most highly enriched proteins also under these conditions, confirming a reproducible interaction between these proteins and MOV10. The majority, 81 out of 91 of the RNA-dependent MOV10 interacting proteins were either previously annotated as RNA-binding or have been experimentally shown to associate with poly(A)-purified mRNA transcripts (Figure 11E) (Baltz et al., 2012; Castello et al., 2012). The RNA-dependent MOV10 protein interactors were enriched in Gene Ontology biological pathway terms such as post-transcriptional gene regulation, regulation of translation and RNA processing (Table 1). Among the enriched proteins, we found AGO2, which has previously been reported to interact with MOV10 (Chendrimada et al., 2007; Frohn et al., 2012; Landthaler et al., 2008; Meister et al., 2005). We also identified TNRC6B (human homolog of GW182) which is part of the miRNA-induced silencing complex (miRISC) (Meister et al., 2005), the 3'UTR binding proteins IGF2BP1-3 (Hafner et al., 2010), heterogeneous nuclear ribonucleoproteins HNRNPA2B1, cold shock domain containing CSDE1, DEAD box RNA helicase DDX3X, PUM1 reported to induce formation of 3'UTR structures resulting in altered miRNA accessibility (Kedde et al., 2010) and the putative RNA helicase YTHDC2 as enriched in both label-swap experiments and with high peptide counts (Table S4).

Table 1: Gene Ontology biological pathway terms enriched among proteins bound in the proximity of MOV10.

Gene Ontology Biological Pathway	# Proteins	P-Value
Post-transcriptional regulation of gene expression	23	4.80E-25
Regulation of translation	15	6.90E-16
mRNA metabolic process	18	2.50E-13
RNA processing	19	1.20E-11
mRNA processing	15	8.80E-11
Negative regulation of translation	8	1.20E-10
Regulation of cellular protein metabolic process	16	1.50E-09
Regulation of mRNA stability	6	3.60E-08
RNA splicing	12	4.00E-08
Regulation of RNA stability	6	5.80E-08

UPF1 Interacts with Components of the EJC in a Separate Complex from MOV10

To confirm the interaction between MOV10 and UPF1 as well as to address the overlap between MOV10 and UPF1 interacting proteins, I performed a similar purification of FLAG/HA-tagged UPF1 as described above. Again we identified both RNA-dependent and RNA-independent protein interactors. Because the spread of the log2-transformed SILAC ratios were less than for MOV10, we chose a cutoff of 1 to classify proteins as enriched. MOV10 was highly enriched in the UPF1 IP samples in both crossover label-swap experiments with log2-transformed SILAC ratios of 2.17 and 2.35 (Figure 12A and Table S5). In addition, we identified PABPC1, PABPC4 and eIF4A3, which were also identified as MOV10 interactions partners. As UPF1-specific interactors we identified Y14 (also known as RBM8A), which is part of the EJC. Both BTZ (also known as CASC3 or MLN51) and MAGOH were identified with ratios of 0.91;1.26 and 1.02;0.99 respectively, meaning that they just barely failed to make the cutoff of 1 in both samples (Figure 12A). Together with eIF4A3, BTZ, Y14 and MAGOH comprise the core components of the EJC (Andersen et al., 2006; Bono et al., 2006; Singh et al., 2012). UPF1's interaction with the EJC is mediated by UPF2 and UPF3 (Chamieh et al., 2008; Le Hir et al., 2001; Melero et al., 2012). Surprisingly, we did not identify the known UPF1 interaction partners, UPF2 or UPF3 with enriched SILAC ratios. UPF3 exists as two paralogous in vertebrates, the X chromosome encoded UPF3B (Gehring et al., 2003; Lykke-Andersen et al., 2000) and the less active UPF3A (Kunz et al., 2006; Lykke-Andersen et al., 2000). Competition between UPF3B or UPF3A binding to UPF2 provides means to regulate the activity of NMD,

but also provides a regulatory robustness in the case of X chromosome inactivation (Chan et al., 2009). Although we did not detect UPF2 or UPF3 with enriched SILAC ratios, we did detect 63, 25 and 19 unique peptides from UPF2, UPF3A and UPF3B in the UPF1 IP, respectively (Figure 12B). In comparison we did not detect any peptides for either UPF2 or UPF3 in the MOV10 IP (data not shown). It has previously been reported that proteins from different labeling states can be exchanged during cell lysis and the IP procedure if the protein interactions occur transiently (Hubner and Mann, 2011), suggesting that this might be the case for the interaction between UPF1, UPF2 and UPF3.

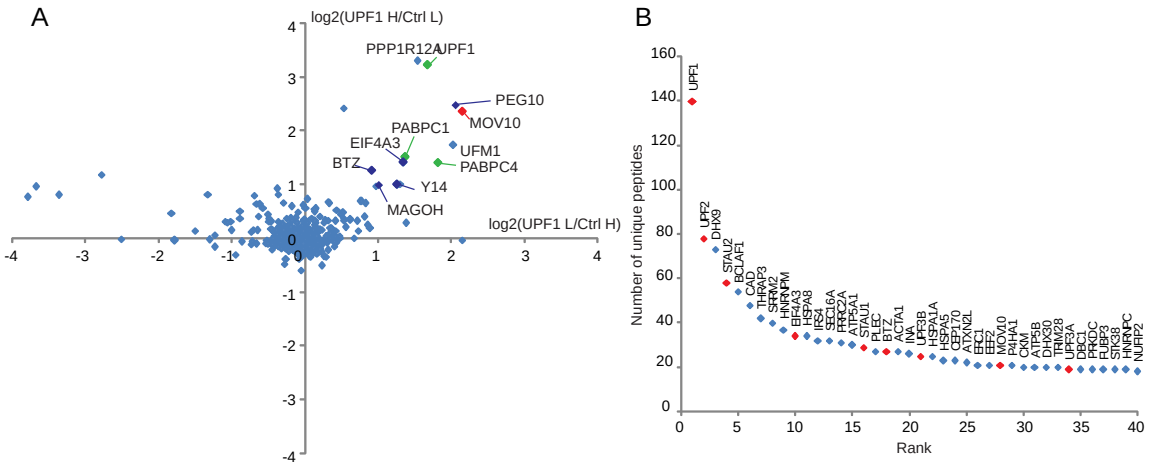

Figure 12. UPF1 interacts with MOV10 as well as core components from the EJC.

(A) Plot of log2-transformed SILAC ratios from the two label-swap experiments for the identification of RNA-independent UPF1 interaction partners. **(B)** Proteins identified with high unique peptide counts in the UPF1 IP. X-axis shows proteins ranked accordingly to the number of unique peptides detected for that given protein. Contaminants and ribosomal proteins were removed from the list.

We also observed a high peptide count for both STAU1 and STAU2 in our UPF1 IPs (Figure 12B). Both STAU1 and STAU2 are involved in STAU-mediated decay together with UPF1 (Kim et al., 2005; Park et al., 2013). STAU-mediated decay is mechanistically different from NMD and reported to involve base pairing between long non-coding RNAs and Alu elements with regions in 3'UTRs which are recognized by STAU to promote target degradation (Gleghorn et al., 2013; Gong and Maquat, 2011). STAU1 was also detected in the MOV10 IP with 5 unique peptides, while STAU2 was only identified with one unique peptide in the MOV10 IP (data not shown). This indicates a stronger interaction between UPF1, STAU1 and STAU2 than for MOV10. Since we only observed one unique peptide for eIF4A3 in our MOV10 IPs and did not observe any peptides for BTZ, MAGOH, Y14, UPF2 or UPF3 in our MOV10 IP, our data suggest that UPF1 is interacting with the EJC, UPF2 and UPF3 in a separate complex from

MOV10 (Table S3 and S5, data not shown). As additional UPF1-specific protein interactors, we identified the retrotransposon derived PEG10 (Ono et al., 2001), the myosin phosphatase target subunit 1 PPP1R12A (Hartshorne et al., 2004) and the ubiquitin-fold modifier 1 UFM1 which is a ubiquitin-like protein conjugated to endogenous proteins (Komatsu et al., 2004). As for MOV10, we also performed a UPF1 IP from 4SU treated and UV-crosslinked cells where cellular extracts were treated under mild RNase to identify proteins bound in the proximity of UPF1 (Figure 13).

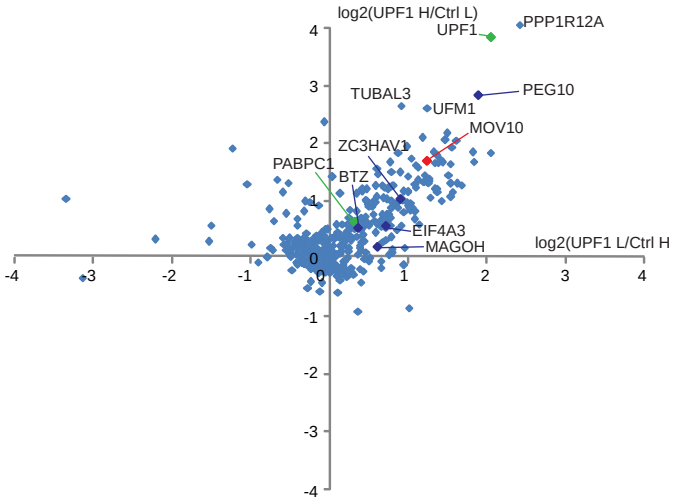

Figure 13. Proteins bound to RNA in the proximity of UPF1.

Plot of log2-transformed SILAC ratios from the two label-swap experiments used for the identification of proteins bound in the proximity of UPF1 (RNA-dependent interactions).

Interestingly, we did not observe as many RNA-dependent interaction partners for UPF1 as we did for MOV10, maybe due to a weaker or more transient binding of UPF1 to its RNA targeted transcripts. In total we identified 44 RNA-dependent interaction partners of UPF1 with log2-transformed SILAC ratios above 1 in both label-swap experiments. Only 23 of the proteins were experimentally validated or annotated as RNA-binding (Baltz et al., 2012; Castello et al., 2012). Among the known RNA-binding proteins detected with high peptide counts were MOV10, PEG10 and the elongation factor EEF2. As proteins not previously known to bind RNA, we identified KANK2, involved in formation of actin stress fibers (Kakinuma et al., 2009), carbamoyl-phosphate synthetase CAD and the direct UPF1 interactor, UFM1 with high peptide counts (Table S6).

MOV10 Interacts with UPF1 in a Partial RNA-Dependent Manner and in a RNA-Dependent Manner with AGO2

Our mass-spectrometry results suggest that MOV10 and UPF1 interact both in the absence and presence of RNA. To validate these results, I performed co-IPs of MOV10, UPF1 and AGO2 followed by Western blotting. In agreement with our mass-spectrometry data, I observed co-IP of UPF1 and MOV10 both in the presence and absence of RNase (Figure 14A). However, the interaction between MOV10 and UPF1 was reduced when the lysates were treated with RNase prior to the IP, indicating that the interaction between MOV10 and UPF1 is partially dependent on RNA.

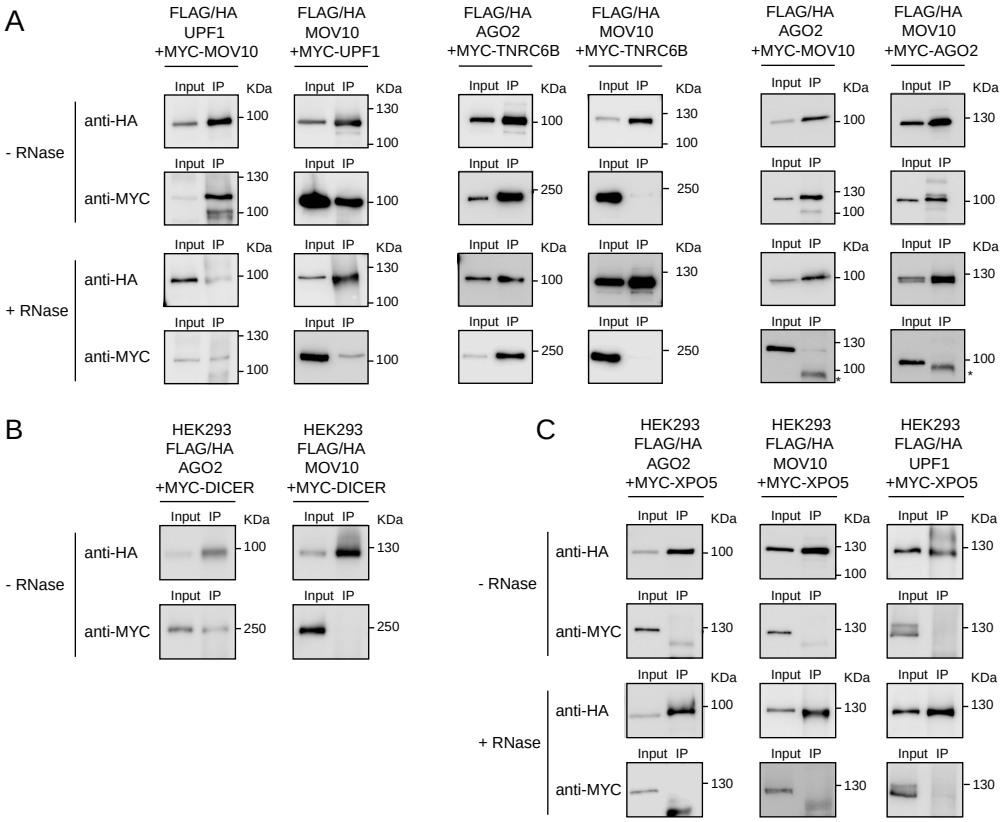

Figure 14. Validation of SILAC IP data.

(A) Western blot of FLAG/HA-tagged MOV10, AGO2 and UPF1 IPs. Flp-In T-REx HEK293 cells stably expressing FLAG/HA-tagged MOV10, AGO2 or UPF1 were transiently transfected with MYC-tagged AGO2, MOV10, UPF1 or TNRC6B expression constructs as indicated. Input and anti-FLAG IPs were analyzed by Western blotting with an antibody against the HA-tag (upper panel) or against the MYC-tag (lower panel). Asterisks indicate unspecific bands. **(B and C)** Western blot of FLAG/HA-tagged MOV10, AGO2 and UPF1 IPs. Flp-In T-REx HEK293 cells stably expressing FLAG/HA-tagged MOV10, AGO2 and UPF1 were transiently transfected with MYC-tagged MYC-tagged DICER **(B)** or MYC-tagged XPO5 **(C)** expression constructs as indicated. Input and anti-FLAG IPs were analyzed by Western blotting with an antibody against the HA-tag (upper panel) or against the MYC-tag (lower panel).

Also confirming the mass-spectrometry results, I found that AGO2 could only be co-IPed with MOV10 in the presence of RNA (Figure 14A). MOV10 has previously been reported to interact directly with AGO2 (Chendrimada et al., 2007; Meister et al., 2005), but more recently the interaction was found to be highly RNA-dependent (Frohn et al., 2012). If MOV10 is involved in miRNA-mediated regulation, we would expect MOV10 binding to be increased in the region complementary to predicted miRNA-binding sites. However, when comparing MOV10 binding sites to the presence of predicted miRNA-binding sites in 3'UTRs (Krek et al., 2005), we found no enrichment of MOV10 PAR-CLIP reads around miRNA sites (Figure 15). This suggests that MOV10 does not have a preference for miRNA-binding sites like AGO2 (Hafner et al., 2010).

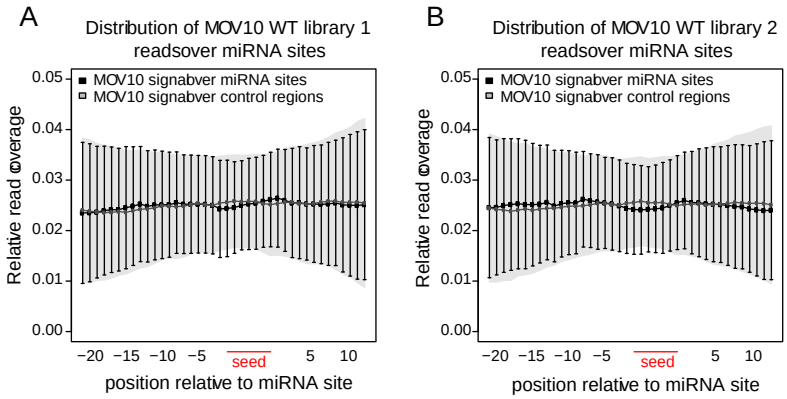

Figure 15. No enrichment of MOV10 binding sites around predicted miRNA binding sites,

MOV10 PAR-CLIP reads around miRNA-binding sites for MOV10 WT PAR-CLIP library 1 **(A)** and MOV10 WT PAR-CLIP library 2 **(B)**. Vertical lines indicate standard deviation. The gray area reflects expectancy gathered from regions shifted 100 nt relative to the miRNA seed site (region complementary to nucleotide 2-7 of the mature miRNA). The region complementary to miRNA seed sites is indicated bellow by the red line.

As a positive control for the co-IP experiments, I used TNRC6B, a known interactions partner of AGO2 (Landthaler et al., 2008; Meister et al., 2005). Confirming our co-IP strategy to validate protein-protein interactions, TNRC6B could readily be co-IP with AGO2 in the presence of RNase (Figure 14A). However TNRC6B was only co-IPed with MOV10 in the absence of RNase treatment (Figure 14A). This is in accordance with our mass-spectrometry results where we identified TNRCB6 as a protein bound in the proximity of MOV10, but not as an RNA-independent interaction partner (Table S2 and S3). To investigate if MOV10 is involved in miRNA processing, I also tested whether DICER1 could be co-IPed with MOV10, but found no co-IP of DICER1 with MOV10 (Figure 14B). Taken together, this indicates that MOV10 is not a component of miRISC together with AGO2 and TNRC6B or involved in DICER1 processing of miRNAs. As a negative control Exportin-5 (XPO5) involved in export of pre-miRNAs from the nucleus (Bohnsack et al., 2004) did not co-IP with MOV10, UPF1 or AGO2 (Figure 14C).

MOV10 and UPF1 Both Bind to Sites in 3'UTRs

Since MOV10 and UPF1 are interacting in a partially RNA-sensitive manner, we next questioned whether they bind the same sites on their RNA targets. UPF1 is the key factor in NMD and known to recognize and target PTC-containing transcripts for rapid decay (Lykke-Andersen et al., 2000). In addition, evidence suggests that UPF1 plays a role in regulation of non-PTC-containing transcripts (Mendell et al., 2004; Tani et al., 2012; Yepiskoposyan et al., 2011), in particular for transcripts with long 3'UTRs (Amrani et al., 2004; Behm-Ansmant et al., 2007; Eberle et al., 2008; Hogg and Goff, 2010; Ivanov et al., 2008; Silva et al., 2008; Singh et al., 2008). UPF1 mRNA targets have been partially characterized as mRNA transcripts deregulated upon UPF1 knockdown in HeLa cells and very recently by CLIP-Seq in murine embryonic stem cells and iCLIP in HeLa cells (Hurt et al., 2013; Zund et al., 2013). Similarly to MOV10, UPF1 binds its RNA targets mainly through interactions with 3'UTRs (Figure 16) (Zund et al., 2013). However, UPF1 binding to coding regions increases upon translational inhibition, indicating that UPF1 bound to coding regions is continuously displaced by translating ribosomes (Hurt et al., 2013; Zund et al., 2013). This is similar to UPF1 displacement from 3'UTRs by translational read-through which has previously been described (Hogg and Goff, 2010; Zund et al., 2013). As an example, UPF1 iCLIP identified binding sites with and without puromycin-induced translation inhibition mapping to the DDX6 transcript are shown in Figure 16. To address whether MOV10 binding to its targets is also affected by translational inhibition we performed PAR-CLIP of MOV10 after treatment with puromycin. However, we did not observe any major change in the location of MOV10 binding upon puromycin treatment, indicating that the RNA-binding pattern of MOV10, unlike UPF1, is independent of translation (Mathias Munschauer, data not shown).

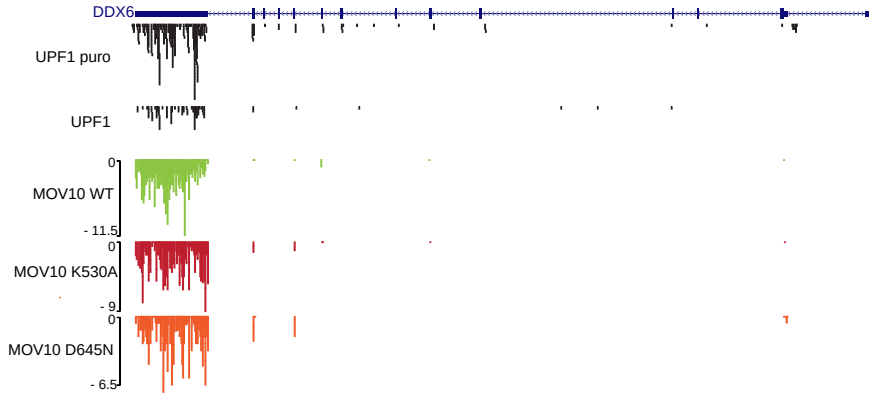

Figure 16. MOV10 and UPF1 share similar 3'UTR binding patterns.

UCSC genome browser view of UPF1 iCLIP identified binding sites (Zund et al., 2013) in untreated and puromycin (puro) treated HeLa cells mapping to the DDX6 transcript. MOV10 consensus T-C transitions are shown below.

MOV10 Knockdown Stabilizes a PTC-containing NMD-Targeted Reporter

To further study the molecular function of MOV10 and its relationship with UPF1 we performed siRNA-mediated knockdown of both proteins. MOV10 has a very long protein half-life (Schwanhausser et al., 2011) and to obtain a good knockdown we had to used a pool of two siRNAs targeting MOV10. 48 hrs post-transfection we observed a good depletion of both MOV10 and UPF1 (Figure 17). Moreover, the depletion of one protein did not seem to affect the level of the other protein (Figure 17). Since UPF1 is involved in targeting PTC-containing transcripts for rapid mRNA decay, we examined whether MOV10 plays a role in mRNA degradation of a well-characterized PTC-containing reporter transcript. β-globin reporters containing either a wild-type β-globin gene (βWT) or the corresponding PTC-containing β-globin (β39) transcript, which is targeted for NMD have previously been described (Lykke-Andersen and Wagner, 2005) and have been widely used to study NMD (Franks et al., 2010; Kurosaki and Maquat, 2013; Lykke-Andersen et al., 2000; Trcek et al., 2013) (Figure 18A). Transcription of both reporter genes is controlled by tetracycline-repressive promoters, which makes it possible to block transcription by addition of tetracycline to the cell culture media and subsequently follow mRNA degradation of the individual reporters over time. A reporter constitutively expressing a wild-type β-globin reporter with an extended open reading frame consisting of the 3'UTR from GAPDH (β-UAC-GAP) is used as an internal normalization control (Lykke-Andersen et al., 2000) (Figure 18A).

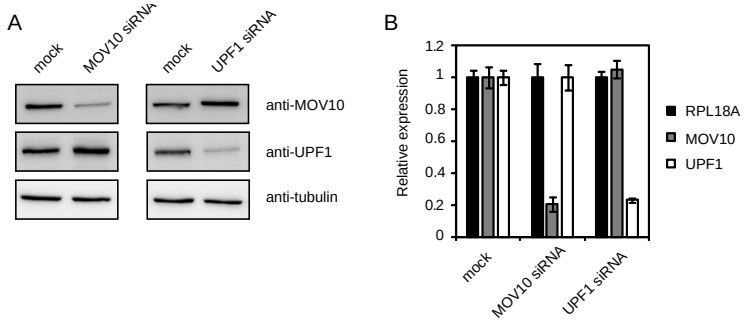

Figure 17. Validation of MOV10 and UPF1 siRNA-mediated knockdown.

(A) Validation of siRNA-mediated knockdown of MOV10 and UPF1 by Western blotting measured 48 hrs post-transfection. Tubulin serves as a loading control. **(B)** siRNA-mediated depletion of MOV10 and UPF1 measured by qRT-PCR 48 hrs post-transfection. Expression levels were normalized to RPL18A levels and are shown relative to mock transfected cells. Error bars show ± standard derivations for three technical replicates.

I observed similar degradation rates of the βWT reporter mRNA upon either MOV10 or UPF1 knockdown compared to mock transfected cells (Figure 18B). However, both upon MOV10 and UPF1 knockdown, the βWT mRNA degradation rates were slightly slower than for mock treated

cells. In contrast, mRNA degradation of the β39 reporter was markedly decreased both upon MOV10 or UPF1 knockdown (Figure 18C). Notably, UPF1 knockdown almost completely abrogated mRNA degradation of the β39 reporter mRNA (Figure 18C). The different time scales used to follow βWT and β39 mRNA decay are due to the accelerated decay of the β39 reporter mRNA caused by introduction of the PTC. To address how MOV10 and UPF1 might work together to mediated decay of the β39 reporter, I tested how a double knockdown of both MOV10 and UPF1 affected the degradation of the β39 mRNA and found that degradation rates were similar to MOV10 knockdown alone (Figure 18D). In the case of the double knockdown, I followed degradation of the β39 mRNA over a longer time interval than for the single knockdown, which is the reason why degradation of the reporter is more evident than for the single knockdowns in Figure 18C. The similar reduction in mRNA degradation rates of the β39 mRNA upon MOV10 knockdown alone and double knockdown of MOV10 and UPF1, indicates that MOV10 works downstream of UPF1, since the additional knockdown of UPF1 did not significantly enhance the effect of MOV10 knockdown.

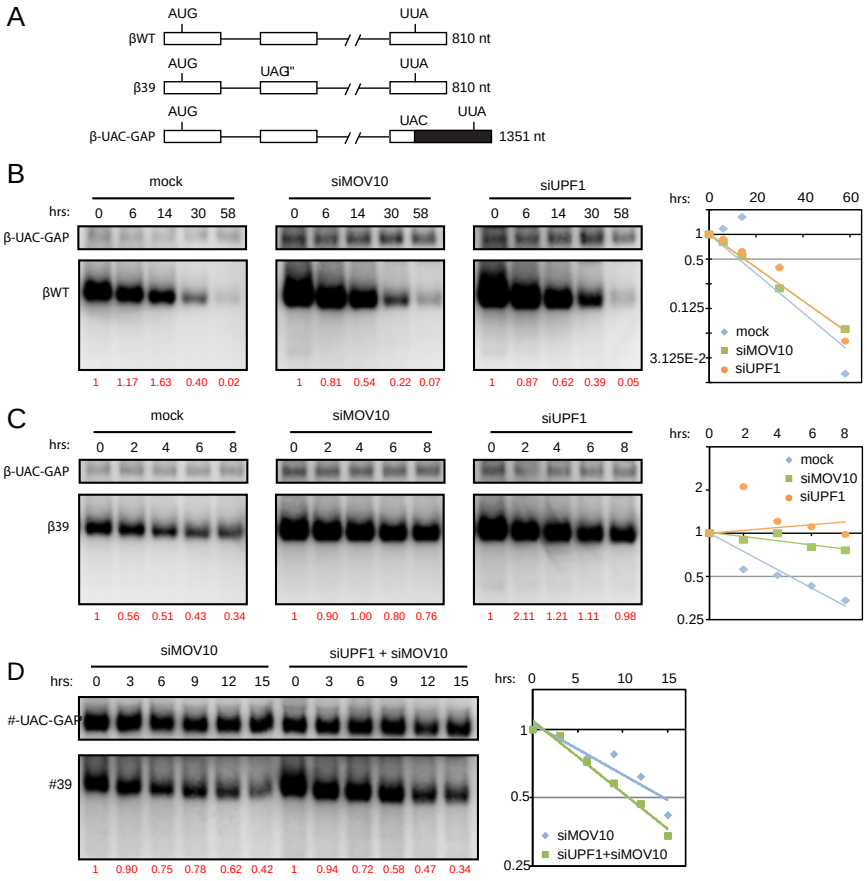

Figure 18. MOV10 knockdown leads to increased mRNA half-life of an NMD targeted β-globin reporter.

(A) Schematic representation of tetracycline responsive β-globin reporters containing either a wild-type β-globin gene (βWT) or the corresponding PTC-containing β-globin (β39) used to follow mRNA decay (Lykke-Andersen and Wagner, 2005). A wild-type

constitutively expressing β-globin reporter with an extended 3'UTR from GAPDH (β-UAC-GAP) was co-transfected together with the tetracycline responsive reporters and used as an internal control (Lykke-Andersen et al., 2000). **(B)** Stable mRNA decay of βWT in mock, MOV10 or UPF1 siRNA transfected cells. Ratios indicated in red represent levels of βWT relative to β-UAC-GAP. Ratios are plotted in log2 scale in graph on the right. **(C)** NMD-mediated decay of β39 mRNA in mock, MOV10 or UPF1 siRNA transfected cells. Ratios indicated in red represent levels of β39 relative to β-UAC-GAP. Ratios are plotted in log2 scale in graph on the right. **(D)** NMD-mediated decay of β39 mRNA in MOV10 siRNA transfected cells or upon double knockdown of MOV10 and UPF1. Ratios indicated in red represent levels of β39 mRNA relative to β-UAC-GAP. Ratios are plotted in log2 scale in graph on the right.

Changes in MOV10-Bound mRNA Levels and Degradation Rates upon MOV10 Knockdown

Considering the widespread binding of MOV10 to 3'UTRs of numerous mRNAs we hypothesized that MOV10 is also involved in regulating mRNA degradation of non-PTC-containing transcripts. To determine if steady-state mRNA levels were affected by MOV10 knockdown, we performed high-throughput sequencing of poly(A)+ mRNAs (hereafter termed RNA-Seq) isolated from mock transfected cells and MOV10 siRNA treated cells harvested 48 hrs post-transfection. We identified 513 up-regulated genes (false discovery rate < 0.05) and 917 down-regulated genes (false discovery rate < 0.05). As an independent validation of the RNA-Seq data we performed a nanostring nCounter analysis. The nCounter analysis allows measurement of mRNA expression levels based on direct hybridization of RNA to a selected probeset and is not dependent on reverse transcription, thus providing an unbiased method for measurement of few hundred mRNAs simultaneously (Geiss et al., 2008). We observed a high correlation between log2-transformed fold-changes determined using either method (Figure 19A).

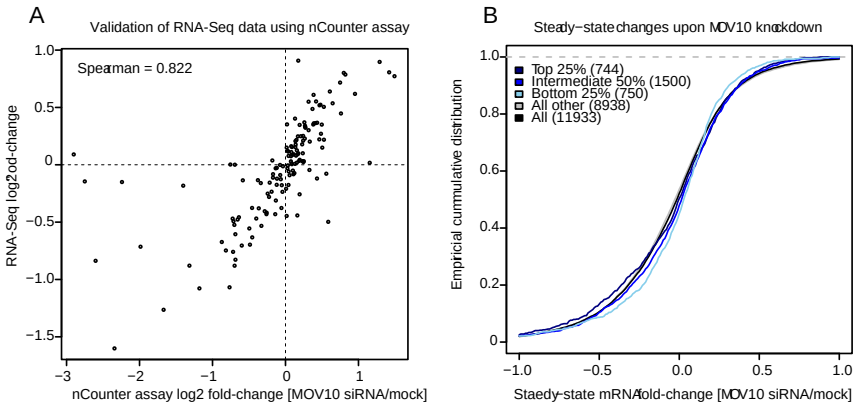

Figure 19. MOV10 knockdown does not affect steady-state mRNA levels of MOV10-targeted transcripts.

(A) Validation of RNA-Seq data using nanostring nCounter assay. Correlation plot of log2-transformed fold-changes determined based on FPKM values (fragments per kilobase of exon per million fragments pairs) from RNA-Seq data and mRNA expression count numbers as determined using the nCounter assay. Spearman correlation coefficient between the two datasets is indicated. **(B)** Changes in mRNA steady-state levels upon MOV10 knockdown (log2-transformed RNA-Seq fold-changes). MOV10-targeted transcripts with more than 5 T-C transitions in their 3'UTR were divided into top 25 %, intermediate 50 % and bottom 25 % target sets based on their number of T-C transitions normalized to the 3'UTR length and the expression level of the transcript (FPKM value).

To correlate changes in steady-state mRNA levels upon MOV10 depletion with the extent of MOV10 binding, we ranked transcripts by the number of T-C transitions in 3'UTRs, normalized to the 3'UTR length and expression level (FPKM - fragments per kilobase of exon per million fragments mapped value) of each individual mRNA transcript. All transcripts with more than 5 T-C transitions in their 3'UTR were considered. To distinguish between differentially MOV10-bound transcripts, we defined three groups based on this ranking, bottom 25 %, intermediate 50 % and top 25 %. Surprisingly, we did not observe any clear change in the steady-state mRNA levels of MOV10 targets compared to non-targets (Figure 19B). However, since changes in mRNA degradation does not necessarily lead to changes in steady-state levels due to feed-back regulation and may also be influenced by indirect effects on transcriptional regulation, steady-state mRNA levels are not directly informative about mRNA turnover rates. To overcome this, we globally determined changes in mRNA half-lives upon MOV10 knockdown using a previously described protocol for metabolic labeling of nascent mRNA transcripts with 4SU followed by RNA-Seq (Dolken et al., 2008; Rabani et al., 2011; Schwanhausser et al., 2011). Newly synthesized RNA transcripts were pulse labeled with 4SU for 60 min (Figure S4D), biotinylated and used for pull-down with streptavidin beads to separate newly synthesized mRNA transcripts (4SU-labeled) from pre-existing transcripts (non-4SU). By comparison with RNA-Seq data of total mRNA from the same samples, mRNA half-lives can be inferred (Dolken et al., 2008; Schwanhausser et al., 2011). In attempts to account for global changes in mRNA half-lives we normalized the RNA-Seq data to spiked-in 4SU-labeled yeast RNA using a simple linear model. Unfortunately, the yeast RNA was labeled with a much higher efficiency than HEK293 RNA and already 6 min after addition of 4TU to the yeast culture (Figure S4). Therefore, it was not possible to spike in sufficient amounts of 4SU-labeled yeast RNA to measure both lowly and highly expressed yeast genes in the input samples as well as the 4SU-labeled fractions, without favoring the pull-out of yeast RNA in the 4SU-labeled fractions to such an extent that we would not obtain enough human reads to a reliable measurement human mRNA half-lives (data not shown). We therefore chose to only spike in 1/200 fraction of 4SU-labeled yeast RNA into our samples and use it as a control for equal sample preparation, instead of using it for normalization, since a robust normalization would not be possible due to the low number of yeast reads in the input samples (Table S7). Only considering the human reads we were able to quantify the mRNA half-life of 7,682 mRNA transcripts in both the mock treated samples and MOV10 knockdown samples (Figure 20). The mean half-life of all quantified transcripts was 13.5 hrs (810 min). Based on a similar method to quantify mRNA half-lives using a 2 hrs 4SU labeling pulse, the mean mRNA half-life in NIH3T3 cells were determined to 9 hrs (Schwanhausser et al., 2011).

1,592 of the transcripts had a half-life below 6.75 hrs (50 % below the mean half-life). These genes are typically highly regulated genes with long 3'UTRs and encode for proteins involved in transcriptional regulation, including numerous zinc finger domain-containing proteins (Table S8). In the other end of the spectrum, long-lived transcripts generally have short 3'UTRs indicative of a reduced need for post-transcriptional regulation in general. 1,245 transcripts had a half-life above 20.25 hrs (50 % above the mean half-life). Genes in this group typically encode for proteins encoding metabolic enzymes or proteins involved in intracellular transport (Table S9). We observed a general tendency of short-lived mRNA transcripts to have longer 3'UTRs and therefore wondered if MOV10-targeted transcripts were associated with long 3'UTRs (Figure 20).

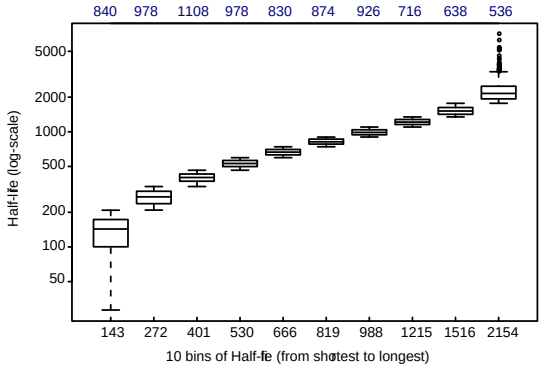

Figure 20. Short-lived mRNA transcripts generally have longer 3'UTRs.

Short-lived mRNA transcripts have longer 3'UTRs. Boxplot depicting the mRNA half-life of 10 equally sized bins of mRNAs ranked accordingly to their mRNA half-life. Mean mRNA half-life for each individual bin is indicated on the x-axis. The mean 3'UTR length for each bin is indicated above the graph.

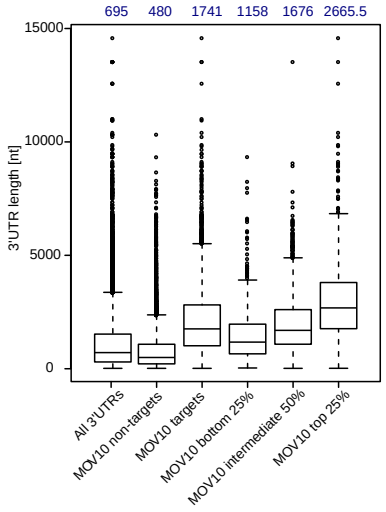

Figure 21. Highly bound MOV10 mRNA transcripts have longer 3'UTRs.

Boxplot of 3'UTR lengths for all Ensembl genes and the indicated PAR-CLIP target groups. The mean 3'UTR length for each group is shown above the plot. MOV10 targets were ranked by 3'UTR T-C counts normalized to both 3'UTR length and expression level (FPKM).

Indeed we found that MOV10-bound mRNAs (after normalization of T-C transition counts to 3'UTR length and expression levels), had long 3'UTRs and that the 3'UTR length was increased with increased MOV10 binding (Figure 21). To test if MOV10 knockdown had an effect on the mRNA half-life of its targeted transcripts we compared the changes in mRNA half-life upon knockdown for our defined MOV10 PAR-CLIP target groups. The mRNA half-lives of both the top 25% and intermediate 50% of MOV10-targeted transcripts were significantly stabilized compared to the bottom 25% of MOV10 targets or all other transcripts upon MOV10 knockdown (Figure 22A). This indicates that MOV10 normally functions to promote degradation of its targets. To validate these results using a different experimental setup we treated cells with actinomycin D to block transcription and followed mRNA degradation by qRT-PCR. We selected 4 transcripts all with numerous MOV10 T-C transitions in their 3'UTR (Figure S5). CBX6, CDKN1B and WEE1 were all stabilized upon MOV10 knockdown based on our RNA-Seq half-life measurement, whereas the half-life of HOXA9 was not determined (Table 2).

Table 2: mRNA half-lives measured by high-throughput sequencing.

mRNA transcript	mRNA half-life, Mock (hrs)	mRNA half-life, siMOV10 (hrs)
CBX6	2.86 (±0.10)[a]	4.35 (±1.48)
CDKN1B	1.61 (±0.03)	2.89 (±0.89)
HOXA9	ND[b]	ND
WEE1	1.96 (±0.09)	2.89 (±0.22)
IMPDH1	17.7 (±0.03)	21.9 (±4.95)
MYC	ND	ND
PANK2	5.26 (±0.40)	7.26 (±0.71)
RPL18A	19.2 (±0.70)	23.6 (±6.11)

[a]Mean value ± standard deviation from two biological replicates. [b]ND = Not determined.

As a normalization control we used the RPL18A gene, since RPL18A was not identified as a MOV10 target and has an mRNA half-life close to 20 hrs in HEK293 cells (Table 2). We observed increased mRNA half-lives of all 4 transcripts upon MOV10 knockdown (Figure 22B). As a control we did not observe increased mRNA half-lives of either IMPDH1 or MYC, which both have very few MOV10 T-C transitions in their 3'UTR (Figure 22B). As further confirmation that MOV10 is regulating degradation of 'real' UPF1 targets, we confirmed that MOV10 knockdown also stabilized the known UPF1 target PANK2 (Chan et al., 2007; Tani et al., 2012) (Figure 22C and Table 2). Taken together with our half-life measurements, our data shows that MOV10 promotes mRNA degradation of its targeted transcripts.

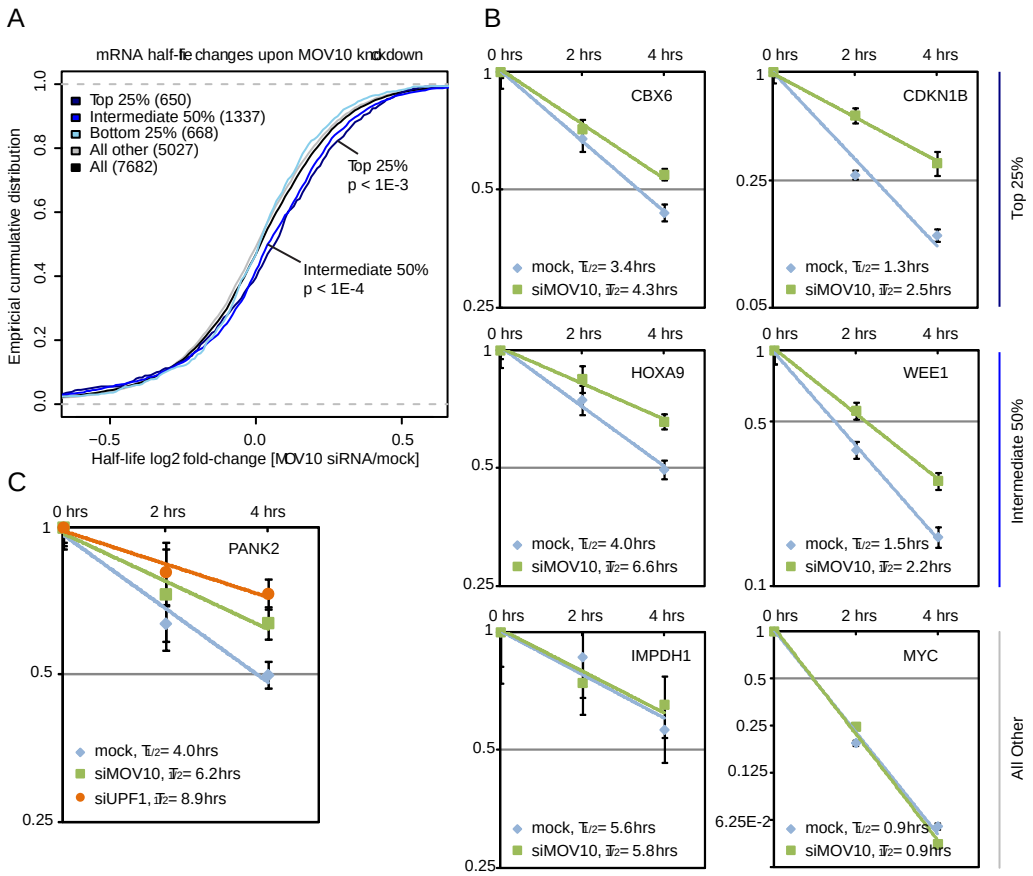

Figure 22. MOV10 knockdown leads to increased mRNA half-lives of its targeted transcripts.

(A) Changes in mRNA half-lives upon MOV10 knockdown. MOV10-targeted transcripts with more than 5 T-C transitions in their 3'UTR were divided into top 25 %, intermediate 50 % and bottom 25 % target sets based on their number of T-C transitions normalized to the 3'UTR length and the expression level of the transcript (FPKM value). P-values comparing the top 25% and intermediate 50% to all are calculated by one-sided Wilcoxon signed rank test. **(B)** Decay of CBX6, CDKN1B, HOXA9, WEE1, IMPDH1 and MYC mRNAs after actinomycin D treatment as measured by qRT-PCR. mRNA levels are shown relative to RPL18A (internal normalization control) and the 0 hr time point ± standard deviation from three technical replicates. **(C)** mRNA decay of the known UPF1 target PANK2 after actinomycin D treatment as measured by qRT-PCR. mRNA levels were normalized to RPL18A (internal normalization control) and shown relative to the 0 hr time point, with ± standard deviation from three technical replicates.

DISCUSSION

Translation and stability of mRNAs are regulated post-transcriptionally by dynamic association of RNA-binding proteins with their mRNA targets (Bessonov et al., 2008; Lee and Lykke-Andersen, 2013). RNA helicases are known to mediate ATP-dependent RNP remodeling, and evidence suggests that they can facilitate the transition between different RNP compositions dictating the fate of associated mRNAs (Franks et al., 2010; Pisareva et al., 2008). In order to gain insight into how mRNP transitions occur and how they are regulated it is necessary to study the molecular function of individual RNA helicases and to identify their RNA targets. Profiling of protein-RNA interactions has proven to be a powerful method to investigate post-transcriptional regulation mediated by numerous RNA-binding proteins present in mammalian cells (Hafner et al., 2010; Jungkamp et al., 2011; Lebedeva et al., 2011; Mukherjee et al., 2011; Wilbert et al., 2012). Recently, protein-RNA interactions have also been studied for a number of RNA helicases (Bohnsack et al., 2009; Hurt et al., 2013; Ilik et al., 2013; Sauliere et al., 2012; Sievers et al., 2012; Singh et al., 2012; Zund et al., 2013). MOV10 belongs to the UPF1-like SF1 helicase subfamily, which includes the RNA helicase UPF1 and the RNA-DNA helicase SETX. The helicase activity of UPF1 is necessary for the release of the surveillance complex from its mRNA targets, which in turn is required for subsequent XRN1-mediated degradation of the 3' NMD intermediate (Franks et al., 2010). In a similar manner, SETX has been shown to resolve RNA-DNA hybrids upstream of XRN2-mediated termination of transcription (Skourti-Stathaki et al., 2011). Even though MOV10 has been implicated in inhibition of retroviral infections and retrotransposition as well as chromatin remodelling, the molecular function of MOV10 remains elusive. To address the functional role of MOV10, we took advantage of a range of high-throughput techniques in order to characterize its molecular function in HEK293 cells. By applying PAR-CLIP to study the RNA-binding pattern of the RNA helicase MOV10 WT and two MOV10 helicase mutants, we were able to provide evidence of MOV10's translocation on its RNA targets at nucleotide resolution. I have shown that MOV10 interacts with UPF1, implicating MOV10 in mRNA degradation and NMD. Based on MOV10 knockdown experiments, I was able to show that MOV10 plays a role in mRNA degradation of UPF1-targeted transcripts and that MOV10 bound transcripts are stabilized upon MOV10 depletion. Below I will discuss our findings in connection with previously published results and elaborate on our proposed model of the function of MOV10.

PAR-CLIP of MOV10

We found that MOV10 displays widespread binding to 3'UTRs of thousands of transcripts. We observed a high number of diagnostic T-C transitions as well as a high correlation between the positions of T-C transitions between biological replicates, indicating that we identified high-confidence binding sites of MOV10. Binding of MOV10 was observed throughout entire 3'UTRs, forming long MOV10 binding clusters. For the two biological replicate MOV10 WT PAR-CLIP libraries, we identified 434,221 and 437,370 putative mRNA-binding clusters, with a mean cluster length of 66.6 and 67.7 nt in more than 12,000 genes. In comparison, a previously published report of nuclear MOV10 PAR-CLIP identified 17,053 MOV10 binding clusters mapping to 6,271 genes with a mean cluster length of 35.7 nt (Sievers et al., 2012). However, it should be noted that Sievers and colleagues used a different algorithm to identify binding clusters and that the numbers therefore are not directly comparable. Overall, the location of MOV10 binding clusters in 3'UTRs agree between our study and the study of Sievers and colleagues, however the resolution of our data is significantly higher, thus allowing for a more detailed study of MOV10 binding. In particular, the long binding clusters in our study made it possible to track the translocation of MOV10 WT compared to its helicase mutants.

Interestingly, MOV10 was found to be the strongest RNA-binder in a validation assay of 23 mRNA-bound proteins in HeLa cells, further underlining MOV10 as a protein extensively bound to mRNAs (Castello et al., 2012). It should be stressed that it is not possible to directly infer how many molecules of MOV10 are associated with one single transcript from our PAR-CLIP data since the observed number of T-C transitions does not necessarily represent an average over all transcripts, but likely reflect a mixed population of transcripts bound by MOV10 to a different extent. Naturally, the extent of MOV10 binding is correlated with the expression level of mRNA transcripts, since highly expressed genes are present at a higher copy number and therefore more available for MOV10 binding. Similarly, mRNA transcripts with longer 3'UTRs also harbor more T-C transitions simply because they provide more contact opportunities for MOV10. In order to classify MOV10-targeted transcripts based on their degree of MOV10 binding, we normalized T-C transitions both to 3'UTR length and FPKM values derived from RNA-Seq data. This way we obtained a measure to quantify the extent of MOV10 binding independently of 3'UTR lengths and gene expression levels.

In addition to MOV10 WT, we also studied the RNA-binding pattern of MOV10 helicase mutants. Our study is the first using PAR-CLIP to compare the RNA-binding pattern of an RNA helicase with its helicase mutants. Using this approach we were able to capture a snapshot of the

RNA-binding sites for both MOV10 and its helicase mutants. Although the extent of RNA-binding to 3'UTRs remained unchanged, we observed clear differences in the location of RNA-contact sites of MOV10 and its helicase mutants throughout 3'UTRs as well as within overlapping binding clusters. Our method for studying the RNA-binding pattern of MOV10 can readily be applied to study the role of other RNA helicases involved in various steps of RNA metabolism. Furthermore, our method can easily be extended to study changes in RNA-binding of helicases in response to changes in cellular conditions or upon viral infections.

Helicase Activity of MOV10

We showed for the first time that MOV10 has 5' to 3' directional RNA unwinding activity *in vitro*. The directionality of MOV10 unwinding *in vitro* is in accordance with the shift of MOV10 WT binding sites 3' relative to its helicase mutants that we observed in our PAR-CLIP experiments. Evidence suggests that processive RNA helicases are tracking along the loading strand, since their unwinding activity is only sensitive to disruptions in that strand (Beran et al., 2006; Jankowsky et al., 2000; Kawaoka et al., 2004). This indicates that we are able to capture MOV10 as it is translocating along 3'UTRs of its mRNA targets. The 5' to 3' directional unwinding activity of MOV10 is similar to other members of the SF1 UPF1-like subfamily of helicases UPF1, IGHMBP2 and the yeast homolog of SETX, Sen1p, which all display 5' to 3' directional unwinding activity *in vitro* (Bhattacharya et al., 2000; Guenther et al., 2009; Kim et al., 1999). Thus it seems like the 5' to 3' directionality is a common feature for all UPF1-like helicases. We found that MOV10 binds to unstructured regions immediately upstream of predicted secondary structures. This is in agreement with results from *in vitro* RNA unwinding assays showing that efficient unwinding is promoted by loading of RNA helicases onto single stranded region adjacent to a duplex (Gross and Shuman, 1996; Yang and Jankowsky, 2006). Thus, the positional accessibility around MOV10 binding sites likely reflects that we were able to capture MOV10 WT while it is working on unwinding structured regions. This implies that the process of unwinding is slower than MOV10's translocation along the RNA, resulting in stalling of MOV10 when it encounters local structures during its tracking along 3'UTRs. In this way, local secondary structures within 3'UTRs can be viewed as roadblocks where MOV10 accumulates until the protein is able to resolve the structure and move on (Figure 23). In contrast to our observation for WT MOV10, we did not observe any decreased positional accessibility downstream of the MOV10 helicase mutants. This is most likely because we captured the MOV10 helicase mutants at their initial binding sites, which are unstructured regions in the

3’UTRs (Figure 23). Similar to our observations, UPF1 has been reported to protect a region immediately upstream of a stable stem loop in PTC-containing reporter construct, while this was not the case for the UPF1 helicase mutant R844C (Shigeoka et al., 2012).

MOV10 Recognizes Accessible Regions without any Clear Sequence Preference

We did not observe any clear enrichment of sequence motifs around MOV10 crosslinking sites. This is in line with the general sequence unspecific recognition of nucleic acids described for other helicases (Appleby et al., 2011; Cheng et al., 2007; Saikrishnan et al., 2009; Sengoku et al., 2006; Singleton et al., 2007; Velankar et al., 1999). Sievers and colleagues reported three sequence motifs as enriched among their identified MOV10 binding sites, however the actual motifs are only observed 10 to 14 times within their 17,053 MOV10 clusters, again indicating that MOV10 recognizes its RNA targets in a sequence unspecific manner (Sievers et al., 2012). If MOV10 works as a general mRNA remodeling factor, this is indeed what would be expected because MOV10 would need to recognize and bind a wide variety of mRNA targets throughout their 3’UTRs. The mode of RNA recognition provided by the helicase domain of MOV10 is therefore perfectly suited for its function as an mRNA scanning factor. Taken together, our PAR-CLIP data indicates a model where MOV10 binds extensively to the vast majority of transcribed transcripts, and that MOV10 is able to translocate along the 3’UTR of those transcripts in a 5’ to 3’ direction.

MOV10 Interacts with UPF1 in a Complex Distinct from UPF2 and UPF3

Using a SILAC based proteomics approach as well as Western blotting of MOV10 and UPF1 IPs, I found that MOV10 and UPF1 proteins interact in a partially RNase sensitive manner. It remains to be determined which domains of MOV10 and UPF1 are responsible for their protein interaction, but we speculate that the previously described CH domains found in both proteins might be involved. Although I identified the core EJC RNA helicase eIF4A3 with enriched SILAC ratios in the MOV10 IPs, the identification was only based on one unique peptide. In contrast, eIF4A3 was identified with 34 unique peptides in the UPF1 IP. Additionally I also identified MAGOH and Y14 as UPF1 interaction partners, but not as MOV10 interaction partners. Together this suggests a stronger interaction between the EJC and UPF1 than for MOV10. The interaction between the EJC complex and UPF1 is bridged by UPF2 and UPF3 (Chamieh et al., 2008; Kim et al., 2001; Le Hir et al., 2001; Melero et al., 2012), which we both

identified with high peptide counts in UPF1 IPs. The interaction between UPF1, UPF2 and UPF3 serves to activate the helicase activity of UPF1 and commits UPF1-targeted transcript to decay (Chakrabarti et al., 2011; Chamieh et al., 2008; Kashima et al., 2006). Since we did not identify any peptides for UPF2 or UPF3 in MOV10 IPs, we expect that MOV10 interacts with UPF1 which have not been activated/committed to promote mRNA decay or alternatively after dissociation of UPF2 and UPF3 from the surveillance complex. Interestingly, the protein level of UPF1 is 3-fold more abundant than MOV10 in NIH3T3 cells, whereas the protein abundances of UPF2 and UPF3 are more than 10-fold less than UPF1 (Schwanhausser et al., 2011). This indicates that UPF1 is not the limiting factor for NMD, but likely associates with several transcripts, and that NMD is only activated under certain circumstances. The partially RNase sensitive interaction between UPF1 and MOV10 suggests that UPF1 and MOV10 might interact before they bind RNA or alternatively that MOV10 could be recruited to UPF1 binding sites in 3'UTRs through direct interaction with RNA-bound UPF1 that has not yet been activated and committed for decay.

UPF1 Binding to 3'UTRs and its Role in NMD

Two recent studies have reported the identification of UPF1 binding sites using CLIP-Seq and iCLIP (Hurt et al., 2013; Zund et al., 2013). UPF1 binds mainly to 3'UTRs in cells with ongoing translation, however upon translational inhibition the fraction of UPF1 bound to coding regions increased, indicating that UPF1 normally gets displaced from coding regions by the ribosome (Hurt et al., 2013; Zund et al., 2013). UPF1 binding to 3'UTRs was first suggested by Hogg and Goff and have also been validated for the well characterized β-globin 39 NMD reporter (Hogg and Goff, 2010; Kurosaki and Maquat, 2013). Both studies found the extent of UPF1 associated with 3'UTRs to correlate with NMD susceptibility (Hogg and Goff, 2010; Kurosaki and Maquat, 2013). In yeast, extended 3'UTRs have also been reported to accelerate UPF1-mediated decay (Muhlrad and Parker, 1999). EJC-independent degradation of the PTC-containing immune-globulin-μ minigene in human cells also depends on its 3'UTR length (Buhler et al., 2006). Increased distance between the stop codon and the end of the 3'UTR stimulates NMD in both *S. cerevisiae*, *C. elegans*, *D. melanogaster* and mammalian cells indicating that increased 3'UTR length is correlated with increased UPF1-mediated targeting across species (Amrani et al., 2004; Behm-Ansmant et al., 2007; Eberle et al., 2008; Ivanov et al., 2008; Longman et al., 2007; Silva et al., 2008; Singh et al., 2008). In *S. cerevisiae* the 3'UTR length typically ranges from 50-200 nt and mRNA transcripts with extremely long 3'UTRs are frequently targeted for UPF1-mediated

decay (Kebaara and Atkin, 2009). In humans, the length of 3'UTRs are generally around 700 nt and also here mRNA transcripts with long 3'UTRs are regulated by UPF1 (Eberle et al., 2008; Ivanov et al., 2008; Silva et al., 2008; Singh et al., 2008), although a subset of mRNAs with long 3'UTRs seem to have evolved mechanisms to evade UPF1-mediated regulation (Singh et al., 2008). However, not the length alone but rather the physical distance between the stop codon and the 3' end of the mRNA transcript might be the determining factor, since 3'UTR fold-back constructs were found to stabilize NMD targeted reporters (Eberle et al., 2008). This effect might be caused by PABPC1, which is known to antagonize NMD when it is tethered to the proximity of a stop codon (Behm-Ansmant et al., 2007; Ivanov et al., 2008; Silva et al., 2008; Singh et al., 2008). Both PABPC1 and UPF1 can interact with the eukaryotic release factors and it has been suggested that whether a termination event is recognized as premature or not depend on competition between PABPC1 and UPF1-EJC for interaction with the release factors eRF1 and eRF3, where formation of the activated SMG-1-UPF1-eRF1-eRF3 (SURF) complex promotes NMD (Czaplinski et al., 1998; Ivanov et al., 2008; Kashima et al., 2006; Singh et al., 2008; Wang et al., 2001). We found increased MOV10 binding to long 3'UTRs, indicating that MOV10 is preferentially promoting mRNA degradation of mRNA transcripts with long 3'UTRs. This could be caused by increased UPF1-mediated degradation of these transcripts, increased length between the termination ribosome and PABPC1 or because transcripts with long 3'UTRs in general are more dependent on removal of secondary structures and 3'UTR protein displacement prior to degradation.

In a similar manner to how translating ribosomes are able to displace UPF1 from coding regions (Hurt et al., 2013; Zund et al., 2013), read-through events are also able to displace 3'UTR-bound UPF1 preventing UPF1-mediated degradation (Hogg and Goff, 2010). Based on the 3'UTR binding pattern of UPF1, it has been suggested that differential disruption of UPF1 binding to 3'UTRs could serve as a mechanism to sense 3'UTR lengths and regulate mRNA degradation (Hogg and Goff, 2010). Interestingly, rare read-through events were found to allow UPF1 binding to 3'UTRs, but prevent a downstream rate-limiting step for mRNA degradation (Hogg and Goff, 2010). Thus it could be speculated that binding of UPF2, UPF3 and/or the SURF complex to UPF1 represent the rate-limiting step when UPF1 is bound to 3'UTRs. A way for the EJC to accelerate decay could be by providing a binding platform for UPF2 and UPF3 and thus facilitating UPF1 activation (Le Hir et al., 2001; Melero et al., 2012). In contrast, activation of 3'UTR-bound UPF1 might depend on diffusion to bring UPF2 and UPF3 to the sites of UPF1. In support of this, EJC-independent NMD was found to be more sensitive to UPF2 and UPF3 levels than EJC-accelerated decay (Metze et al., 2013). According to this model, NMD can take place in

an EJC-accelerated manner or in a slower 3'UTR length sensing manner. Indeed evidence suggests that this is the case for two widely used NMD reporters, namely the immunoglobulin-μ minigene and the β-globin reporter. Presence of a downstream EJC was found not to be required for NMD-mediated decay, but only to accelerate the decay of both reporter (Metze et al., 2013). This implies that a large fraction of UPF1 associated with MOV10 is not necessarily bound to RNA at the sites of the EJC or associated with UPF2 and UPF3, but instead represents independent binding of UPF1 to 3'UTRs. To complicate matters more, the different NMD reporters also showed different dependencies on the decay factors SMG5, SMG6 and SMG7, indicating that transcripts targeted for NMD can be degraded through different routes (Metze et al., 2013; Schweingruber et al., 2013). Interestingly, the helicase activity of UPF1 is necessary for the disassembly of mRNPs undergoing NMD (Franks et al., 2010). It is believed that in the absence of mRNP disassembly, the exonuclease XRN1 is unable to degrade the 3' NMD decay RNA intermediate generated by SMG6-mediated endonucleolytic cleavage. However, while UPF1's helicase activity is required for the release of the NMD surveillance complex from the 3' NMD decay intermediate, it is not required for the displacement of PABPC1 or components of the EJC, suggesting a downstream step required for complete mRNP disassembly (Franks et al., 2010).

Regulation of PTC-containing NMD-Targeted Reporter by MOV10

To investigate whether MOV10 is involved in NMD-mediated degradation of PTC-containing mRNAs, I tested the effect of MOV10 depletion on the well-characterized β-globin reporter with a PTC at position 39 (Lykke-Andersen et al., 2000; Lykke-Andersen and Wagner, 2005). This reporter is rapidly degraded by the NMD pathway in a manner that is highly EJC-dependent (Metze et al., 2013). Movement of the PTC to the last exon, where there is no upstream EJC greatly reduces the degradation rate of the transcript (Hall and Thein, 1994; Kurosaki and Maquat, 2013). Compared to mock transfected cells, we observed decreased degradation rates upon both UPF1 and MOV10 depletion, indicating that MOV10 is involved in promoting degradation of PTC-containing transcripts. Strikingly, we observe much higher levels of the reporter at the 0 hr time points both in the case of UPF1 and MOV10 depletion compared to mock transfected cells. We speculate that this might be caused by increased accumulation of the mRNA reporter during the 12 hrs where the transcription of the reporter is turned on. Supporting this, shortening of the transcriptional pulse to 3 hrs reduced the difference in the starting amount between mock and knockdown samples. Unfortunately, the amount of transcribed reporter

transcript after 3 hrs transcriptional pulse was not sufficient to measure decay over time and was therefore not used (data not shown).

Stabilization of MOV10-targeted Transcripts upon MOV10 Depletion

The lifespan of an mRNA is largely regulated through association with mRNA-binding proteins as well as non-coding RNA targeting mRNAs for degradation. Since we observed an extensive binding of MOV10 to thousands of transcripts, we wondered whether the function of MOV10 is restricted to its involvement in degradation of PTC-containing transcripts or if MOV10 is able to function as a general factor in regulation of mRNA turnover. To address this issue, we determined the mRNA half-lives globally upon MOV10 depletion using a protocol for metabolic labeling of RNA. We found that mRNA transcripts heavily covered by MOV10-binding sites in their 3'UTR were up-regulated upon MOV10 knockdown, indicating that MOV10 normally is promoting degradation of its mRNA target transcripts. This was validated for 4 fast turnover MOV10 targets by qRT-PCR after actinomycin D treatment. In addition, degradation of the known UPF1 target PANK2 was also stabilized upon MOV10 knockdown (Chan et al., 2007; Tani et al., 2012). Despite the changes in mRNA half-lives, we did not observe a corresponding change of MOV10 targets on steady-state mRNA levels. We speculate that this could be due to feedback mechanisms or compensatory effects that buffer global changes in mRNA half-lives (Sun et al., 2012).

MOV10 May Affect miRNA Regulation Through Displacement of AGO2 From its Target Sites in 3'UTRs

Several reports have indicated that MOV10 plays a role in miRNA-mediated regulation (Banerjee et al., 2009; Chendrimada et al., 2007; Meister et al., 2005). However, a recent study comparing AGO2 co-IPs in the presence and absence of RNase found the interaction between MOV10 and AGO2 to be highly dependent on the presence of RNA (Frohn et al., 2012). In agreement with Frohn and colleagues, we also found that the interaction between MOV10 and AGO2 is sensitive to RNase treatment, suggesting that MOV10 is not directly involved in miRNA-mediated regulation, but may simply contact regions of 3'UTRs also occupied by AGO2. Our data also does not suggest that MOV10 recognizes miRNA-binding sites, since MOV10 binding around miRNA-binding sites were not enriched. Interestingly, we observed an almost uniform distribution of MOV10 PAR-CLIP reads around miRNA-binding sites. This is in contrast to

ELAVL1 PAR-CLIP sites that are clearly depleted around predicted miRNA-binding sites (Lebedeva et al., 2011). This indicates that MOV10, unlike other 3'UTR binding proteins such as ELAVL1, may be able to displace AGO2 bound to miRNA-binding sites in 3'UTRs. We speculated that MOV10 'meets' AGO2 during its translocation along 3'UTRs and that MOV10 is involved in displacement of AGO2 from its mRNA targets. In this scenario, MOV10 would promote recycling of AGO2, allowing it to bind to additional transcripts, and thus indirectly affecting the miRNA-mediated regulation. This might explain why other studies have found that MOV10 knockdown affects miRNA-mediated repression (Chendrimada et al., 2007; Meister et al., 2005). If MOV10 works to displace AGO2 from its targets, then MOV10 depletion would result in impaired AGO2 recycling.

Implication for MOV10 Regulation of Retroviral Activity and Retrotransposable Elements

That MOV10 is able to regulate mRNA degradation suggests that MOV10 may function in regulation of HIV-1 expression as well as regulation of retrotransposable elements by regulating mRNA degradation and/or mRNP disassembly. MOV10's ability to inhibit LINE-1 retrotransposition was suggested to be due to accelerated mRNA decay of LINE-1 upon MOV10 over-expression (Li et al., 2013). An intact helicase core of MOV10 is required for inhibition of both LINE-1 and IAP replication, indicating that MOV10 needs to translocate and/or unwind structures in order to regulate retrotransposition (Goodier et al., 2012; Li et al., 2013). Similarly, MOV10's regulation of retroviral activity was also found to be dependent on the presence of its helicase domain raising the possibility that MOV10 regulates the stability of viral transcripts by promoting degradation and mRNP disassembly (Goodier et al., 2012; Li et al., 2013). Interestingly, we found ZC3HAV1 as a MOV10 interaction partner. ZC3HAV1 has HIV-1 anti-viral activity and works by recruiting the poly(A)-specific ribonuclease (PARN) to viral mRNA which leads to poly(A) shortening and mRNA degradation (Zhu et al., 2011). Thus, it could be speculated that MOV10 and ZC3HAV1 work together to promote degradation of viral mRNAs.

No Implication of MOV10 in Chromatin Remodeling

In agreement with numerous reports we found MOV10 to be localized primarily to the cytoplasm and P-bodies (Burdick et al., 2010; Gallois-Montbrun et al., 2007; Goodier et al., 2012; Izumi et al., 2013; Lu et al., 2012; Meister et al., 2005). Both studies reporting a nuclear localization of MOV10 used antibodies, which have not been used in any of the papers reporting a cytoplasmic

localization of MOV10, raising the possibility that the different reports of MOV10's localization is due to the different antibodies used (El Messaoudi-Aubert et al., 2010; Sievers et al., 2012). Epitope-tagged MOV10 has consistently been found to localize to the cytoplasm and P-bodies (Burdick et al., 2010; Gallois-Montbrun et al., 2007; Goodier et al., 2012; Izumi et al., 2013; Lu et al., 2012; Meister et al., 2005). MOV10 localization to P-bodies is dependent on the presence of helicase motif V, indicating that MOV10 needs to bind RNA in order to localize to P-bodies (Izumi et al., 2013).

We observe no support of MOV10's role in chromatin remodeling based on our PAR-CLIP data or identification of MOV10's protein interaction partners. A study performing proteomics of purified CBX7 protein complexes did not find MOV10 among the identified CBX7 interacting proteins (Yap et al., 2010). Moreover, electrophoretic mobility shift assays showed that the chromodomain of CBX7 interacts directly with *ANRIL* (Yap et al., 2010). Similarly to previously reported we also we did not observe any binding of MOV10 to the long non-coding RNA *ANRIL* (Sievers et al., 2012) , however this could also be due to its low expression level in HEK293 cells.

Possible Role of MOV10 in Post-Transcriptional Subcellular Regulation of mRNAs

MOV10 has an extremely long protein half-life of more than 100 hrs in NIH3T3 cells (Schwanhausser et al., 2011). For comparison the median protein half-life is 48 hrs (Schwanhausser et al., 2011). Evidence suggests that MOV10 expression is regulated in a subcellular manner by ubiquitination and proteasome mediated degradation in active synapses (Banerjee et al., 2009). This provides a mechanism for local subcellular regulation of mRNP remodeling, allowing mRNA turnover and protein synthesis to be regulated differentially in different compartments of the cell. In light of the long half-life of MOV10 it seems appropriate that the cells have a way to regulate the protein level of MOV10 through promoting its protein degradation, thus allowing a fine-tuning of its post-transcriptional regulation. The ubiquitin ligase responsible for MOV10 ubiquitination is unknown. In our proteomics of MOV10 IPs, we identified RNF166 as highly enriched in both label-swap experiments. RNF166 together with RNF114, RNF125 and RNF138 comprise a novel family of ubiquitin ligases that in addition to an N-terminal RING domain also contain an C-terminal zinc finger domain as well as a ubiquitin binding domain (UIM domain) (Giannini et al., 2008). Our finding that MOV10 and RNF166 interact suggests that RNF166 may be responsible for the reported ubiquitination of MOV10. Like MOV10, eIF4A3 is also localized to subcellular compartments of neuronal cells allowing for

differential mRNA repression of the synaptic mRNA Arc through NMD in neuronal granules (Giorgi et al., 2007). In addition, a recent study reported that local regulation of axonal mRNAs mediated by NMD at the tip of axonal growth cones are required for proper growth of axons across the midline floor plate (Colak et al., 2013). Together these studies provide examples of how local gene-regulation can be achieved through regulation of mRNA-binding proteins that in turn are involved in mRNP remodeling and underline the complexity of post-transcriptional regulation of mRNP dynamics mediated by RNA helicases.

Model of MOV10 Target Regulation

Considering the binding pattern of MOV10 and its helicase mutants throughout 3'UTRs we propose a model where MOV10 is recruited to sites in the beginning of 3'UTRs from where it is able to translocate in a 5' to 3' direction along the 3'UTR stalling at sites upstream of secondary structures and potentially displaces proteins involved in post-transcriptional regulation (summarized in Figure 23). We do not know how MOV10 gets recruited to the beginning of 3'UTRs, but we speculate that its recruitment might involve UPF1 or interactions with the terminating ribosome due to the strong binding of MOV10 helicase mutant 30 nt downstream of the stop codon. We observed increased mRNA half-lives of transcripts highly bound by MOV10 upon MOV10 depletion, indicating that MOV10 is able to promote mRNA degradation of its targeted transcripts. This was further validated for 4 MOV10-targeted transcripts as well as for a known UPF1 target using a different experimental setup to measure mRNA degradation. Based on the predicted positional accessibility around MOV10 bound sites, we postulate that MOV10 is involved in resolving local RNA secondary structures in 3'UTRs. Protein displacement activity has been shown for other processive RNA helicases (Jankowsky et al., 2000) and we suspect that MOV10 also has protein displacement activity due to the nature of its RNA-binding pattern and lack of depletion around AGO2 occupied sites. Taken together with MOV10's role in mRNA turnover, we hypothesize a model where MOV10 works as a mRNP remodeling/clearance factor paving the way for 5' to 3' exonucleolytic decay. mRNP remodeling prior to mRNA degradation might be especially crucial for UPF1-targeted transcripts that are turned over rapidly by NMD.

It is not possible to say whether all MOV10-targeted transcripts are also UPF1 targets. Al UPF1 is 3-fold more abundant than MOV10, its binding to 3'UTRs is much more modest than MOV10, indicating that it may not be possible to compressively capture UPF1-regulated mRNA transcripts based on CLIP techniques because UPF1 is only briefly associated with its targets (Hurt et al., 2013; Zund et al., 2013). A recent study has indicated that degradation of PTC-

containing transcripts targeted for NMD may occur in less than 1 min after export from the nucleus, emphasizing the difficulties in capturing UPF1 bound to PTC-containing targets (Trcek et al., 2013). Based on this, it is tempting to speculate that the transcripts we captured with PAR-CLIP are devoid of PTC-containing NMD targets, but instead represent non-PTC-containing transcripts regulated by UPF1 through 3'UTR length sensing as previously described (Hogg and Goff, 2010).

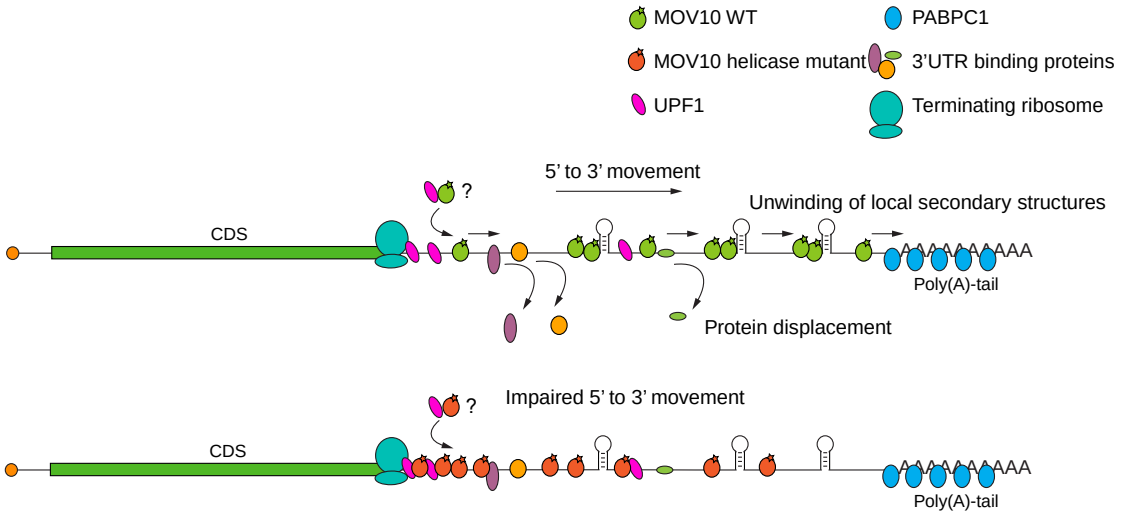

Figure 23. Model of MOV10 function as a 3'UTR mRNP clearance factor.

MOV10 binds to the beginning of 3'UTRs and translocate along 3'UTRs in a 5' to 3' direction. This translocation may result in displacement of proteins bound to 3'UTRs. When MOV10 encounters local secondary structures it accumulates upstream of the structures, likely because RNA unwinding is rate-limiting. In case of catalytically inactive helicase mutants (lacking ATPase activity) the 5' to 3' translocation of MOV10 along 3'UTRs is impaired (lower panel) and we do not observe any accumulation of the helicase mutants immediately upstream of local secondary structures. MOV10 helicase mutants accumulate in the beginning of 3'UTRs with the highest binding 30 nt downstream of the stop codon. It remains unresolved how MOV10 is recruited to 3'UTRs, but we speculate that UPF1 might be able to recruit MOV10 possibly through interactions with the terminating ribosome.

Taken together our study has demonstrated a role of MOV10 in mRNA degradation together with UPF1. How the interplay between MOV10 and UPF1 exactly affects mRNA degradation remains to be addressed in the future. However, based on our data, we suggest that MOV10 is recruited to UPF1-targeted transcripts downstream of UPF1. Since UPF1 interacts with the eukaryotic release factors and both UPF1 and MOV10 preferentially bind to the 5' end of 3'UTRs, it is possible that UPF1 can recruit MOV10 to the beginning of 3'UTR through interaction with the terminating ribosome (Czaplinski et al., 1998; Ivanov et al., 2008; Kashima et al., 2006; Wang et al., 2001; Zund et al., 2013). Because the UPF1's helicase activity is inhibited when it is not associated with UPF2, we speculate that MOV10 represents a more processive RNA helicase than UPF1 with the ability to translocate along 3'UTRs. UPF1 on the contrary,

might be caught in a clamping mode similarly to the eIF4A3 RNA helicase in the EJC when it is associated to 3'UTRs without bound UPF2. Thus whereas UPF1 is essential for marking mRNA transcripts for degradation through its recognition of PTC-containing transcripts, MOV10 might be the facilitator to promote the mRNA degradation through its 3'UTR mRNP clearance activity.

Evolutionary Perspective on the Role of MOV10 and UPF1

As mentioned in the introduction MOV10 is related to Armitage in *D. melanogaster* and SDE3 in *A. thaliana*. In addition, MOV10 has a human paralog MOV10L1. Armitage likely represents the ancestor of MOV10L1, because both function in the piRNA-mediated repression of retrotransposable elements in the germline (Cook et al., 2004; Malone et al., 2009), although Armitage unlike MOV10L1 also has been shown to function in somatic cells (Haase et al., 2010; Olivieri et al., 2010). The ping-pong cycle used for amplification of piRNAs in the germline of *D. melanogaster* might work in a similar manner to the SDE3-RDR6 amplification of viral RNA in *A. thaliana*. However, the ping-pong cycle in *D. melanogaster* was shown to act independently of both PIWI and Armitage, but instead requires the RNA helicases Spindle-E and Vasa (Malone et al., 2009). Thus it seems that there might be some mechanistic differences in the roles of SDE3, Armitage and MOV10L1 in RNAi pathways, although a common function for all proteins is the silencing of retroelements. We speculate that MOV10 evolved from MOV10L1 as a result of a gene duplication event. At some point MOV10 must have acquired somatic expression or MOV10L1 expression must have been restricted to the germline. Unlike SDE3, Armitage and MOV10L1, there is no evidence suggesting that MOV10's role in inhibition of somatic retroelements requires the involvement of RNAi pathways. On the contrary MOV10's ability to inhibit LINE-1 elements was shown to be unaffected by AGO2 knockdown (Li et al., 2013). A common theme for all proteins is the removal of potential harmful RNA species. In a similar manner, UPF1 has also been suggested as a general factor working to reduce genomic noise, through removal of non-functional RNAs, such as transcribed pseudogenes, transposons, natural antisense transcript and RNA-like non-coding RNAs (Kurihara et al., 2009; Mendell et al., 2004; Mitrovich and Anderson, 2005). The UPF1 homolog in *C. elegans* has been shown to suppress expression of transcribed pseudogenes (Mitrovich and Anderson, 2005). Similarly, mutation of the *A. thaliana* UPF1 homolog, upf1, resulted in up-regulation of natural antisense transcripts and non-coding RNAs resembling protein-coding mRNAs (Kurihara et al., 2009). In yeast, mRNAs with extended 3'UTRs are degraded in a manner dependent on Upf1, Upf2 and Upf3 as well as the decapping enzyme Dcp1 and Xrn1, suggesting that Upf1 is also involved in 3'UTR length

sensing in yeast (Muhlrad and Parker, 1999). MOV10 has no known yeast homolog, meaning that UPF1-mediated decay in yeast must take place independently of MOV10. However, since the lengths of human 3'UTRs generally are much longer than in yeast, this may explain the additional need for MOV10 to remodel mRNPs prior to mRNA degradation in humans.

In contrast to mammals, NMD in *A. thaliana*, yeast, *C. elegans* and *D. melanogaster* occurs independently of the EJC (Behm-Ansmant et al., 2007; Gatfield et al., 2003; Kerenyi et al., 2008; Longman et al., 2007; Wen and Brogna, 2010). Deletion of *upf1* in yeast is not lethal, but in mice *Upf1* knockout is embryonic lethal (Behm-Ansmant et al., 2007; Longman et al., 2007; Medghalchi et al., 2001). This is also the case for Upf2 knockout mice, suggesting that the embryonic lethality of *Upf1* knockout is due to its role in NMD (Weischenfeldt et al., 2008). Whereas *Mov10l1* knockout mice display male infertility (Frost et al., 2010; Zheng et al., 2010), no knockout mouse model for *Mov10* has been described to date. It is plausible that the function of MOV10 is in some ways redundant to UPF1 and that MOV10 works as a facilitator to promote degradation of UPF1-targeted transcripts. In addition, MOV10 seems to be involved in inhibition of retroviral infections and retrotranspositions in somatic cells, indicative of MOV10-mediated regulation of mRNA turnover beyond UPF1-mediated degradation.

CONCLUSIONS AND OUTLOOK

Here I have presented a role for the RNA helicase MOV10 in mRNA degradation and provided evidence of its 5' to 3' directional translocation on its RNA targeted transcripts. Furthermore I have shown that MOV10 interacts with the related RNA helicase UPF1. As evidence that MOV10 plays a role in promoting mRNA degradation of UPF1-targeted transcripts I found that MOV10 depletion results in impaired degradation of a PTC-containing reporter transcript and the known non-PTC-containing transcript PANK2.

The field of mapping RNA-protein interactions together with the study of mRNP remodeling is rapidly evolving, especially due to the introduction of methods such as CLIP and global occupancy profiles of RNA interacting proteins, which allows studies of RNA-protein interactions on a genome-wide scale. The development of these new techniques has opened the door to study the interplay between different RNA interacting proteins and higher order structures of mRNPs. However questions still remain as to how dynamic mRNP remodeling is regulated in a spatial temporal manner. How fast are mRNPs targeted for decay and how is the localization and dynamic remodeling of mRNPs regulated? Studies of eIF4A3 and UPF1 indicate that they can trigger a certain mRNP fate only to a subset of mRNPs based on their localization within cells. Moreover the activity of UPF1 is tightly regulated through phosphorylation and re-arrangement of its CH domain providing an 'on-off' switch for UPF1 mediated regulation. MOV10 can be targeted for degradation by ubiquitination. We found the ubiquitin ligase RNF166 as an interaction partner of MOV10 raising the possibility that RNF166 might regulate the MOV10 levels in response to signals yet to be determined. Thus, an interesting area of study would be the influence of RNF166 on MOV10-mediated mRNA target regulation.

RNA surveillance mechanisms exist for every step of RNA processing and function to remove non-functional and potentially harmful RNA spices, including viral RNA transcripts and retrotransposons. However, RNA surveillance mechanisms allow the formation of novel functional RNA species for instance as generated by alternative splicing and thus provide means for the exploration of new RNA species and expansion of the RNA diversity within the framework set up by the RNA surveillance mechanisms. MOV10 functions both in retroviral defense, to restrict retrotransposons and to promote the degradation of UPF1-targeted transcripts.

It is likely that the function of MOV10 in all processes is based on the same molecular mechanism, namely MOV10's ability to translocate along its RNA targets in a 5' to 3' directional manner. In this study I have focused on MOV10 binding sites located within coding transcripts, however it would be interesting to expand the catalog of MOV10 binding sites to retrotransposable elements or to map MOV10's binding sites within retroviral RNA transcripts following a cellular infection.

REFERENCES

Abudu, A., Wang, X., Dang, Y., Zhou, T., Xiang, S.H., and Zheng, Y.H. (2012). Identification of molecular determinants from Moloney leukemia virus 10 homolog (MOV10) protein for virion packaging and anti-HIV-1 activity. J Biol Chem *287*, 1220-1228.

Aitken, C.E., and Lorsch, J.R. (2012). A mechanistic overview of translation initiation in eukaryotes. Nature Structural & Molecular Biology *19*, 568-576.

Amrani, N., Ganesan, R., Kervestin, S., Mangus, D.A., Ghosh, S., and Jacobson, A. (2004). A faux 3'-UTR promotes aberrant termination and triggers nonsense-mediated mRNA decay. Nature *432*, 112-118.

Anantharaman, V., Koonin, E.V., and Aravind, L. (2002). Comparative genomics and evolution of proteins involved in RNA metabolism. Nucleic Acids Res *30*, 1427-1464.

Andersen, C.B., Ballut, L., Johansen, J.S., Chamieh, H., Nielsen, K.H., Oliveira, C.L., Pedersen, J.S., Seraphin, B., Le Hir, H., and Andersen, G.R. (2006). Structure of the exon junction core complex with a trapped DEAD-box ATPase bound to RNA. Science *313*, 1968-1972.

Appleby, T.C., Anderson, R., Fedorova, O., Pyle, A.M., Wang, R., Liu, X., Brendza, K.M., and Somoza, J.R. (2011). Visualizing ATP-dependent RNA translocation by the NS3 helicase from HCV. J Mol Biol *405*, 1139-1153.

Arjan-Odedra, S., Swanson, C.M., Sherer, N.M., Wolinsky, S.M., and Malim, M.H. (2012). Endogenous MOV10 inhibits the retrotransposition of endogenous retroelements but not the replication of exogenous retroviruses. Retrovirology *9*, 53.

Auweter, S.D., Oberstrass, F.C., and Allain, F.H. (2006). Sequence-specific binding of single-stranded RNA: is there a code for recognition? Nucleic Acids Res *34*, 4943-4959.

Ballut, L., Marchadier, B., Baguet, A., Tomasetto, C., Seraphin, B., and Le Hir, H. (2005). The exon junction core complex is locked onto RNA by inhibition of eIF4AIII ATPase activity. Nat Struct Mol Biol *12*, 861-869.

Baltz, A.G., Munschauer, M., Schwanhausser, B., Vasile, A., Murakawa, Y., Schueler, M., Youngs, N., Penfold-Brown, D., Drew, K., Milek, M., *et al.* (2012). The mRNA-bound proteome and its global occupancy profile on protein-coding transcripts. Mol Cell *46*, 674-690.

Banerjee, S., Neveu, P., and Kosik, K.S. (2009). A coordinated local translational control point at the synapse involving relief from silencing and MOV10 degradation. Neuron *64*, 871-884.

Bartel, D.P. (2009). MicroRNAs: target recognition and regulatory functions. Cell *136*, 215-233.

Behm-Ansmant, I., Gatfield, D., Rehwinkel, J., Hilgers, V., and Izaurralde, E. (2007). A conserved role for cytoplasmic poly(A)-binding protein 1 (PABPC1) in nonsense-mediated mRNA decay. EMBO J *26*, 1591-1601.

Belancio, V.P., Roy-Engel, A.M., Pochampally, R.R., and Deininger, P. (2010). Somatic expression of LINE-1 elements in human tissues. Nucleic Acids Res *38*, 3909-3922.

Bentley, D.L. (2005). Rules of engagement: co-transcriptional recruitment of pre-mRNA processing factors. Curr Opin Cell Biol *17*, 251-256.

Beran, R.K., Bruno, M.M., Bowers, H.A., Jankowsky, E., and Pyle, A.M. (2006). Robust translocation along a molecular monorail: the NS3 helicase from hepatitis C virus traverses unusually large disruptions in its track. J Mol Biol *358*, 974-982.

Bessonov, S., Anokhina, M., Will, C.L., Urlaub, H., and Luhrmann, R. (2008). Isolation of an active step I spliceosome and composition of its RNP core. Nature *452*, 846-850.

Bhattacharya, A., Czaplinski, K., Trifillis, P., He, F., Jacobson, A., and Peltz, S.W. (2000). Characterization of the biochemical properties of the human Upf1 gene product that is involved in nonsense-mediated mRNA decay. RNA *6*, 1226-1235.

Bhattacharyya, S.N., Habermacher, R., Martine, U., Closs, E.I., and Filipowicz, W. (2006). Relief of microRNA-mediated translational repression in human cells subjected to stress. Cell *125*, 1111-1124.

Bleichert, F., and Baserga, S.J. (2007). The long unwinding road of RNA helicases. Mol Cell *27*, 339-352.

Bohnsack, M.T., Czaplinski, K., and Gorlich, D. (2004). Exportin 5 is a RanGTP-dependent dsRNA-binding protein that mediates nuclear export of pre-miRNAs. RNA *10*, 185-191.

Bohnsack, M.T., Martin, R., Granneman, S., Ruprecht, M., Schleiff, E., and Tollervey, D. (2009). Prp43 bound at different sites on the pre-rRNA performs distinct functions in ribosome synthesis. Mol Cell *36*, 583-592.

Bono, F., Ebert, J., Lorentzen, E., and Conti, E. (2006). The crystal structure of the exon junction complex reveals how it maintains a stable grip on mRNA. Cell *126*, 713-725.

Brengues, M., Teixeira, D., and Parker, R. (2005). Movement of eukaryotic mRNAs between polysomes and cytoplasmic processing bodies. Science *310*, 486-489.

Brouha, B., Schustak, J., Badge, R.M., Lutz-Prigge, S., Farley, A.H., Moran, J.V., and Kazazian, H.H., Jr. (2003). Hot L1s account for the bulk of retrotransposition in the human population. Proc Natl Acad Sci U S A *100*, 5280-5285.

Buhler, M., Steiner, S., Mohn, F., Paillusson, A., and Muhlemann, O. (2006). EJC-independent degradation of nonsense immunoglobulin-mu mRNA depends on 3' UTR length. Nat Struct Mol Biol *13*, 462-464.

Burdick, R., Smith, J.L., Chaipan, C., Friew, Y., Chen, J., Venkatachari, N.J., Delviks-Frankenberry, K.A., Hu, W.S., and Pathak, V.K. (2010). P body-associated protein Mov10 inhibits HIV-1 replication at multiple stages. J Virol *84*, 10241-10253.

Castello, A., Fischer, B., Eichelbaum, K., Horos, R., Beckmann, B.M., Strein, C., Davey, N.E., Humphreys, D.T., Preiss, T., Steinmetz, L.M., *et al.* (2012). Insights into RNA biology from an atlas of mammalian mRNA-binding proteins. Cell *149*, 1393-1406.

Chakrabarti, S., Jayachandran, U., Bonneau, F., Fiorini, F., Basquin, C., Domcke, S., Le Hir, H., and Conti, E. (2011). Molecular mechanisms for the RNA-dependent ATPase activity of Upf1 and its regulation by Upf2. Mol Cell *41*, 693-703.

Chamieh, H., Ballut, L., Bonneau, F., and Le Hir, H. (2008). NMD factors UPF2 and UPF3 bridge UPF1 to the exon junction complex and stimulate its RNA helicase activity. Nat Struct Mol Biol *15*, 85-93.

Chan, W.K., Bhalla, A.D., Le Hir, H., Nguyen, L.S., Huang, L., Gecz, J., and Wilkinson, M.F. (2009). A UPF3-mediated regulatory switch that maintains RNA surveillance. Nat Struct Mol Biol *16*, 747-753.

Chan, W.K., Huang, L., Gudikote, J.P., Chang, Y.F., Imam, J.S., MacLean, J.A., 2nd, and Wilkinson, M.F. (2007). An alternative branch of the nonsense-mediated decay pathway. EMBO J *26*, 1820-1830.

Chendrimada, T.P., Finn, K.J., Ji, X., Baillat, D., Gregory, R.I., Liebhaber, S.A., Pasquinelli, A.E., and Shiekhattar, R. (2007). MicroRNA silencing through RISC recruitment of eIF6. Nature *447*, 823-828.

Cheng, Z., Muhlrad, D., Lim, M.K., Parker, R., and Song, H. (2007). Structural and functional insights into the human Upf1 helicase core. EMBO J *26*, 253-264.

Chi, S.W., Zang, J.B., Mele, A., and Darnell, R.B. (2009). Argonaute HITS-CLIP decodes microRNA-mRNA interaction maps. Nature *460*, 479-486.

Colak, D., Ji, S.J., Porse, B.T., and Jaffrey, S.R. (2013). Regulation of axon guidance by compartmentalized nonsense-mediated mRNA decay. Cell *153*, 1252-1265.

Coller, J.M., Tucker, M., Sheth, U., Valencia-Sanchez, M.A., and Parker, R. (2001). The DEAD box helicase, Dhh1p, functions in mRNA decapping and interacts with both the decapping and deadenylase complexes. RNA *7*, 1717-1727.

Cook, H.A., Koppetsch, B.S., Wu, J., and Theurkauf, W.E. (2004). The Drosophila SDE3 homolog armitage is required for oskar mRNA silencing and embryonic axis specification. Cell *116*, 817-829.

Cox, J., and Mann, M. (2008). MaxQuant enables high peptide identification rates, individualized p.p.b.-range mass accuracies and proteome-wide protein quantification. Nat Biotechnol *26*, 1367-1372.

Cox, J., Neuhauser, N., Michalski, A., Scheltema, R.A., Olsen, J.V., and Mann, M. (2011). Andromeda: a peptide search engine integrated into the MaxQuant environment. J Proteome Res *10*, 1794-1805.

Czaplinski, K., Ruiz-Echevarria, M.J., Paushkin, S.V., Han, X., Weng, Y., Perlick, H.A., Dietz, H.C., Ter-Avanesyan, M.D., and Peltz, S.W. (1998). The surveillance complex interacts with the translation release factors to enhance termination and degrade aberrant mRNAs. Genes Dev *12*, 1665-1677.

Dalmay, T., Horsefield, R., Braunstein, T.H., and Baulcombe, D.C. (2001). SDE3 encodes an RNA helicase required for post-transcriptional gene silencing in Arabidopsis. EMBO J *20*, 2069-2078.

Das, R., Yu, J., Zhang, Z., Gygi, M.P., Krainer, A.R., Gygi, S.P., and Reed, R. (2007). SR proteins function in coupling RNAP II transcription to pre-mRNA splicing. Mol Cell *26*, 867-881.

Dolken, L., Ruzsics, Z., Radle, B., Friedel, C.C., Zimmer, R., Mages, J., Hoffmann, R., Dickinson, P., Forster, T., Ghazal, P., *et al.* (2008). High-resolution gene expression profiling for simultaneous kinetic parameter analysis of RNA synthesis and decay. RNA *14*, 1959-1972.

Doucet, A.J., Hulme, A.E., Sahinovic, E., Kulpa, D.A., Moldovan, J.B., Kopera, H.C., Athanikar, J.N., Hasnaoui, M., Bucheton, A., Moran, J.V., *et al.* (2010). Characterization of LINE-1 ribonucleoprotein particles. PLoS Genet *6*.

Eberle, A.B., Stalder, L., Mathys, H., Orozco, R.Z., and Muhlemann, O. (2008). Posttranscriptional gene regulation by spatial rearrangement of the 3' untranslated region. PLoS Biol *6*, e92.

El Messaoudi-Aubert, S., Nicholls, J., Maertens, G.N., Brookes, S., Bernstein, E., and Peters, G. (2010). Role for the MOV10 RNA helicase in polycomb-mediated repression of the INK4a tumor suppressor. Nat Struct Mol Biol *17*, 862-868.

Ernoult-Lange, M., Baconnais, S., Harper, M., Minshall, N., Souquere, S., Boudier, T., Benard, M., Andrey, P., Pierron, G., Kress, M., *et al.* (2012). Multiple binding of repressed mRNAs by the P-body protein Rck/p54. RNA *18*, 1702-1715.

Eulalio, A., Behm-Ansmant, I., and Izaurralde, E. (2007). P bodies: at the crossroads of post-transcriptional pathways. Nat Rev Mol Cell Biol *8*, 9-22.

Fairman-Williams, M.E., Guenther, U.P., and Jankowsky, E. (2010). SF1 and SF2 helicases: family matters. Curr Opin Struct Biol *20*, 313-324.

Fairman, M.E., Maroney, P.A., Wang, W., Bowers, H.A., Gollnick, P., Nilsen, T.W., and Jankowsky, E. (2004). Protein displacement by DExH/D "RNA helicases" without duplex unwinding. Science *304*, 730-734.

Fenger-Gron, M., Fillman, C., Norrild, B., and Lykke-Andersen, J. (2005). Multiple processing body factors and the ARE binding protein TTP activate mRNA decapping. Mol Cell *20*, 905-915.

Fiorini, F., Boudvillain, M., and Le Hir, H. (2013). Tight intramolecular regulation of the human Upf1 helicase by its N- and C-terminal domains. Nucleic Acids Res *41*, 2404-2415.

Franks, T.M., Singh, G., and Lykke-Andersen, J. (2010). Upf1 ATPase-dependent mRNP disassembly is required for completion of nonsense- mediated mRNA decay. Cell *143*, 938-950.

Frohn, A., Eberl, H.C., Stohr, J., Glasmacher, E., Rudel, S., Heissmeyer, V., Mann, M., and Meister, G. (2012). Dicer-dependent and -independent Argonaute2 Protein Interaction Networks in Mammalian Cells. Mol Cell Proteomics *11*, 1442-1456.

Frost, R.J., Hamra, F.K., Richardson, J.A., Qi, X., Bassel-Duby, R., and Olson, E.N. (2010). MOV10L1 is necessary for protection of spermatocytes against retrotransposons by Piwi-interacting RNAs. Proc Natl Acad Sci U S A *107*, 11847-11852.

Furtak, V., Mulky, A., Rawlings, S.A., Kozhaya, L., Lee, K., Kewalramani, V.N., and Unutmaz, D. (2010). Perturbation of the P-body component Mov10 inhibits HIV-1 infectivity. PLoS One *5*, e9081.

Gallois-Montbrun, S., Holmes, R.K., Swanson, C.M., Fernandez-Ocana, M., Byers, H.L., Ward, M.A., and Malim, M.H. (2008). Comparison of cellular ribonucleoprotein complexes associated with the APOBEC3F and APOBEC3G antiviral proteins. J Virol *82*, 5636-5642.

Gallois-Montbrun, S., Kramer, B., Swanson, C.M., Byers, H., Lynham, S., Ward, M., and Malim, M.H. (2007). Antiviral protein APOBEC3G localizes to ribonucleoprotein complexes found in P bodies and stress granules. J Virol *81*, 2165-2178.

Garcia, D., Garcia, S., Pontier, D., Marchais, A., Renou, J.P., Lagrange, T., and Voinnet, O. (2012). Ago hook and RNA helicase motifs underpin dual roles for SDE3 in antiviral defense and silencing of nonconserved intergenic regions. Mol Cell *48*, 109-120.

Garneau, N.L., Wilusz, J., and Wilusz, C.J. (2007). The highways and byways of mRNA decay. Nat Rev Mol Cell Biol *8*, 113-126.

Gatfield, D., Unterholzner, L., Ciccarelli, F.D., Bork, P., and Izaurralde, E. (2003). Nonsense-mediated mRNA decay in Drosophila: at the intersection of the yeast and mammalian pathways. EMBO J *22*, 3960-3970.

Gehring, N.H., Neu-Yilik, G., Schell, T., Hentze, M.W., and Kulozik, A.E. (2003). Y14 and hUpf3b form an NMD-activating complex. Mol Cell *11*, 939-949.

Geiss, G.K., Bumgarner, R.E., Birditt, B., Dahl, T., Dowidar, N., Dunaway, D.L., Fell, H.P., Ferree, S., George, R.D., Grogan, T., *et al.* (2008). Direct multiplexed measurement of gene expression with color-coded probe pairs. Nat Biotechnol *26*, 317-325.

Giannini, A.L., Gao, Y., and Bijlmakers, M.J. (2008). T-cell regulator RNF125/TRAC-1 belongs to a novel family of ubiquitin ligases with zinc fingers and a ubiquitin-binding domain. Biochem J *410*, 101-111.

Giorgi, C., Yeo, G.W., Stone, M.E., Katz, D.B., Burge, C., Turrigiano, G., and Moore, M.J. (2007). The EJC factor eIF4AIII modulates synaptic strength and neuronal protein expression. Cell *130*, 179-191.

Gleghorn, M.L., Gong, C., Kielkopf, C.L., and Maquat, L.E. (2013). Staufen1 dimerizes through a conserved motif and a degenerate dsRNA-binding domain to promote mRNA decay. Nat Struct Mol Biol *20*, 515-524.

Gong, C., and Maquat, L.E. (2011). lncRNAs transactivate STAU1-mediated mRNA decay by duplexing with 3' UTRs via Alu elements. Nature *470*, 284-288.

Goodier, J.L., Cheung, L.E., and Kazazian, H.H., Jr. (2012). MOV10 RNA Helicase Is a Potent Inhibitor of Retrotransposition in Cells. PLoS Genet *8*, e1002941.

Greenberg, J.R. (1979). Ultraviolet light-induced cross-linking of mRNA to proteins. Nucleic Acids Res *6*, 715–732.

Gross, C.H., and Shuman, S. (1996). Vaccinia virus RNA helicase: nucleic acid specificity in duplex unwinding. J Virol *70*, 2615-2619.

Gu, M., and Rice, C.M. (2010). Three conformational snapshots of the hepatitis C virus NS3 helicase reveal a ratchet translocation mechanism. Proc Natl Acad Sci U S A *107*, 521-528.

Guenther, U.P., Handoko, L., Laggerbauer, B., Jablonka, S., Chari, A., Alzheimer, M., Ohmer, J., Plottner, O., Gehring, N., Sickmann, A., *et al.* (2009). IGHMBP2 is a ribosome-associated helicase inactive in the neuromuscular disorder distal SMA type 1 (DSMA1). Hum Mol Genet *18*, 1288-1300.

Gupta, R.A., Shah, N., Wang, K.C., Kim, J., Horlings, H.M., Wong, D.J., Tsai, M.C., Hung, T., Argani, P., Rinn, J.L., *et al.* (2010). Long non-coding RNA HOTAIR reprograms chromatin state to promote cancer metastasis. Nature *464*, 1071-1076.

Haase, A.D., Fenoglio, S., Muerdter, F., Guzzardo, P.M., Czech, B., Pappin, D.J., Chen, C., Gordon, A., and Hannon, G.J. (2010). Probing the initiation and effector phases of the somatic piRNA pathway in Drosophila. Genes Dev *24*, 2499-2504.

Hafner, M., Landthaler, M., Burger, L., Khorshid, M., Hausser, J., Berninger, P., Rothballer, A., Ascano, M., Jr., Jungkamp, A.C., Munschauer, M., *et al.* (2010). Transcriptome-wide identification of RNA-binding protein and microRNA target sites by PAR-CLIP. Cell *141*, 129-141.

Hall, G.W., and Thein, S. (1994). Nonsense codon mutations in the terminal exon of the beta-globin gene are not associated with a reduction in beta-mRNA accumulation: a mechanism for the phenotype of dominant beta-thalassemia. Blood *83*, 2031-2037.

Harbers, K., Schnieke, A., Stuhlmann, H., and Jaenisch, R. (1982). Infectivity and structure of molecular clones obtained from two genetically transmitted Moloney leukemia proviral genomes. Nucleic Acids Res *10*, 2521-2537.

Hartshorne, D.J., Ito, M., and Erdodi, F. (2004). Role of protein phosphatase type 1 in contractile functions: myosin phosphatase. J Biol Chem *279*, 37211-37214.

Hogg, J.R., and Goff, S.P. (2010). Upf1 senses 3'UTR length to potentiate mRNA decay. Cell *143*, 379-389.

Huang da, W., Sherman, B.T., and Lempicki, R.A. (2009). Systematic and integrative analysis of large gene lists using DAVID bioinformatics resources. Nat Protoc *4*, 44-57.

Hubner, N.C., and Mann, M. (2011). Extracting gene function from protein-protein interactions using Quantitative BAC InteraCtomics (QUBIC). Methods *53*, 453-459.

Hurt, J.A., Robertson, A.D., and Burge, C.B. (2013). Global analyses of UPF1 binding and function reveals expanded scope of nonsense-mediated mRNA decay. Genome Res.

Ilik, I.A., Quinn, J.J., Georgiev, P., Tavares-Cadete, F., Maticzka, D., Toscano, S., Wan, Y., Spitale, R.C., Luscombe, N., Backofen, R., *et al.* (2013). Tandem Stem-Loops in roX RNAs Act Together to Mediate X Chromosome Dosage Compensation in Drosophila. Mol Cell *51*, 156-173.

Ingolia, N.T., Ghaemmaghami, S., Newman, J.R., and Weissman, J.S. (2009). Genome-wide analysis in vivo of translation with nucleotide resolution using ribosome profiling. Science *324*, 218-223.

Ivanov, P.V., Gehring, N.H., Kunz, J.B., Hentze, M.W., and Kulozik, A.E. (2008). Interactions between UPF1, eRFs, PABP and the exon junction complex suggest an integrated model for mammalian NMD pathways. EMBO J *27*, 736-747.

Izumi, T., Burdick, R., Shigemi, M., Plisov, S., Hu, W.S., and Pathak, V.K. (2013). Mov10 and APOBEC3G Localization to Processing Bodies is not Required for Virion Incorporation and Antiviral Activity. J Virol.

Jaenisch, R., Jahner, D., Nobis, P., Simon, I., Lohler, J., Harbers, K., and Grotkopp, D. (1981). Chromosomal position and activation of retroviral genomes inserted into the germ line of mice. Cell *24*, 519-529.

Jankowsky, E., and Fairman, M.E. (2007). RNA helicases--one fold for many functions. Curr Opin Struct Biol *17*, 316-324.

Jankowsky, E., Gross, C.H., Shuman, S., and Pyle, A.M. (2000). The DExH protein NPH-II is a processive and directional motor for unwinding RNA. Nature *403*, 447-451.

Jankowsky, E., Gross, C.H., Shuman, S., and Pyle, A.M. (2001). Active disruption of an RNA-protein interaction by a DExH/D RNA helicase. Science *291*, 121-125.

Jensen, T.H., Dower, K., Libri, D., and Rosbash, M. (2003). Early formation of mRNP: license for export or quality control? Mol Cell *11*, 1129-1138.

Jungkamp, A.C., Stoeckius, M., Mecenas, D., Grun, D., Mastrobuoni, G., Kempa, S., and Rajewsky, N. (2011). In vivo and transcriptome-wide identification of RNA binding protein target sites. Mol Cell *44*, 828-840.

Kakinuma, N., Zhu, Y., Wang, Y., Roy, B.C., and Kiyama, R. (2009). Kank proteins: structure, functions and diseases. Cell Mol Life Sci *66*, 2651-2659.

Kashima, I., Yamashita, A., Izumi, N., Kataoka, N., Morishita, R., Hoshino, S., Ohno, M., Dreyfuss, G., and Ohno, S. (2006). Binding of a novel SMG-1-Upf1-eRF1-eRF3 complex (SURF) to the exon junction complex triggers Upf1 phosphorylation and nonsense-mediated mRNA decay. Gene Dev *20*, 355-367.

Kawaoka, J., Jankowsky, E., and Pyle, A.M. (2004). Backbone tracking by the SF2 helicase NPH-II. Nat Struct Mol Biol *11*, 526-530.

Kawaoka, J., and Pyle, A.M. (2005). Choosing between DNA and RNA: the polymer specificity of RNA helicase NPH-II. Nucleic Acids Res *33*, 644-649.

Kebaara, B.W., and Atkin, A.L. (2009). Long 3'-UTRs target wild-type mRNAs for nonsense-mediated mRNA decay in Saccharomyces cerevisiae. Nucleic Acids Res *37*, 2771-2778.

Kedde, M., van Kouwenhove, M., Zwart, W., Oude Vrielink, J.A., Elkon, R., and Agami, R. (2010). A Pumilio-induced RNA structure switch in p27-3' UTR controls miR-221 and miR-222 accessibility. Nat Cell Biol *12*, 1014-1020.

Keene, J.D., Komisarow, J.M., and Friedersdorf, M.B. (2006). RIP-Chip: the isolation and identification of mRNAs, microRNAs and protein components of ribonucleoprotein complexes from cell extracts. Nat Protoc *1*, 302-307.

Kerenyi, Z., Merai, Z., Hiripi, L., Benkovics, A., Gyula, P., Lacomme, C., Barta, E., Nagy, F., and Silhavy, D. (2008). Inter-kingdom conservation of mechanism of nonsense-mediated mRNA decay. EMBO J *27*, 1585-1595.

Kervestin, S., and Jacobson, A. (2012). NMD: a multifaceted response to premature translational termination. Nat Rev Mol Cell Biol *13*, 700-712.

Kim, H.D., Choe, J., and Seo, Y.S. (1999). The sen1(+) gene of Schizosaccharomyces pombe, a homologue of budding yeast SEN1, encodes an RNA and DNA helicase. Biochemistry *38*, 14697-14710.

Kim, J.L., Morgenstern, K.A., Griffith, J.P., Dwyer, M.D., Thomson, J.A., Murcko, M.A., Lin, C., and Caron, P.R. (1998). Hepatitis C virus NS3 RNA helicase domain with a bound oligonucleotide: the crystal structure provides insights into the mode of unwinding. Structure *6*, 89-100.

Kim, V.N., Kataoka, N., and Dreyfuss, G. (2001). Role of the nonsense-mediated decay factor hUpf3 in the splicing-dependent exon-exon junction complex. Science *293*, 1832-1836.

Kim, Y.K., Furic, L., Desgroseillers, L., and Maquat, L.E. (2005). Mammalian Staufen1 recruits Upf1 to specific mRNA 3'UTRs so as to elicit mRNA decay. Cell *120*, 195-208.

Koito, A., and Ikeda, T. (2012). Apolipoprotein B mRNA-editing, catalytic polypeptide cytidine deaminases and retroviral restriction. Wiley Interdiscip Rev RNA *3*, 529-541.

Komatsu, M., Chiba, T., Tatsumi, K., Iemura, S., Tanida, I., Okazaki, N., Ueno, T., Kominami, E., Natsume, T., and Tanaka, K. (2004). A novel protein-conjugating system for Ufm1, a ubiquitin-fold modifier. EMBO J *23*, 1977-1986.

Konig, J., Zarnack, K., Rot, G., Curk, T., Kayikci, M., Zupan, B., Turner, D.J., Luscombe, N.M., and Ule, J. (2010). iCLIP reveals the function of hnRNP particles in splicing at individual nucleotide resolution. Nat Struct Mol Biol *17*, 909-915.

Kotake, Y., Nakagawa, T., Kitagawa, K., Suzuki, S., Liu, N., Kitagawa, M., and Xiong, Y. (2011). Long non-coding RNA ANRIL is required for the PRC2 recruitment to and silencing of p15(INK4B) tumor suppressor gene. Oncogene *30*, 1956-1962.

Krek, A., Grun, D., Poy, M.N., Wolf, R., Rosenberg, L., Epstein, E.J., MacMenamin, P., da Piedade, I., Gunsalus, K.C., Stoffel, M., *et al.* (2005). Combinatorial microRNA target predictions. Nat Genet *37*, 495-500.

Kundu, P., Fabian, M.R., Sonenberg, N., Bhattacharyya, S.N., and Filipowicz, W. (2012). HuR protein attenuates miRNA-mediated repression by promoting miRISC dissociation from the target RNA. Nucleic Acids Res *40*, 5088-5100.

Kunz, J.B., Neu-Yilik, G., Hentze, M.W., Kulozik, A.E., and Gehring, N.H. (2006). Functions of hUpf3a and hUpf3b in nonsense-mediated mRNA decay and translation. RNA *12*, 1015-1022.

Kurihara, Y., Matsui, A., Hanada, K., Kawashima, M., Ishida, J., Morosawa, T., Tanaka, M., Kaminuma, E., Mochizuki, Y., Matsushima, A., *et al.* (2009). Genome-wide suppression of aberrant mRNA-like noncoding RNAs by NMD in Arabidopsis. Proc Natl Acad Sci U S A *106*, 2453-2458.

Kurosaki, T., and Maquat, L.E. (2013). Rules that govern UPF1 binding to mRNA 3' UTRs. Proc Natl Acad Sci U S A *110*, 3357-3362.

Lander, E.S., Linton, L.M., Birren, B., Nusbaum, C., Zody, M.C., Baldwin, J., Devon, K., Dewar, K., Doyle, M., FitzHugh, W., *et al.* (2001). Initial sequencing and analysis of the human genome. Nature *409*, 860-921.

Landthaler, M., Gaidatzis, D., Rothballer, A., Chen, P.Y., Soll, S.J., Dinic, L., Ojo, T., Hafner, M., Zavolan, M., and Tuschl, T. (2008). Molecular characterization of human Argonaute-containing ribonucleoprotein complexes and their bound target mRNAs. RNA *14*, 2580-2596.

Lange, S.J., Maticzka, D., Mohl, M., Gagnon, J.N., Brown, C.M., and Backofen, R. (2012). Global or local? Predicting secondary structure and accessibility in mRNAs. Nucleic Acids Res *40*, 5215-5226.

Le Hir, H., Gatfield, D., Izaurralde, E., and Moore, M.J. (2001). The exon-exon junction complex provides a binding platform for factors involved in mRNA export and nonsense-mediated mRNA decay. EMBO J *20*, 4987-4997.

Lebedeva, S., Jens, M., Theil, K., Schwanhausser, B., Selbach, M., Landthaler, M., and Rajewsky, N. (2011). Transcriptome-wide analysis of regulatory interactions of the RNA-binding protein HuR. Mol Cell *43*, 340-352.

LeBlanc, J.J., and Beemon, K.L. (2004). Unspliced Rous sarcoma virus genomic RNAs are translated and subjected to nonsense-mediated mRNA decay before packaging. J Virol *78*, 5139-5146.

Lee, S.R., and Lykke-Andersen, J. (2013). Emerging roles for ribonucleoprotein modification and remodeling in controlling RNA fate. Trends in cell biology.

Leppek, K., Schott, J., Reitter, S., Poetz, F., Hammond, M.C., and Stoecklin, G. (2013). Roquin promotes constitutive mRNA decay via a conserved class of stem-loop recognition motifs. Cell *153*, 869-881.

Li, X., Zhang, J., Jia, R., Cheng, V., Xu, X., Qiao, W., Guo, F., Liang, C., and Cen, S. (2013). The MOV10 Helicase Inhibits LINE-1 Mobility. J Biol Chem *288*, 21148-21160.

Linder, P., and Jankowsky, E. (2011). From unwinding to clamping - the DEAD box RNA helicase family. Nat Rev Mol Cell Biol *12*, 505-516.

Liu, C., Zhang, X., Huang, F., Yang, B., Li, J., Liu, B., Luo, H., Zhang, P., and Zhang, H. (2012). APOBEC3G inhibits microRNA-mediated repression of translation by interfering with the interaction between Argonaute-2 and MOV10. J Biol Chem *287*, 29373-29383.

Longman, D., Plasterk, R.H., Johnstone, I.L., and Caceres, J.F. (2007). Mechanistic insights and identification of two novel factors in the C. elegans NMD pathway. Genes Dev *21*, 1075-1085.

Lorgeoux, R.P., Guo, F., and Liang, C. (2012). From promoting to inhibiting: diverse roles of helicases in HIV-1 Replication. Retrovirology *9*, 79.

Lu, C., Luo, Z., Jager, S., Krogan, N.J., and Peterlin, B.M. (2012). Moloney leukemia virus type 10 inhibits reverse transcription and retrotransposition of intracisternal a particles. J Virol *86*, 10517-10523.

Lykke-Andersen, J., Shu, M.D., and Steitz, J.A. (2000). Human Upf proteins target an mRNA for nonsense-mediated decay when bound downstream of a termination codon. Cell *103*, 1121-1131.

Lykke-Andersen, J., and Wagner, E. (2005). Recruitment and activation of mRNA decay enzymes by two ARE-mediated decay activation domains in the proteins TTP and BRF-1. Genes Dev *19*, 351-361.

Malone, C.D., Brennecke, J., Dus, M., Stark, A., McCombie, W.R., Sachidanandam, R., and Hannon, G.J. (2009). Specialized piRNA pathways act in germline and somatic tissues of the Drosophila ovary. Cell *137*, 522-535.

Maquat, L.E. (2004). Nonsense-mediated mRNA decay: splicing, translation and mRNP dynamics. Nat Rev Mol Cell Biol *5*, 89-99.

Medghalchi, S.M., Frischmeyer, P.A., Mendell, J.T., Kelly, A.G., Lawler, A.M., and Dietz, H.C. (2001). Rent1, a trans-effector of nonsense-mediated mRNA decay, is essential for mammalian embryonic viability. Hum Mol Genet *10*, 99-105.

Meinhart, A., and Cramer, P. (2004). Recognition of RNA polymerase II carboxy-terminal domain by 3'-RNA-processing factors. Nature *430*, 223-226.

Meister, G., Landthaler, M., Peters, L., Chen, P.Y., Urlaub, H., Luhrmann, R., and Tuschl, T. (2005). Identification of novel argonaute-associated proteins. Curr Biol *15*, 2149-2155.

Melero, R., Buchwald, G., Castano, R., Raabe, M., Gil, D., Lazaro, M., Urlaub, H., Conti, E., and Llorca, O. (2012). The cryo-EM structure of the UPF-EJC complex shows UPF1 poised toward the RNA 3' end. Nat Struct Mol Biol *19*, 498-505, S491-492.

Mendell, J.T., Sharifi, N.A., Meyers, J.L., Martinez-Murillo, F., and Dietz, H.C. (2004). Nonsense surveillance regulates expression of diverse classes of mammalian transcripts and mutes genomic noise. Nat Genet *36*, 1073-1078.

Metze, S., Herzog, V.A., Ruepp, M.D., and Muhlemann, O. (2013). Comparison of EJC-enhanced and EJC-independent NMD in human cells reveals two partially redundant degradation pathways. RNA.

Minshall, N., Kress, M., Weil, D., and Standart, N. (2009). Role of p54 RNA helicase activity and its C-terminal domain in translational repression, P-body localization and assembly. Mol Biol Cell *20*, 2464-2472.

Minshall, N., Thom, G., and Standart, N. (2001). A conserved role of a DEAD box helicase in mRNA masking. RNA *7*, 1728-1742.

Mischo, H.E., Gomez-Gonzalez, B., Grzechnik, P., Rondon, A.G., Wei, W., Steinmetz, L., Aguilera, A., and Proudfoot, N.J. (2011). Yeast Sen1 helicase protects the genome from transcription-associated instability. Mol Cell *41*, 21-32.

Mitrovich, Q.M., and Anderson, P. (2005). mRNA surveillance of expressed pseudogenes in C. elegans. Curr Biol *15*, 963-967.

Mozaffari-Jovin, S., Santos, K.F., Hsiao, H.H., Will, C.L., Urlaub, H., Wahl, M.C., and Luhrmann, R. (2012). The Prp8 RNase H-like domain inhibits Brr2-mediated U4/U6 snRNA unwinding by blocking Brr2 loading onto the U4 snRNA. Genes Dev *26*, 2422-2434.

Mozaffari-Jovin, S., Wandersleben, T., Santos, K.F., Will, C.L., Luhrmann, R., and Wahl, M.C. (2013). Inhibition of RNA helicase Brr2 by the C-terminal tail of the spliceosomal protein Prp8. Science *341*, 80-84.

Muhlrad, D., and Parker, R. (1999). Aberrant mRNAs with extended 3' UTRs are substrates for rapid degradation by mRNA surveillance. RNA *5*, 1299-1307.

Mukherjee, N., Corcoran, D.L., Nusbaum, J.D., Reid, D.W., Georgiev, S., Hafner, M., Ascano, M., Jr., Tuschl, T., Ohler, U., and Keene, J.D. (2011). Integrative regulatory mapping indicates that the RNA-binding protein HuR couples pre-mRNA processing and mRNA stability. Mol Cell *43*, 327-339.

Muller-McNicoll, M., and Neugebauer, K.M. (2013). How cells get the message: dynamic assembly and function of mRNA-protein complexes. Nature reviews Genetics *14*, 275-287.

Neugebauer, K.M. (2002). On the importance of being co-transcriptional. J Cell Sci *115*, 3865-3871.

Ohnishi, T., Yamashita, A., Kashima, I., Schell, T., Anders, K.R., Grimson, A., Hachiya, T., Hentze, M.W., Anderson, P., and Ohno, S. (2003). Phosphorylation of hUPF1 induces formation of mRNA surveillance complexes containing hSMG-5 and hSMG-7. Molecular Cell *12*, 1187-1200.

Olivieri, D., Sykora, M.M., Sachidanandam, R., Mechtler, K., and Brennecke, J. (2010). An in vivo RNAi assay identifies major genetic and cellular requirements for primary piRNA biogenesis in Drosophila. EMBO J *29*, 3301-3317.

Ong, S.E., Blagoev, B., Kratchmarova, I., Kristensen, D.B., Steen, H., Pandey, A., and Mann, M. (2002). Stable isotope labeling by amino acids in cell culture, SILAC, as a simple and accurate approach to expression proteomics. Mol Cell Proteomics *1*, 376-386.

Ono, R., Kobayashi, S., Wagatsuma, H., Aisaka, K., Kohda, T., Kaneko-Ishino, T., and Ishino, F. (2001). A retrotransposon-derived gene, PEG10, is a novel imprinted gene located on human chromosome 7q21. Genomics *73*, 232-237.

Pang, P.S., Jankowsky, E., Planet, P.J., and Pyle, A.M. (2002). The hepatitis C viral NS3 protein is a processive DNA helicase with cofactor enhanced RNA unwinding. EMBO J *21*, 1168-1176.

Park, E., Gleghorn, M.L., and Maquat, L.E. (2013). Staufen2 functions in Staufen1-mediated mRNA decay by binding to itself and its paralog and promoting UPF1 helicase but not ATPase activity. Proc Natl Acad Sci U S A *110*, 405-412.

Parker, R., and Sheth, U. (2007). P bodies and the control of mRNA translation and degradation. Mol Cell *25*, 635-646.

Parsyan, A., Svitkin, Y., Shahbazian, D., Gkogkas, C., Lasko, P., Merrick, W.C., and Sonenberg, N. (2011). mRNA helicases: the tacticians of translational control. Nat Rev Mol Cell Biol *12*, 235-245.

Pisareva, V.P., Pisarev, A.V., Komar, A.A., Hellen, C.U., and Pestova, T.V. (2008). Translation initiation on mammalian mRNAs with structured 5'UTRs requires DExH-box protein DHX29. Cell *135*, 1237-1250.

Pyle, A.M. (2008). Translocation and unwinding mechanisms of RNA and DNA helicases. Annual review of biophysics *37*, 317-336.

Rabani, M., Levin, J.Z., Fan, L., Adiconis, X., Raychowdhury, R., Garber, M., Gnirke, A., Nusbaum, C., Hacohen, N., Friedman, N., *et al.* (2011). Metabolic labeling of RNA uncovers principles of RNA production and degradation dynamics in mammalian cells. Nat Biotechnol *29*, 436-442.

Rappsilber, J., Ishihama, Y., and Mann, M. (2003). Stop and go extraction tips for matrix-assisted laser desorption/ionization, nanoelectrospray, and LC/MS sample pretreatment in proteomics. Anal Chem *75*, 663-670.

Rebbapragada, I., and Lykke-Andersen, J. (2009). Execution of nonsense-mediated mRNA decay: what defines a substrate? Curr Opin Cell Biol *21*, 394-402.

Rinn, J.L., Kertesz, M., Wang, J.K., Squazzo, S.L., Xu, X., Brugmann, S.A., Goodnough, L.H., Helms, J.A., Farnham, P.J., Segal, E., *et al.* (2007). Functional demarcation of active and silent chromatin domains in human HOX loci by noncoding RNAs. Cell *129*, 1311-1323.

Rocak, S., and Linder, P. (2004). Dead-box proteins: The driving forces behind RNA metabolism. Nat Rev Mol Cell Bio *5*, 232-241.

Saikrishnan, K., Powell, B., Cook, N.J., Webb, M.R., and Wigley, D.B. (2009). Mechanistic basis of 5'-3' translocation in SF1B helicases. Cell *137*, 849-859.

Sauliere, J., Murigneux, V., Wang, Z., Marquenet, E., Barbosa, I., Le Tonqueze, O., Audic, Y., Paillard, L., Roest Crollius, H., and Le Hir, H. (2012). CLIP-seq of eIF4AIII reveals transcriptome-wide mapping of the human exon junction complex. Nat Struct Mol Biol *19*, 1124-1131.

Schnieke, A., Stuhlmann, H., Harbers, K., Chumakov, I., and Jaenisch, R. (1983). Endogenous Moloney leukemia virus in nonviremic Mov substrains of mice carries defects in the proviral genome. J Virol *45*, 505-513.

Schoenberg, D.R., and Maquat, L.E. (2012). Regulation of cytoplasmic mRNA decay. Nature Reviews Genetics *13*, 448-448.

Schoggins, J.W., Wilson, S.J., Panis, M., Murphy, M.Y., Jones, C.T., Bieniasz, P., and Rice, C.M. (2011). A diverse range of gene products are effectors of the type I interferon antiviral response. Nature *472*, 481-485.

Schwalb, B., Schulz, D., Sun, M., Zacher, B., Dumcke, S., Martin, D.E., Cramer, P., and Tresch, A. (2012). Measurement of genome-wide RNA synthesis and decay rates with Dynamic Transcriptome Analysis (DTA). Bioinformatics *28*, 884-885.

Schwanhausser, B., Busse, D., Li, N., Dittmar, G., Schuchhardt, J., Wolf, J., Chen, W., and Selbach, M. (2011). Global quantification of mammalian gene expression control. Nature *473*, 337-342.

Schwartz, Y.B., and Pirrotta, V. (2007). Polycomb silencing mechanisms and the management of genomic programmes. Nature reviews Genetics *8*, 9-22.

Schweingruber, C., Rufener, S.C., Zund, D., Yamashita, A., and Muhlemann, O. (2013). Nonsense-mediated mRNA decay - mechanisms of substrate mRNA recognition and degradation in mammalian cells. Biochim Biophys Acta *1829*, 612-623.

Sengoku, T., Nureki, O., Nakamura, A., Kobayashi, S., and Yokoyama, S. (2006). Structural basis for RNA unwinding by the DEAD-box protein Drosophila Vasa. Cell *125*, 287-300.

Serman, A., Le Roy, F., Aigueperse, C., Kress, M., Dautry, F., and Weil, D. (2007). GW body disassembly triggered by siRNAs independently of their silencing activity. Nucleic Acids Res *35*, 4715-4727.

Sheth, U., and Parker, R. (2006). Targeting of aberrant mRNAs to cytoplasmic processing bodies. Cell *125*, 1095-1109.

Shibuya, T., Tange, T.O., Sonenberg, N., and Moore, M.J. (2004). eIF4AIII binds spliced mRNA in the exon junction complex and is essential for nonsense-mediated decay. Nat Struct Mol Biol *11*, 346-351.

Shigeoka, T., Kato, S., Kawaichi, M., and Ishida, Y. (2012). Evidence that the Upf1-related molecular motor scans the 3'-UTR to ensure mRNA integrity. Nucleic Acids Res *40*, 6887-6897.

Sievers, C., Schlumpf, T., Sawarkar, R., Comoglio, F., and Paro, R. (2012). Mixture models and wavelet transforms reveal high confidence RNA-protein interaction sites in MOV10 PAR-CLIP data. Nucleic Acids Res.

Silva, A.L., Ribeiro, P., Inacio, A., Liebhaber, S.A., and Romao, L. (2008). Proximity of the poly(A)-binding protein to a premature termination codon inhibits mammalian nonsense-mediated mRNA decay. RNA *14*, 563-576.

Silverman, E., Edwalds-Gilbert, G., and Lin, R.J. (2003). DExD/H-box proteins and their partners: helping RNA helicases unwind. Gene *312*, 1-16.

Singh, G., Kucukural, A., Cenik, C., Leszyk, J.D., Shaffer, S.A., Weng, Z., and Moore, M.J. (2012). The Cellular EJC Interactome Reveals Higher-Order mRNP Structure and an EJC-SR Protein Nexus. Cell.

Singh, G., Rebbapragada, I., and Lykke-Andersen, J. (2008). A competition between stimulators and antagonists of Upf complex recruitment governs human nonsense-mediated mRNA decay. PLoS Biol *6*, e111.

Singleton, M.R., Dillingham, M.S., and Wigley, D.B. (2007). Structure and mechanism of helicases and nucleic acid translocases. Annual review of biochemistry *76*, 23-50.

Skourti-Stathaki, K., Proudfoot, N.J., and Gromak, N. (2011). Human senataxin resolves RNA/DNA hybrids formed at transcriptional pause sites to promote Xrn2-dependent termination. Mol Cell *42*, 794-805.

Soto-Rifo, R., Rubilar, P.S., Limousin, T., de Breyne, S., Decimo, D., and Ohlmann, T. (2012). DEAD-box protein DDX3 associates with eIF4F to promote translation of selected mRNAs. EMBO J *31*, 3745-3756.

Sun, M., Schwalb, B., Schulz, D., Pirkl, N., Etzold, S., Lariviere, L., Maier, K.C., Seizl, M., Tresch, A., and Cramer, P. (2012). Comparative dynamic transcriptome analysis (cDTA) reveals mutual feedback between mRNA synthesis and degradation. Genome Res *22*, 1350-1359.

Tai, C.L., Chi, W.K., Chen, D.S., and Hwang, L.H. (1996). The helicase activity associated with hepatitis C virus nonstructural protein 3 (NS3). J Virol *70*, 8477-8484.

Tanaka, M., Sasaki, K., Kamata, R., Hoshino, Y., Yanagihara, K., and Sakai, R. (2009). A novel RNA-binding protein, Ossa/C9orf10, regulates activity of Src kinases to protect cells from oxidative stress-induced apoptosis. Mol Cell Biol *29*, 402-413.

Tani, H., Imamachi, N., Salam, K.A., Mizutani, R., Ijiri, K., Irie, T., Yada, T., Suzuki, Y., and Akimitsu, N. (2012). Identification of hundreds of novel UPF1 target transcripts by direct determination of whole transcriptome stability. RNA Biol *9*, 1370-1379.

Tarpey, P.S., Raymond, F.L., Nguyen, L.S., Rodriguez, J., Hackett, A., Vandeleur, L., Smith, R., Shoubridge, C., Edkins, S., Stevens, C., *et al.* (2007). Mutations in UPF3B, a member of the nonsense-mediated mRNA decay complex, cause syndromic and nonsyndromic mental retardation. Nat Genet *39*, 1127-1133.

Tomari, Y., Du, T., Haley, B., Schwarz, D.S., Bennett, R., Cook, H.A., Koppetsch, B.S., Theurkauf, W.E., and Zamore, P.D. (2004). RISC assembly defects in the Drosophila RNAi mutant armitage. Cell *116*, 831-841.

Trcek, T., Sato, H., Singer, R.H., and Maquat, L.E. (2013). Temporal and spatial characterization of nonsense-mediated mRNA decay. Genes Dev *27*, 541-551.

Tsai, M.C., Manor, O., Wan, Y., Mosammaparast, N., Wang, J.K., Lan, F., Shi, Y., Segal, E., and Chang, H.Y. (2010). Long noncoding RNA as modular scaffold of histone modification complexes. Science *329*, 689-693.

Ule, J., Jensen, K.B., Ruggiu, M., Mele, A., Ule, A., and Darnell, R.B. (2003). CLIP identifies Nova-regulated RNA networks in the brain. Science *302*, 1212-1215.

Umate, P., Tuteja, N., and Tuteja, R. (2011). Genome-wide comprehensive analysis of human helicases. Communicative & integrative biology *4*, 118-137.

Velankar, S.S., Soultanas, P., Dillingham, M.S., Subramanya, H.S., and Wigley, D.B. (1999). Crystal structures of complexes of PcrA DNA helicase with a DNA substrate indicate an inchworm mechanism. Cell *97*, 75-84.

Wagenmakers, A.J., Reinders, R.J., and van Venrooij, W.J. (1980). Cross-linking of mRNA to proteins by irradiation of intact cells with ultraviolet light. Eur J Biochem *112*, 323-330.

Wahl, M.C., Will, C.L., and Luhrmann, R. (2009). The spliceosome: design principles of a dynamic RNP machine. Cell *136*, 701-718.

Wang, W., Czaplinski, K., Rao, Y., and Peltz, S.W. (2001). The role of Upf proteins in modulating the translation read-through of nonsense-containing transcripts. EMBO J *20*, 880-890.

Wang, X., Han, Y., Dang, Y., Fu, W., Zhou, T., Ptak, R.G., and Zheng, Y.H. (2010). Moloney leukemia virus 10 (MOV10) protein inhibits retrovirus replication. J Biol Chem *285*, 14346-14355.

Weischenfeldt, J., Damgaard, I., Bryder, D., Theilgaard-Monch, K., Thoren, L.A., Nielsen, F.C., Jacobsen, S.E., Nerlov, C., and Porse, B.T. (2008). NMD is essential for hematopoietic stem and progenitor cells and for eliminating by-products of programmed DNA rearrangements. Genes Dev *22*, 1381-1396.

Wen, J., and Brogna, S. (2010). Splicing-dependent NMD does not require the EJC in Schizosaccharomyces pombe. EMBO J *29*, 1537-1551.

Wilbert, M.L., Huelga, S.C., Kapeli, K., Stark, T.J., Liang, T.Y., Chen, S.X., Yan, B.Y., Nathanson, J.L., Hutt, K.R., Lovci, M.T., *et al.* (2012). LIN28 Binds Messenger RNAs at GGAGA Motifs and Regulates Splicing Factor Abundance. Mol Cell *48*, 195-206.

Yang, Q., and Jankowsky, E. (2006). The DEAD-box protein Ded1 unwinds RNA duplexes by a mode distinct from translocating helicases. Nat Struct Mol Biol *13*, 981-986.

Yap, K.L., Li, S., Munoz-Cabello, A.M., Raguz, S., Zeng, L., Mujtaba, S., Gil, J., Walsh, M.J., and Zhou, M.M. (2010). Molecular interplay of the noncoding RNA ANRIL and methylated histone H3 lysine 27 by polycomb CBX7 in transcriptional silencing of INK4a. Mol Cell *38*, 662-674.

Yepiskoposyan, H., Aeschimann, F., Nilsson, D., Okoniewski, M., and Muhlemann, O. (2011). Autoregulation of the nonsense-mediated mRNA decay pathway in human cells. RNA *17*, 2108-2118.

Zhang, C., and Darnell, R.B. (2011). Mapping in vivo protein-RNA interactions at single-nucleotide resolution from HITS-CLIP data.

Nat Biotechnol *29*, 607-614.

Zheng, K., Xiol, J., Reuter, M., Eckardt, S., Leu, N.A., McLaughlin, K.J., Stark, A., Sachidanandam, R., Pillai, R.S., and Wang, P.J. (2010). Mouse MOV10L1 associates with Piwi proteins and is an essential component of the Piwi-interacting RNA (piRNA) pathway. Proc Natl Acad Sci U S A *107*, 11841-11846.

Zhu, Y., Chen, G., Lv, F., Wang, X., Ji, X., Xu, Y., Sun, J., Wu, L., Zheng, Y.T., and Gao, G. (2011). Zinc-finger antiviral protein inhibits HIV-1 infection by selectively targeting multiply spliced viral mRNAs for degradation. Proc Natl Acad Sci U S A *108*, 15834-15839.

Zund, D., Gruber, A.R., Zavolan, M., and Muhlemann, O. (2013). Translation-dependent displacement of UPF1 from coding sequences causes its enrichment in 3' UTRs. Nat Struct Mol Biol.

SUPPLEMENATAL MATERIAL

Supplemental Figure S1.

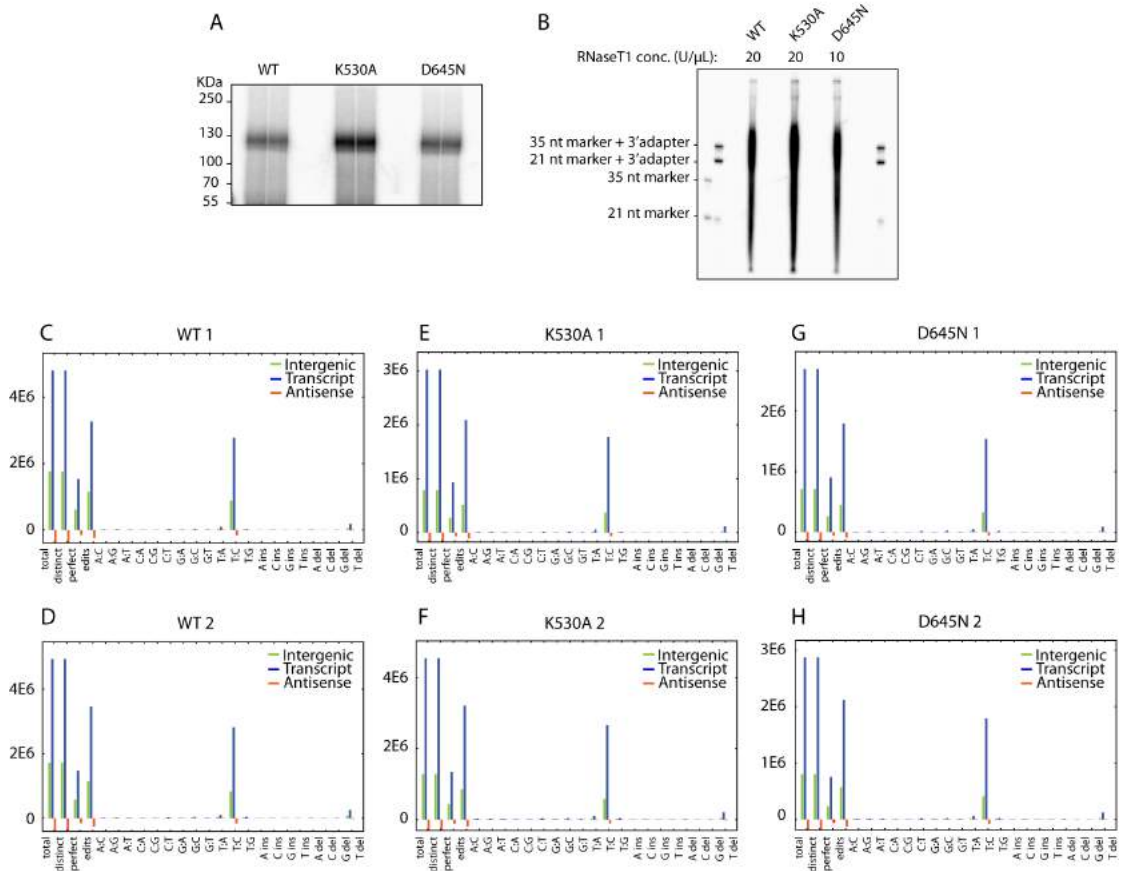

Figure S1. PAR-CLIP diagnostics.

(A) Autoradiograph of MOV10–RNA complexes used for PAR-CLIP library generation separated on a Tris-Acetate gel from Flp-In T-REx HEK293 cells labeled with 100 µM 4SU for 16 hrs prior to crosslinking. **(B)** 3' adapter ligation of MOV10 WT, K530A and D645N UV-crosslinked and radiolabeled RNA. 21 nt and 35 nt oligos, were used as size markers. RNA co-IPed with MOV10 WT and K530A were digested with 20 U/µL RNaseT1 for 15 min at 22 °C. RNA co-IPed with MOV10 D645N was digested with 10 U/µL RNaseT1 for 15 min at 22 °C. **(C-H)** Number of uniquely mapping PAR-CLIP reads, total number of reads, perfectly mapping reads (without mismatches) or reads containing 1 nucleotide edit (1 mismatch, insertion or deletion) as indicated for WT library 1 and 2 **(C-D)**, K530A library 1 and 2 **(E-F)**, D645N library 1 and 2 **(G-H)**. 'Antisense' refers to reads mapping antisense to annotated transcripts.

Supplemental Figure S2.

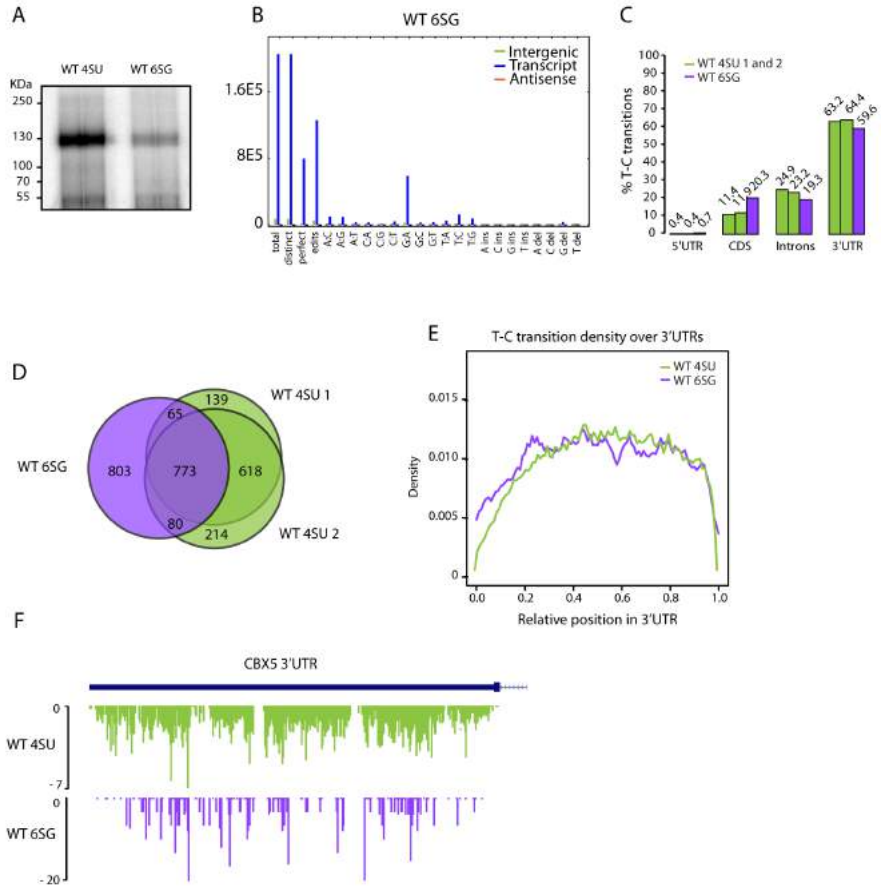

Figure S2. MOV10 6SG PAR-CLIP library compared to 4SU PAR-CLIP libraries.

(A) Autoradiograph of MOV10–RNA complexes used for PAR-CLIP library generation separated on a Tris-Acetate gel from Flp-In T-REx HEK293 cells labeled with either 100 µM 4SU or 100 µM 6SG for 16 hrs prior to crosslinking. **(B)** Number of uniquely mapping PAR-CLIP reads, total number of reads, perfect mapping reads (without mismatches), reads containing 1 nucleotide edit (1 mismatch) for MOV10 WT 6SG library. **(C)** Location of MOV10 binding sites identified by PAR-CLIP. Barplot depicting the percentage of G-A or T-C transitions located in 5'UTRs, coding regions, introns and 3'UTRs. **(D)** Venn diagram displaying the overlap between mRNA targets containing the top 5,000 PAR-CLIP clusters from MOV10 WT 6SG, MOV10 WT 4SU 1 and MOV10 WT 4SU 2 PAR-CLIPs. **(E)** Relative position of T-C transitions of MOV10 WT 6SG and MOV10 4SU consensus throughout 3'UTRs of mRNA target transcripts. Y-axis shows density of the median relative coverage over all 3'UTRs of target genes. **(F)** Example of MOV10 WT 6SG and MOV10 WT 4SU consensus T-C transition counts found in the 3'UTR of CBX5 transcript.

Supplemental Figure S3.

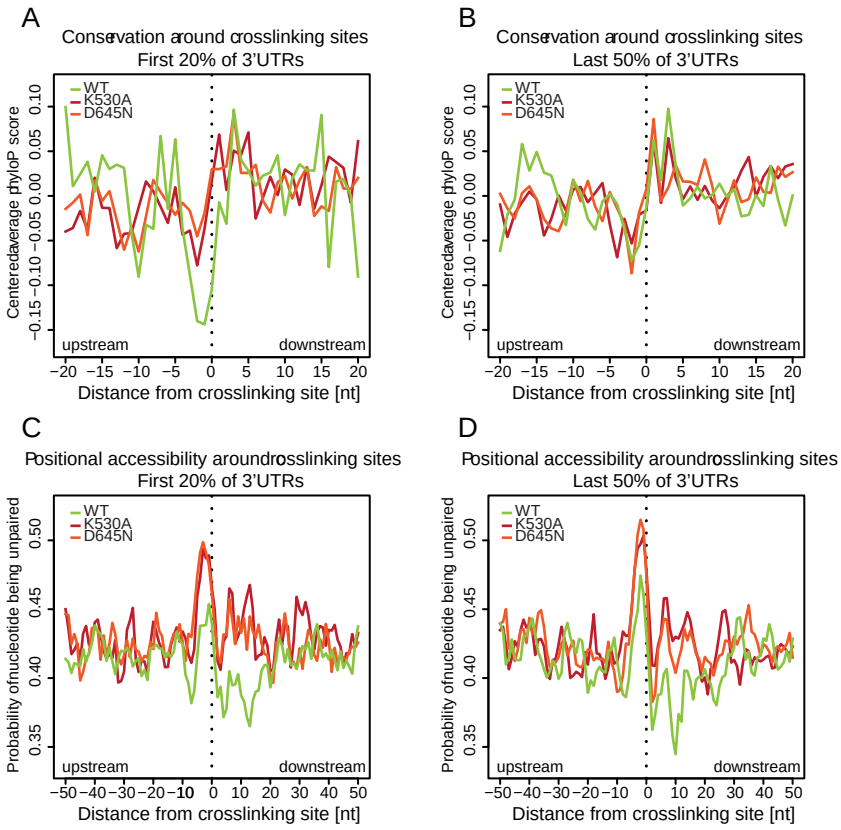

Figure S3. Conservation and positional accessibility around MOV10 binding sites located either in the beginning or end of 3'UTRs.

(A) PhastCons conservation score around MOV10 WT, K530A and D645N sites as described in Figure 9A but restricted to sites located in the first 20% of the 3'UTRs. **(B)** PhastCons conservation score around MOV10 WT, K530A and D645N sites as described in Figure 9A but restricted to sites located in the last 50% of the 3'UTRs. **(C)** Positional site accessibility around MOV10 WT, K530A and D645N sites as described in Figure 9B but restricted to sites located in the first 20% of the 3'UTRs. **(D)** Site accessibility around MOV10 WT, K530A and D645N sites as described in Figure 9B but restricted to sites located in the last 50% of the 3'UTRs.

Supplemental Figure S4.

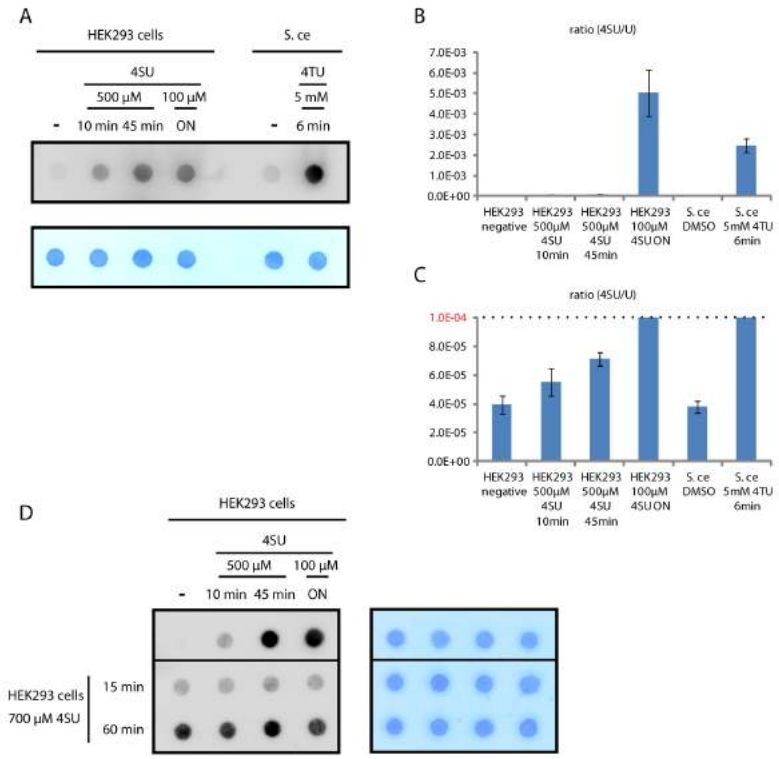

Figure S3. Pulse 4SU labeling of mRNAs.

(A) Dot blot of 4SU- or 4TU-labeled and biotinylated RNA visualized by anti-Streptavidin HRP-conjugated antibody (upper panel). Staining with NaOAc, 0.5 % methylene blue solution was used to control for loading (lower panel). **(B)** LC-MS measurement of 4SU incorporation rates for samples shown in **(A)**. Ratio of 4SU nucleosides relative to U nucleosides are blotted for the indicated samples. HEK239 negative are cells not treated with any 4SU and *S. cerevisiae* DMSO are treated with DMSO only. Both serve as negative controls. Values are shown as mean ± standard derivation measured for three technical replicates. **(C)** Zoom of the bar plot shown in with the y-axis cutoff shown in red **(B)**. **(D)** Dot blot of 4SU-labeled and biotinylated RNA used for global mRNA half-life measurements. RNA was labeled with 700 µM 4SU for 60 min. Samples used for LC-MS 4SU incorporation measurement, labeled for 10 and 45 min with 500 µM 4SU or labeled ON with 100 µM 4SU were blotted on same membrane as a reference.

Supplemental Figure S5 .

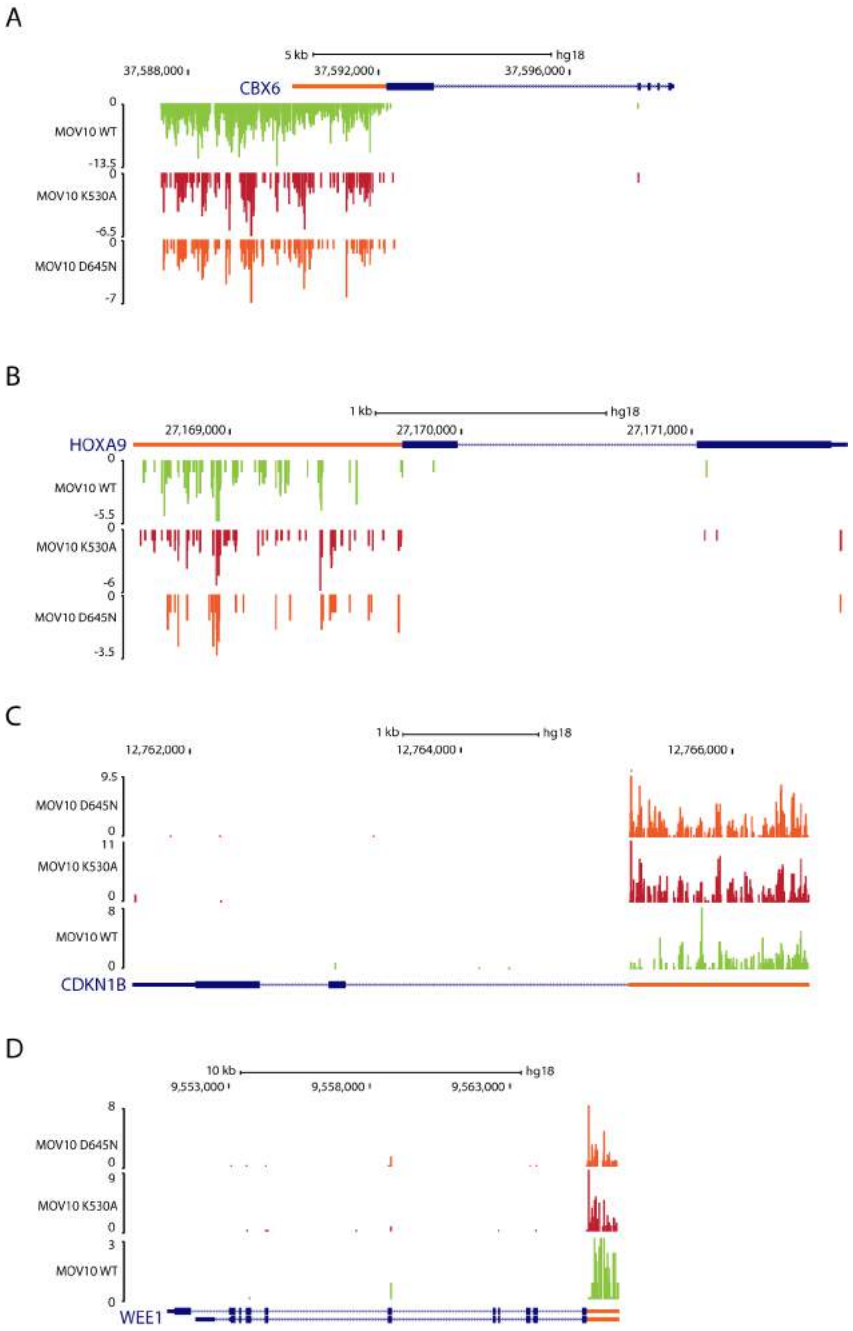

Figure S4: Genome browser view of MOV10 binding sites mapping to CBX6, HOXA9, CDKN1B and WEE1.

MOV10 PAR-CLIP consensus T-C transitions mapping to the CBX6 **(A)**, HOXA9 **(B)**, CDKN1B **(C)** and WEE1 **(D)** transcripts. 3'UTRs are indicated in orange. Note that CBX6 has an unannotated extended 3'UTR.

Supplemental Table S1.

Primer sequences.

Primer Name	Sequence 5’ to 3’
MOV10 K530A sense	5'- CCTCCAGGCACCGGCGCGACTGTCACGTTAGT -3'
MOV10 K530A antisense	5'- ACTAACGTGACAGTCGCGCCGGTGCCTGGAGG -3'
MOV10 D645N sense	5'- CACACACATCTTCATCAATGAGGCTGGCCACTG -3'
MOV10 D645N antisense	5'- CAGTGGCCAGCCTCATTGATGAAGATGTGTGTG -3'
pENTR4 UPF1 XmnI	5’-ATGAGCGTGGAGGCGTACGGG-3’
pENTR4 UPF1 NotI	5’-ATAAGAATGCGGCCGCTTAATACTGGGACAGCCCCGTCAC-3’
pENTR4 XPO5 SalI	5’-ACGCGTCGACATGGCGATGGATCAAGTAAACGCGCTG-3’
pENTR4 XPO5 NotI	5’-ATAAGAATGCGGCCGCTCAGGGTTCAAAGATGGTGGCCAG-3’
RPL18A Q-PCR FW	5'- GGAGAGCACGCCATGAAG -3'
RPL18A Q-PCR RV	5'- AAGATTCGCATGCGGTAGAG -3'
MOV10 Q-PCR FW	5'- ACAGGTGGAGAAAATCCGTTAC -3'
MOV10 Q-PCR RV	5'- TCTTGGCCTTGGAATTCTTC-3'
UPF1 Q-PCR FW	5'- AGATCACGGCACAGCAGA -3'
UPF1 Q-PCR RV	5'- GTGGCAGAAGGGTTTTCCTT -3'
CDKN1B Q-PCR FW	5'- TTTGACTTGCATGAAGAGAAGC-3'
CDKN1B Q-PCR RV	5'- AGCTGTCTCTGAAAGGGACATT-3'
HOXA9 Q-PCR FW	5'- CCCCATCGATCCCAATAA-3'
HOXA9 Q-PCR RV	5'- CACCGCTTTTTCCGAGTG-3'
WEE1 Q-PCR FW	5'- TCTGCGTGGGCAGAAGAT-3'
WEE1 Q-PCR RV	5'- TCTGTAGTTTTCACTTATAGCATCAGC-3'
CXB6 Q-PCR FW	5'- GCTGAGCAAGATGGAGCTGT-3'
CXB6 Q-PCR RV	5'- CCCTTCCATTTCACCAGGTA-3'
IMPDH1 Q-PCR FW	5'- GGCTCCATCTGCATCACC-3'
IMPDH1 Q-PCR RV	5'- GGGCATACTCAGCCACCTT-3'
MYC Q-PCR FW	5'- GCTGCTTAGACGCTGGATTT-3'
MYC Q-PCR RV	5'- TAACGTTGAGGGGCATCG-3'
PANK2 Q-PCR FW	5'- GGATTATTGGTCCAAGGG-3'
PANK2 Q-PCR RV	5'- GTAATGATCACGGGATCTTC-3'
β-globin CDS HindIII	5'- ATAAGAATAAGCTTATGGTGCATCTGACTCCTGAGGAGAAGTCTG-3'

β-globin CDS XbaI	5'- ACGCTCTAGATTAGTGATACTTGTGGGCCAGGGCATTAGCCA-3'
CMV FW	5'- CGCAAATGGGCGGTAGGCGTG-3'

Supplemental Table S2.

PAR-CLIP and poly(A)+ RNA-Seq sequencing library statistics.

PAR-CLIP	Raw reads	After adapter removal		Unique sequences		Mapped reads
MOV10_WT_4SU_1	2.19E+07	91.3	%	71.2	%	1.40E+07
MOV10_WT_4SU_2	2.89E+07	92.3	%	47.9	%	1.30E+07
MOV10_K530A_4SU_1	2.36E+07	94.3	%	60.0	%	1.33E+07
MOV10_K530A_4SU_2	2.20E+07	95.7	%	37.6	%	7.90E+06
MOV10_D645N_4SU_1	2.01E+07	94.5	%	46.9	%	8.92E+06
MOV10_D645N_4SU_2	2.40E+07	84.4	%	36.4	%	7.30E+06
MOV10_WT_6SG	4.06E+07	76.1	%	6.3	%	1.90E+06

Sample	Raw reads	After adapter removal		Unique sequences		Mapped reads
mock_1 (P1A)	1.51E+07	94.6	%	81.3	%	1.34E+07
mock_2 (P1B)	1.88E+07	94.1	%	79.7	%	1.67E+07
MOV10 siRNA_1 (P3A)	1.83E+07	94.6	%	79.3	%	1.63E+07
MOV10 siRNA_2 (P3B)	2.02E+07	94.2	%	78.6	%	1.79E+07
mock_T1 (P1C Total)	1.82E+07	92.5	%	73.6	%	1.58E+07
mock_T2 (P2C Total)	2.22E+07	93.4	%	72.4	%	1.92E+07
MOV10 siRNA _T1 (P3C Total)	1.57E+07	93.2	%	75.3	%	1.37E+07
MOV10 siRNA_T2 (P4C Total)	1.58E+07	93.1	%	75.9	%	1.37E+07
mock_F1 (P1C Flow-through)	2.06E+07	94.2	%	67.9	%	1.82E+07
mock_F2 (P2C Flow-through)	2.48E+07	93.8	%	67.0	%	2.16E+07
MOV10 siRNA_F1 (P3C Flow-through)	1.98E+07	92.5	%	68.6	%	1.71E+07
MOV10 siRNA _F2 (P4C Flow-through)	1.30E+07	93.5	%	72.6	%	1.13E+07
mock_E1 (P1C Eluate)	2.33E+07	89.3	%	75.2	%	1.93E+07
mock_E2 (P2C Eluate)	2.36E+07	89.6	%	76.6	%	1.97E+07
MOV10 siRNA_E1 (P3C Eluate)	2.36E+07	89.7	%	75.9	%	1.97E+07
MOV10 siRNA E2 (P4C Eluate)	3.01E+07	88.0	%	73.3	%	2.45E+07

Supplemental Table S3.

Proteomics of MOV10 protein-protein complexes.

Official Gene Symbol	Razor + unique Peptides MOV10 L, Ctrl H	Razor + unique Peptides MOV10 H, Ctrl L	Unique Peptides MOV10 L, Ctrl H	Unique Peptides MOV10 H, Ctrl L	LOG2 (MOV10 L/Ctrl H)	LOG2 (MOV10 H/Ctrl L)
MOV10	145	135	145	135	4.71	2.39
UPF1	22	18	22	18	3.54	3.26
FAM120A	4	4	4	4	1.88	1.88
PABPC1	24	22	14	15	3.43	3.24
PABPC4	9	10	8	9	3.57	3.33
EIF4A3	1	1	1	1	1.94	2.16
ZC3HAV1	1	1	1	1	2.77	2.39
ZCCHC3	6	6	6	6	1.96	1.81
RNF166	5	5	5	5	5.42	3.49
PCBP1	8	9	8	9	2.82	1.93

Supplemental Table S4.

Proteomics of protein-protein complexes bound to RNA in the proximity of MOV10.

Official Gene Symbol	Razor + unique Peptides MOV10 L, Ctrl H	Razor + unique Peptides MOV10 H, Ctrl L	Unique Peptides MOV10 L, Ctrl H	Unique Peptides MOV10 H, Ctrl L	LOG2 (MOV10 H/Ctrl L)	LOG2 (MOV10 L/Ctrl H)	RNA-binding
PFDN2	2	2	2	2	2.85	3.72	
C14orf166	5	5	5	5	3.91	2.52	x
CDS2	6	6	6	6	4.42	2.60	
RNF166	4	6	4	6	5.44	2.35	
ABHD16B	2	2	2	2	8.10	1.77	
CAMSAP3	4	4	4	4	2.50	1.51	
TUBA1C	2	3	1	1	2.37	2.13	x
CDC20	3	2	3	2	2.86	1.81	x
SCGB3A1	2	1	2	1	5.15	2.46	
LSM12	4	5	4	5	3.12	2.18	
CDNA FLJ27423	1	1	1	1	2.51	2.31	
FAM195B	3	4	3	4	2.99	1.98	
MYCBP	2	3	2	3	3.97	2.72	
ZFP36	3	2	3	2	3.42	2.13	x
MSI1	3	3	3	3	4.12	1.51	x
NUFIP2	14	10	14	10	2.64	1.72	x
LSM1	2	2	2	2	3.69	2.99	x
TIAL1	1	1	1	1	5.47	2.46	x
PABPC1	33	30	21	18	5.73	3.25	x
IGF2BP1	27	22	10	9	4.30	2.65	x
G3BP2	2	2	2	2	3.23	2.66	x
EIF4A3	3	3	3	3	2.69	2.30	x
EIF4B	5	2	5	2	4.20	2.62	x
G3BP1	12	9	10	8	4.37	2.66	x
FXR2	4	3	3	3	2.73	1.85	x
PCBP1	12	11	12	11	3.86	2.23	x
MBNL1	6	6	6	6	3.21	1.84	x
PUM2	5	7	5	7	4.14	2.21	x
RBM3	4	3	4	3	4.20	2.41	x
TARDBP	4	3	4	3	2.60	2.15	x
DHX36	7	5	7	5	2.67	1.51	x
CSDA	4	3	4	3	4.30	2.30	x

YBX1	16	13	8	7	4.03	2.44	x
UPF1	43	45	43	45	5.80	3.17	x
PTBP3	4	3	4	3	3.79	2.59	x
DAZAP1	5	5	5	5	2.96	1.52	x
IGF2BP2	36	35	8	8	2.54	1.65	x
PTBP1	15	14	13	12	2.98	1.62	x
ATXN2	12	7	12	7	3.22	1.87	x
DDX3X	21	23	20	22	3.80	2.29	x
TIA1	3	2	3	2	5.84	2.75	x
SRP14	1	1	1	1	2.87	1.77	x
DDX1	12	10	12	10	3.98	2.55	x
MEX3B	3	4	2	3	4.79	1.96	x
ZC3HAV1	11	9	11	9	3.82	2.17	x
CPEB4	13	10	11	7	4.61	2.46	x
FUBP3	24	24	24	23	4.54	2.63	x
FAM120A	20	8	19	8	4.08	2.54	x
MEX3A	15	9	12	7	5.07	2.41	x
TNRC6B	18	13	18	13	4.04	1.86	x
HNRNPA2B1	27	26	25	25	2.99	1.53	x
CPEB3	6	2	6	2	4.13	2.21	x
SYNCRIP	27	22	20	16	4.88	2.75	x
LSM14A	5	3	5	3	4.43	2.07	x
CNBP	5	4	5	4	5.55	3.18	x
MOV10	147	125	147	125	6.12	2.44	x
CSDE1	22	15	22	15	4.56	2.51	x
C22orf28	9	11	9	11	4.76	2.99	x
PUM1	16	10	12	7	4.78	2.55	x
PABPC4	19	16	18	15	6.04	3.35	x
BRF2	5	3	3	1	4.54	1.66	x
SRP9	2	6	2	6	2.39	2.00	x
TIAL1	6	9	1	1	5.56	2.97	x
IGF2BP3	22	21	21	20	4.33	2.68	x
EIF2C2	5	5	5	5	2.32	1.50	x
CAPRIN1	7	4	7	4	4.97	3.15	x
PATL1	5	3	5	3	4.58	2.39	x
cDNA FLJ55578	1	1	1	1	7.89	3.76	x
RBMS1	4	6	3	4	3.84	2.29	x
LARP4B	8	5	3	3	3.72	2.01	x
IGF2BP2	2	2	2	2	2.17	1.96	x
YTHDC2	12	4	12	4	2.72	1.65	x
ZCCHC3	15	21	15	21	4.75	2.75	x
PURA	5	4	5	4	2.51	3.06	x
PURB	5	7	5	6	5.33	3.17	x

KIF1C	6	2	5	1	2.36	2.09	x
TOP3B	3	3	3	3	3.58	2.30	x
ZCCHC11	22	14	22	14	2.58	1.58	x
MKRN2	2	2	2	2	4.03	1.59	x
PRRC2A	38	18	36	17	4.37	2.27	x
UBAP2L	16	9	16	9	4.84	2.98	x
PRRC2C	7	3	7	3	3.67	2.56	x
FAM98A	3	3	2	2	3.85	2.52	x
YTHDF2	3	5	2	3	3.05	1.77	x
FAM120C	8	3	8	3	5.28	2.18	x
ATXN2L	27	24	27	24	3.57	1.74	x
TRIM56	6	4	6	4	3.97	2.04	x
PRRC2B	7	2	7	2	3.22	1.80	x
GIGYF2	4	2	4	2	3.97	2.20	x
TDRD3	7	5	7	5	3.50	2.39	x
YTHDF3	1	2	1	1	4.99	2.92	x

Supplemental Table S5.

Proteomics of UPF1 protein-protein complexes.

Official Gene Symbol	Razor + unique Peptides UPF1 H, Ctrl L	Razor + unique Peptides MOV10 L, Ctrl H	Unique Peptides MOV10 H, Ctrl L	Unique Peptides MOV10 L, Ctrl H	LOG2 (UPF1 H/Ctrl L)	LOG2 (UPF1 L/Ctrl H)
Y14	4	4	4	4	1.30	1.01
PABPC1	8	5	6	4	1.36	1.52
EIF4A3	28	25	27	24	1.33	1.42
UFM1	2	3	2	3	2.02	1.74
PPP1R12A	1	1	1	1	1.53	3.30
UPF1	129	131	123	125	1.66	3.24
MOV10	10	5	10	5	2.17	2.35
PABPC4	7	7	7	7	1.81	1.42
PEG10	10	11	10	11	2.06	2.45

Supplemental Table S6.

Proteomics of protein-protein complexes bound to RNA in the proximity of UPF1.

Official Gene Symbol	Razor + unique Peptides UPF1 H, Ctrl L	Razor + unique Peptides MOV10 L, Ctrl H	Unique Peptides MOV10 H, Ctrl L	Unique Peptides MOV10 L, Ctrl H	LOG2 (UPF1 H/Ctrl L)	LOG2 (UPF1 L/Ctrl H)	RNA-binding
CCT2	2	2	2	2	1.47	2.06	
KANK2	10	14	10	13	1.20	1.33	
PRRC2C	4	3	4	3	1.09	1.24	x
UFM1	4	4	4	4	1.25	2.61	
CCT8	1	3	1	3	1.83	1.68	
CAD	41	46	41	46	1.38	1.66	
TCP1	4	4	4	4	1.33	1.20	x
CCT6A	1	1	1	1	1.54	1.64	
RUVBL2	4	6	4	6	1.34	1.66	x
CKAP2	2	2	2	2	1.55	1.07	
COPA	2	2	2	2	1.28	1.07	
EID2	3	3	3	3	1.10	1.62	
CSDA	2	2	2	2	1.41	1.72	x
KRT18	7	8	7	8	1.42	1.01	
TUBB	34	36	0	0	1.26	1.31	
DDX3X	2	3	2	3	1.62	1.30	x
EIF4A1	2	4	2	4	1.12	1.36	x
PEG10	10	14	10	14	1.89	2.85	x
EEF2	15	21	15	21	1.50	2.18	x
EIF2S3	1	1	1	1	1.18	2.10	x
EIF4B	2	2	2	2	2.04	1.84	x
GART	2	3	2	3	1.21	1.45	
PUM1	3	4	2	3	1.52	1.45	x
PCBP3	3	2	3	2	1.36	1.78	x
SYNCRIP	2	2	2	2	1.12	1.58	x
HPS6	1	1	1	1	1.20	1.33	
ISYNA1	1	1	1	1	1.04	1.74	
RUVBL1	4	4	4	4	1.09	1.29	
UPF1	125	134	120	128	2.05	3.85	x
TAB2	2	3	2	3	1.27	1.35	
KIAA1217	1	2	1	2	1.26	1.39	
VPS18	1	1	1	1	1.33	1.85	
MOV10	18	19	18	19	1.25	1.71	x

LUZP1	5	6	5	6	1.82	1.85	
MAGED1	2	3	2	3	1.37	1.22	
MAP3K7	2	3	2	3	1.68	1.27	
MAP7D2	2	1	2	1	1.56	1.93	
PPP1R12A	1	2	1	2	2.48	3.91	
OGT	1	1	1	1	1.37	1.16	
POLR2B	5	6	5	6	1.21	1.35	x
TCP11L1	1	1	1	1	1.61	2.05	
TUBA1A	4	4	1	1	1.44	1.67	
TUBA1C	2	2	2	2	1.54	1.30	
TUBB3	2	2	2	2	1.56	1.16	

Supplemental Table S7.

Number of reads mapping uniquely to human and yeast from the mRNA half-life RNA-Seq data.

Sample	Human reads only	Human reads only %		Yeast reads only %	Yeast reads only	
mock_T1 (P1C Total)	1.61E+07	99.8	%	8.55E+03	0.05	%
mock_T2 (P2C Total)	1.96E+07	99.9	%	1.09E+04	0.05	%
MOV10 siRNA _T1 (P3C Total)	1.40E+07	99.9	%	8.06E+03	0.06	%
MOV10 siRNA_T2 (P4C Total)	1.40E+07	99.9	%	7.07E+03	0.05	%
mock_F1 (P1C Flow-through)	1.85E+07	99.9	%	5.65E+03	0.03	%
mock_F2 (P2C Flow-through)	2.19E+07	99.9	%	7.42E+03	0.03	%
MOV10 siRNA_F1 (P3C Flow-through)	1.74E+07	99.8	%	6.64E+03	0.04	%
MOV10 siRNA _F2 (P4C Flow-through)	1.15E+07	99.9	%	4.10E+03	0.04	%
mock_E1 (P1C Eluate)	1.95E+07	99.4	%	7.52E+04	0.38	%
mock_E2 (P2C Eluate)	2.00E+07	99.3	%	8.15E+04	0.41	%
MOV10 siRNA_E1 (P3C Eluate)	2.00E+07	99.4	%	7.47E+04	0.37	%
MOV10 siRNA E2 (P4C Eluate)	2.48E+07	99.2	%	0.97E+04	0.40	%

Supplemental Table S8.

Gene Ontology terms enriched among short-lived transcripts (half-life below 6.75 hrs).

Gene Ontology Biological Pathway	# Proteins	P-Value
Regulation of transcription	697	6.50E-129
Regulation of RNA metabolic process	506	2.70E-93
Negative regulation of gene expression	137	7.50E-22
Negative regulation of nucleobase, nucleoside, nucleotide and nucleic acid metabolic process	137	3.50E-21
Negative regulation of transcription	127	5.33E-21
Negative regulation of nitrogen compound metabolic process	137	1.30E-20
Embryonic development ending in birth or egg hatching	88	2.74E-13
Pattern specification process	73	5.47E-12
Regionalization	58	4.56E-11
Embryonic skeletal system development	32	1.62E-10

Supplemental Table S9.

Gene Ontology terms enriched among long-lived transcripts (half-life above 20.25 hrs).

Gene Ontology Biological Pathway	# Proteins	P-Value
Generation of precursor metabolites and energy	85	3.34E-20
Intracellular transport	127	3.45E-16
Establishment of protein localization	139	3.93E-15
Translational elongation	39	7.15E-15
Purine ribonucleotide metabolic process	43	1.23E-12
Electron transport chain	36	7.07E-11
Nucleoside triphosphate metabolic process	39	7.19E-11
Cellular respiration	31	1.32E-09
Nitrogen compound biosynthetic process	65	3.14E-09
Negative regulation of ubiquitin-protein ligase activity	24	1.20E-08